UNIVERSITY OF OKLAHOMA

GRADUATE COLLEGE

ENVIRONMENTAL CONDITIONS PRODUCING THUNDERSTORMS WITH ANOMALOUS VERTICAL POLARITY OF CHARGE STRUCTURE

A THESIS

SUBMITTED TO THE GRADUATE FACULTY

in partial fulfillment of the requirements for the

Degree of

MASTER OF SCIENCE IN METEOROLOGY

By

ALEXANDER JOSEPH EDDY
Norman, Oklahoma
2018

ENVIRONMENTAL CONDITIONS PRODUCING THUNDERSTORMS WITH ANOMALOUS VERTICAL POLARITY OF CHARGE STRUCTURE

A THESIS APPROVED FOR THE
SCHOOL OF METEOROLGY

BY

_____
Dr. Cameron Homeyer, Chair

_____
Dr. Don MacGorman, Co-Chair

_____
Dr. Mike Biggerstaff

_____
Dr. Earle Williams

This thesis is dedicated to Jesus Christ, my family, and my friends, to whom I owe everything.

Acknowledgements

The author would like to thank the following people: first and foremost his advisor, Dr. Don MacGorman, for his insightful and patient guidance throughout this whole process, for teaching the author how to think critically and be a better researcher and writer, and for taking the time to proofread and edit this thesis; Dr. Cameron Homeyer for serving as the chair of his committee and for always having his door open to offer help; Dr. Mike Biggerstaff and Dr. Earle Williams for providing useful literature on the topic and for providing helpful ideas; Liz DiGangi for her help in learning software and for her helpful tips on writing a thesis; Dr. Kristin Calhoun for providing the Python scripts that were modified to make the violin plots; Dr. Jason Furtado and Dr. Michael Richman for their help with the statistical analysis; Dr. Conrad Ziegler for his script that was modified to perform the Lambert Conformal conic projection on the data; and Lara Keddissi for her help in making the table of contents, list of figures, and list of tables, as well as her support and encouragement. Finally, the author would like to thank the National Science Foundation for providing the funding for this project through grants NSF AGS-1063945 and NSF AGS-1523331.

Table of Contents

List of Tables

List of Figures

Abstract

Electric field soundings and Lightning Mapping Arrays have confirmed the existence of thunderstorms with vertical charge structure that is inverted from the usual polarity. This inverted charge structure can be described grossly as a large upper-level negative charge at roughly the -40°C level, which lies immediately above a large midlevel positive charge, at roughly the -20°C level. This charge structure is often accompanied by a third charge, a smaller negative charge, closer to the freezing level. Cloud-to-ground (CG) flashes lowering positive charge to ground (+CG flashes) instead of the usual negative charge (-CG flashes) make up an unusually large fraction of CG flash activity in these anomalous storms. In this study, we gridded CG flashes from 2004-2014 in order to identify storm cells with high flash rates and having either ≥80% +CG flashes, or having ≥90% -CG flashes. Those with at least 80% +CG flashes were assumed to have an inverted-polarity charge structure, and those with at least 90% -CG flashes were assumed to have a normal-polarity charge structure. We then partitioned the contiguous United States into seven regions, and in each region, we compared the environmental conditions of the inverted-polarity storm cells to those of the normal-polarity storm cells.

We analyzed 17 different environmental parameters, which we divided into 3 categories: dynamic parameters, thermodynamic parameters, and moisture parameters. The dynamic parameters are: 0-3 km shear, 0-6 km shear, 0-3 km storm-relative helicity, and storm-relative wind speed at the equilibrium level. The thermodynamic parameters are: surface equivalent potential temperature, convective available potential energy (CAPE) and normalized CAPE from the level of free convection (LFC) to the

equilibrium level (EL), from the LFC to -20°C, and from 0°C to -20°C, convective inhibition, and EL. The moisture parameters are: dew point depression 2 m above ground level, cloud base height, warm cloud depth, and precipitable water. Hypotheses for the mechanism behind the formation of inverted-polarity thunderstorms are based on conditions causing high supercooled liquid water content in the updraft, thereby favoring positive charging of graupel during rebounding collisions with small ice crystals throughout the depth of the mixed-phase region. Therefore, the environmental parameters we studied are those thought to influence liquid water content in the mixed-phase region of the storm.

Our results show that a storm cell's polarity is determined by no single environmental parameter, but rather by a combination of parameters. Furthermore, different combinations of parameters appear to affect supercooled liquid water content, and hence storm polarity, from region to region. In every region, at least one parameter that was expected to enhance supercooled liquid water content instead had a more favorable median value for normal-polarity cells than for inverted-polarity cells. However, in every region at least four parameters expected to enhance supercooled liquid water content had more favorable values for inverted-polarity cells than for normal-polarity cells. This suggests compensating effects in each region, whereby environmental parameters with values that are unfavorable for maximizing supercooled liquid water content are sufficiently offset by enough environmental parameters with values that are favorable, to produce inverted-polarity storms.

1. Introduction

1.1 Basic Charge Structure of a Thunderstorm

Observations by electric field mills, rocket-borne, ground-based, aircraft-based and balloon-borne electric field meters, and lightning mapping arrays, as well as other instruments have over the years shaped our understanding of atmospheric electricity in both fair-weather and thunderstorm environments. The ability of thunderstorms to generate electric fields on the order of 100 kV m^{-1} and lightning discharges with peak currents well over 100 kA has made them prime objects of study by the atmospheric electricity community. In electrostatics, an electric discharge (e.g., lightning) can occur between two regions of opposite charge if they contain enough charge and are close enough to one another that the electric field between them increases to the breakdown threshold of air. Thus, understanding the mechanisms by which thunderstorm charge is separated and how it is spatially distributed are crucial to better understanding the origin of electric discharges in a thunderstorm.

One of the earliest studies of charge distribution in thunderstorms was carried out by Wilson (1921). Wilson hypothesized that the vertical distribution of charge in a thunderstorm could be described as a positive dipole, defined as a large region of positive charge above a large region of negative charge. Since Wilson's work, others have also described parts of a storm as having a positive or "normal" dipole structure (e.g., Takeuti et al. 1978; Brook et al. 1982; Takagi et al. 1986; Rutledge et al. 1993). In addition to this main dipole, there has often been observed a smaller lower positive charge beneath the dipole, forming a net tripole structure. This has been documented as

far back as Simpson and Robinson (1941), who measured corona current from a balloon-borne instrument to estimate the vertical component of the electric field of storms and thus infer the vertical charge distribution. Others have confirmed the same net tripole structure in many storms, with a large, upper positive charge at roughly -40°C, a large midlevel negative charge at roughly -20°C, and a smaller lowest positive charge near or below the freezing level (e.g., Takahashi 1978; Williams 1989; Stolzenburg et al. 1998; Fuchs et al. 2015).

The tripole description of vertical charge structure is only an approximation and applies mainly to simpler storms with approximately cylindrical symmetry and classic updraft-downdraft motions. In more complicated storms, the classic tripole distribution applies mainly to the updraft core (Bruning et al. 2014). In fact, many storms have a charge structure that is far more complicated, even in the updraft region. Stolzenburg et al. (1998) analyzed 10 electric field soundings through updrafts and five soundings outside of the updrafts in the convective regions of mesoscale convective systems (MCSs). The updraft regions tended to have four main charge regions, alternating in polarity, with the lowest charge region being positive. Outside of the updraft, six charge regions were found, alternating in polarity, with the lowest charge region being positive. The authors suggested that in the updraft regions, the main negative region above the lowest positive charge and the positive charge above it could correspond to the normal dipole distribution that others had observed. Furthermore, Bruning et al. (2014) suggested that the majority of storms have some semblance of the classic tripole structure although some storms have a markedly different structure, which is the topic of this thesis and will be discussed in following sections.

1.2 The Noninductive Graupel-Ice Mechanism

The primary mechanism behind electrification in the updraft region of a storm that leads to the normal tripole structure involves charge transfer during rebounding collisions between ice crystals and larger graupel particles in the presence of supercooled liquid water. MacGorman and Rust (1998) refer to this mechanism as the "noninductive graupel-ice mechanism," and we will do the same. Takahashi (1978) and Jayaratne et al. (1983) showed in laboratory experiments that the sign of charge transferred between graupel and ice crystals depends on the temperature and amount of supercooled liquid water content (SLWC) in the environment. For very high SLWCs (around 8 g m^{-3} in Takahashi 1978) graupel (ice crystals) tended to charge positively (negatively) for all temperatures. Williams et al. (1991) compared the results from Takahashi (1978) to theoretical results that they derived and found that some high SLWCs would also allow wet growth of the graupel. For typical SLWCs of around 1-2 g m^{-3}, graupel (ice crystals) tended to charge negatively (positively) at temperatures colder than around -10°C and positively (negatively) at warmer temperatures. The temperature at which a reversal occurs in the sign of charge that graupel acquires is termed the reversal temperature.

Takahashi (1978) explained the formation of the typical tripole structure of storms as follows: Ice crystals, which have relatively slow terminal velocities, tend to become displaced vertically from graupel particles, which have faster terminal velocities in the updraft. Ice crystals would be lofted to the upper levels of the storm, and before reaching their highest altitudes would have collided with graupel particles in the mixed-phase region at temperatures lower than the reversal temperature, acquiring a

positive charge. This would establish the large upper positive charge of the tripole. Graupel particles would have gained negative charge from collisions with these ice crystals and would be heavy enough to fall in the periphery of the updraft, thereby establishing the large midlevel negative charge of the tripole. Some of the graupel, however, would fall to the lower portions of the storm with temperatures greater than around -10°C. These graupel particles would acquire a positive charge after colliding with ice crystals in temperatures greater than the reversal temperature, establishing the lower positive charge. Similar studies have been conducted on the noninductive graupel-ice mechanism with similar results (e.g., Jayaratne et al. 1983; Jayaratne and Saunders 1984; Saunders et al. 1991).

More recently, Saunders and Peck (1998) showed that the charge transferred to graupel is dependent on temperature and the rime accretion rate (RAR), rather than simply on SLWC, according to:

$$RAR = GDCE\ x\ SLWC\ x\ GCRV,$$

where GDCE is the graupel-droplet collection efficiency, SLWC is the supercooled liquid water content, as before, and GCRV is the graupel-crystal relative velocity. Nonetheless, there is still a reversal temperature. Figure 1 shows the sign of the charge imparted to graupel as a function of RAR and temperature from both Saunders et al. (1991) (piecewise curve) and Saunders and Peck (1998) (black points with polynomial fit). In general, for a moderate RAR, graupel charges positively at warmer temperatures and negatively at colder temperatures. For high RAR, graupel charges positively for all temperatures.

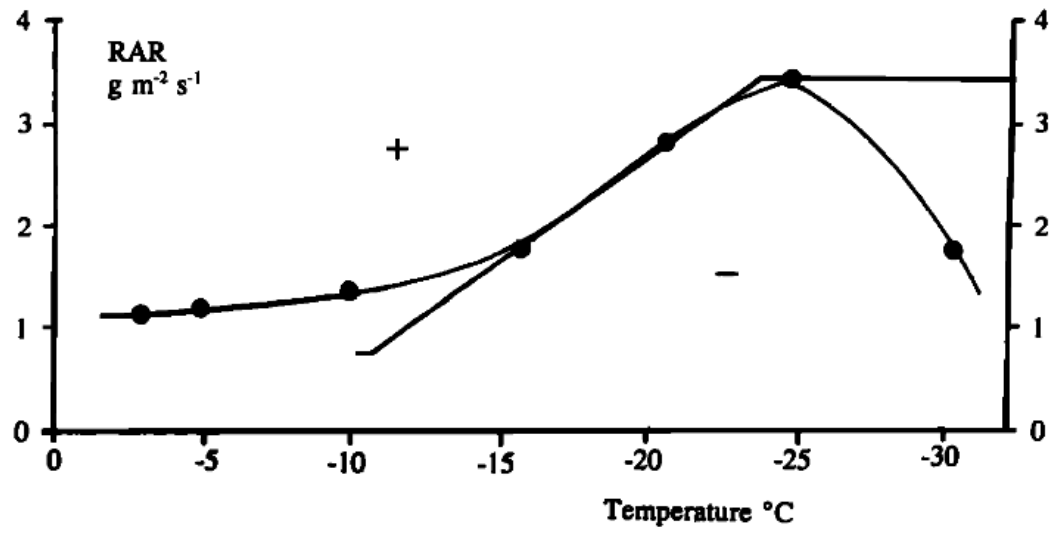

Figure 1: Sign of charge gained by graupel after colliding with and rebounding from ice crystals in the presence of supercooled liquid water content as a function of rime accretion rate and temperature. Black points with polynomial fit are results from and Saunders and Peck (1998), and piecewise curve is from Saunders et al. (1991). Taken from Saunders and Peck (1998).

1.3 Negative and Positive Cloud-to-Ground Flashes

In observations (e.g., Clarence and Malan 1957; Gilmore and Wicker 2002; MacGorman et al. 2011) and modeling (e.g., Mansell et al. 2002) studies, the lower positive charge of a normal tripole is important for enabling lightning to strike ground and lower negative charge from the cloud to the ground (-CG flashes). Similarly, a lower negative charge is thought to be important for enabling +CG flashes. Since the gross vertical charge structure of most warm season thunderstorms approximates a normal tripole, it is no surprise that the dominant polarity of CG flashes is negative.

Using very high frequency (VHF) lightning mapping systems to measure total

lightning (strikes to ground plus strikes remaining in the cloud) and the US National Lightning Detection Network (NLDN) to measure ground strikes, MacGorman et al. (2011) analyzed lightning in storms that occurred from May to August 2005 in Oklahoma and north Texas and from May to July 2000 in Colorado, Kansas, and Nebraska to determine the timing of the first cloud-to-ground (CG) flash relative to the first intra-cloud (IC) flash. They found that the first cloud-to-ground flash was delayed much longer in the drier subcloud environment of the more northern of these regions. Because the more western storms of the High Plains tend to take much longer to develop significant low-level precipitation, and the precipitation was believed to carry the lowest charge in the tripole of the storm, they suggested the delay in precipitation formation also explained why it took much longer for those storms to produce their first CG flash, even in the presence of abundant in-cloud flashes. They suggested also that the much shallower layer for warm-cloud processes and the much stronger exhaust of particles high in updrafts in the northern storms also allowed more liquid water content to be present and thereby caused the vertical distribution of charge to be inverted and caused the CG flash activity they and others observed to be dominated by +CG flashes.

Some of the earliest studies of flashes that lower positive charge to ground (+CG flashes) had been carried out by Takeuti et al. (1978); Rust et al. (1981a,b); Fuquay (1982); Takagi et al. (1986). In fact, prior to 1980, there were fewer than 100 records of +CG flashes documented with their accompanied changes in electric field (Rust et al. 1981b). In the contiguous United States (CONUS), approximately 90% of flashes that strike the earth's surface are -CG flashes, and the remaining 10% are +CG flashes (e.g., Orville and Huffines 2001; Cooray 2015). The two types of ground flashes tend to have

somewhat different characteristics. +CG flashes tend to have larger peak currents, fewer strokes, and are more likely to exhibit continuing current (Rust et al. 1981a; Brook et al. 1982; Fuquay 1982; Orville et al. 1987, 2002; Fleenor et al. 2009). The tendency for +CG flashes to have a longer duration of current to the ground makes +CG flashes ideal candidates for igniting forest fires (e.g., Rudlosky and Fuelberg 2011).

While it is true that most CG flashes in most storms are -CG flashes, some storms have been documented in which most CG flashes were +CG flashes, and correlations between severe weather and storms producing mainly +CG flashes have been observed. Lang and Rutledge (2002) analyzed radar, thermodynamic, and lightning characteristics from 11 storms from the midlatitudes and the tropics and concluded that storms producing predominantly +CG flashes were often severe, had larger updraft volumes of vertical velocity greater than 20 m s^{-1}, and had more hail. Carey et al. (2003) compared severe storm reports to CG flash polarity across the CONUS from 1989-1998 and found that, for all regions of the CONUS, there was a positive correlation between the percentage of +CG flashes and hail size as the diameter of hail increased from 2-8 cm. For larger hail, there was a flat to slightly decreasing trend, which they claimed could perhaps be attributed to an insufficient sample size of storms with larger hail.

1.4 Characteristics and Early Explanations of +CG Flashes

The advent of modern lightning detection networks such as the National Lightning Detection Network (NLDN) (Cummins and Murphy 2009) have provided the data needed to determine geographic variations in the fraction of ground flashes that are

+CG flashes. Similarly, the availability of satellite-borne sensors for detecting all types of lightning flashes has been used to determine the ratio of intracloud flashes to cloud-to-ground flashes (IC:CG flash ratio) (Boccippio et al. 2001). Boccippio et al. (2001) used data from the NASA Optical Transient Detector and from the NLDN to produce the geographic trends shown in Figure 2 in both parameters throughout the CONUS. The +CG flash percentage is highest along parts of the west coast, the northwest, and in the great plains from eastern Colorado and western Kansas stretching northeast through Nebraska, South Dakota, North Dakota, and Minnesota, and this latter region overlaps much of the region of large IC:CG flash ratios in the central CONUS. A similar pattern was also observed by Medici et al. (2017), who expanded on the analysis in Boccippio et al. (2001).

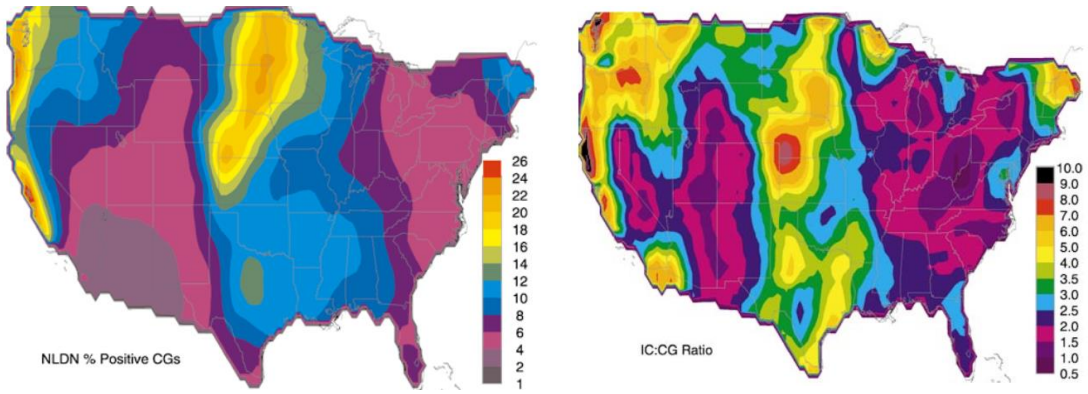

Figure 2: Average percentage of CG flashes that are +CG flashes (left) and average IC:CG flash ratio (right) across the CONUS from May 1995-April 1999. Taken from Boccippio et al. (2001).

That +CG flashes comprise a larger fraction of CG flashes in certain regions of the CONUS implies an environmental influence on the underlying storm electrification and/or the prevalence of a particular storm type conducive to +CG flashes. However, the specific aspect of the environment responsible for the observed trend was uncertain

and remains uncertain today. Boccippio et al. (2001) tentatively hypothesized that the collocated anomalies in percentage of +CG flashes and IC:CG flash ratio in the great plains region were possibly due to the prevalence of storms with stronger updrafts there. A stronger updraft would act to elevate the charge regions composing the thunderstorm tripole. They suggested that this would decrease the number of CG flashes by increasing the distance between the lower positive charge and the earth's surface, as had been suggested by MacGorman et al. (1989) and MacGorman and Nielsen (1991). They also suggested that a stronger updraft would deepen the lower positive charge and that the enhanced lower positive charge would increase the prevalence of +CG flashes (MacGorman and Nielsen 1991; Boccippio et al. 2001).

Earlier, Williams (1989) had also hypothesized that an enhanced lower dipole in the tripolar storm charge distribution might explain observations by others that +CG flashes were frequently associated with electric field measurements at the surface having a vertical polarity opposite to the polarity normally measured under thunderstorms. However, he cautioned that a major problem with the enhanced lower dipole hypothesis was that in deep convection, even though the two lowest charge regions of the thunderstorm tripole form an enhanced inverted dipole, there are often few if any +CG flashes. Qie et al. (2005) studied a thunderstorm on the Tibetan Plateau in China with an enhanced lower dipole and found that no +CG flashes occurred. However, Pawar and Kamra (2009) studied a storm in India that developed in the drier conditions of the premonsoon season that had an enhanced lower dipole and some +CG flashes.

Another hypothesis of the cause of anomalously high +CG percentages in

storms was that large wind shear with height would tilt the main dipole of the thunderstorm enough that some of the upper level positive charge would no longer be shielded from the ground by the midlevel negative charge. A direct path could, therefore, be established for a +CG flash to travel from the positive charge to the ground. Studies of winter storms with anomalously high percentages of +CG flashes in Japan have supported this theory (Takeuti et al. 1978; Brook et al. 1982; Takagi et al. 1986). Brook et al. (1982) suggested that the threshold of shear in the horizontal winds necessary between the altitudes of the negative and positive charge to produce +CG flashes was 1.5 m s^{-1} km^{-1}.

Two papers (Vonnegut and Moore 1958; Marshall et al. 1995) mentioned evidence for a storm having a vertical distribution of charge in which the polarity of the charge in each region was inverted from the polarity observed in most storms, and this would have also contributed to +CG flashes being produced. However, the evidence in neither instance was definitive and was not credited elsewhere in the scientific literature until 2005. From measurements by an electric field mill on the roof of a building approximately 90 km from the storm, Vonnegut and Moore (1958) reported that their measurements were consistent with the storm having inverted-polarity charge structure, but other interpretations of their data were possible. Similarly, Marshall et al. (1995) presented without comment a balloon-borne electric field sounding consistent with four vertically displaced charge regions opposite in polarity from the polarity usually observed at each height. However, the process of inferring charge from electric field soundings has some ambiguities, and they neither had independent confirmation of the charge distribution nor discussed the inverted-polarity structure.

1.5 The STEPS Field Campaign and an Answer to the Problem of +CG Flashes

Observations from the Severe Thunderstorm Electrification and Precipitation Study (STEPS) (Lang et al. 2004) led to a major breakthrough in understanding the origin of +CG flashes. The STEPS field program, conducted in May-July 2000 near the Colorado-Kansas border, collected data using Doppler radars, a Lightning Mapping Array, the National Lightning Detection Network, T-28 armored research aircraft, mobile mesonets, and balloon-borne electric field meters. Two of its main goals were: (1) to understand lightning behavior in different storm types in the drier surface conditions prevalent in the STEPS region; and (2) to better understand the causes of +CG lightning. Rust and MacGorman (2002), Rust et al. (2005), and MacGorman et al. (2005) launched balloon-borne electric field meters into storms to obtain soundings of the vertical component of the electric field (E_z).

Rust and MacGorman (2002) presented soundings of E_z from three storms and suggested the electric field soundings were consistent with a vertical sequence of charge regions in which the polarity of the charge appeared to be inverted from the polarities usually observed. They cautioned, however, that the storms with apparent inverted-polarity charges structures could actually be normal-polarity storms with extra regions of charge in the vertical and that the difficulty in determining the height of cloud base and cloud top introduced ambiguity in the location of each charge region relative to storm structure. Nonetheless, they suggested that the disproportionate frequency of storms that appeared to have inverted-polarity charge distributions in the STEPS domain compared to other regions could explain the higher percentages of +CG flashes

found there.

Rust et al. (2005) expanded the study of Rust and MacGorman (2002) by analyzing Lightning Mapping Array data and the three-dimensional electric field measured by their soundings, rather than just E_z. They studied three storms that occurred during STEPS: a storm near Bird City, Kansas on June 4, 2000; a storm in Haigler, Nebraska on June 25, 2000; and a storm in Idalia, Colorado on June 23, 2000. Unlike the inverted-polarity structure described in Williams (1989) and Boccippio et al. (2001), in which the inversion simply consisted of the inverted dipole composed of the two lowest charges in the normal tripole structure, the polarity of some or all of the layers of vertical charge in all three storms studied by Rust et al. (2005) were opposite to the polarity of charge usually found at those heights. The lightning charge structure they inferred from the Lightning Mapping Array data in all three storms indicated inverted-polarity cloud flashes, and the altitude of the charge regions involved in lightning agreed with the altitude of some of the charge regions inferred from the electric field soundings in those storms. The Bird City storm produced no cloud-to-ground lightning, but the ground flashes produced by the Haigler and Idalia storms produced were mainly +CG flashes. Because of the agreement between the charge regions inferred from lightning and those inferred from the electric field soundings, they concluded that these storms did have inverted-polarity charge structure and that the midlevel positive charge found in those storms was the charge source region for +CG flashes. Because it was very unusual for a storm to produce as many IC flashes without any -CG flashes as produced by the Bird City storm, they suggested a potential link between inverted-polarity charge structure and a delay or complete lack of CG flash

activity.

MacGorman et al. (2005) analyzed balloon soundings of two supercell thunderstorms from STEPS, one on June 29, 2000 and one on July 5, 2000, and found that both storms had an inverted-polarity charge structure and produced mainly +CG flashes. In addition, most +CG flashes drained charge from the midlevel positive charge region located at around 6-8 km MSL, where the midlevel negative charge would reside in a normal-polarity storm. They suggested that the inverted-polarity charge structure was the result of high supercooled liquid water content, leading to a large rime accretion rate of graupel particles. The noninductive graupel-ice mechanism would cause the graupel (ice crystals with which they collide) to charge positively (negatively) for all temperature ranges and thus the entire depth of the mixed-phase region, shown in Figure 1. Differential terminal velocities of the graupel and ice crystals in the updraft would send the negatively charged ice crystals to the upper part of the storm (which is normally positively charged in a normal-polarity storm) and the positively charged graupel to the midlevels (which are normally negatively charged). Since a lower charge of opposite polarity (negative in this case) closer to the ground is crucial for the occurrence of CG flashes (Mansell et al. 2002), the two supercells would have to have negative charge introduced in the lower levels, below the midlevel positive charge. This negative charge could come from graupel that had been negatively charged by the noninductive graupel-ice mechanism in nearby regions having smaller updraft speeds or by other charging processes (MacGorman et al. 2005).

Other studies of storms during STEPS reached similar conclusions, with some additional findings. For example, Wiens et al. (2005) also studied the June 29, 2000

supercell studied by MacGorman et al. (2005) and reached similar conclusions. Nearly 90% of the CGs produced by the storm were +CG flashes, and the storm had an inverted tripole structure when it became severe. Again they attributed the inverted structure to positive charging of graupel in very strong updrafts having large liquid water contents and attributed the +CG flashes to having a lower negative charge below the midlevel positive charge. Tessendorf et al. (2007) studied both a normal-polarity storm (on June 19, 2000) and an inverted-polarity storm (on June 22, 2000). The inverted-polarity storm produced mainly +CG flashes. It was much more intense than the normal-polarity storm and had a stronger, broader updraft. Weiss et al. (2008) expanded the study of the June 25, 2000 storm in Haigler, Nebraska analyzed previously by Rust et al. (2005). While all +CG flashes involved the lowest-altitude negative charge and the positive charge region immediately above it, they cautioned against classifying the entire storm as normal- or inverted-polarity because the vertical distribution of charge regions inferred from lightning evolved both in number of regions and order of polarity. The polarity of a storm region could change in time by the addition or removal of charge layers, and this was sometimes sufficient to change the polarity of its vertical charge distribution according to the inverted-polarity criterion of Rust and MacGorman (2002) (they required the lowest charge to be negative with alternating charges above it).

1.6 Environmental Influences on the Polarity of Thunderstorm Charge Structure

With a clear link established between inverted-polarity storms and high percentages of +CG flashes, and an understanding of the geographic preference for higher percentages of +CG flashes in the High Plains region of the CONUS, several studies sought to understand how environmental characteristics unique to the High Plains, of which the STEPS domain is a part, could be conducive to the formation of inverted-polarity storms. Hypotheses involved maximizing the amount of supercooled liquid water content (SLWC) in the thunderstorm updraft core, as this would allow graupel to charge positively throughout most if not all of the mixed-phase region, leading to the inverted-polarity charge structure.

Williams et al. (2005) suggested that the intersection of high convective available potential energy (CAPE) values and high cloud base heights (CBHs) in the STEPS domain likely played an important role. Higher values of CAPE would allow stronger updrafts. Air parcels in the storm's updraft would, therefore, spend less time below the freezing level, where the scavenging of cloud droplets by larger precipitation droplets through collision and coalescence reduces the amount of cloud water being lofted into the mixed-phase region. Minimizing the time spent in the cloud below the freezing level (warm cloud residence time) therefore helps to maximize SLWC in the mixed-phase region. Higher CBHs would also reduce the warm cloud residence time of an ascending air parcel by reducing the warm cloud depth (WCD), the depth of the cloud below the freezing level. Additionally, higher CBHs lead to broader updrafts, which reduce dry air and cold air entrainment in the updraft core, making for more

efficient processing of CAPE and less dilution of the cloud water content in the updraft core. This would lead to stronger updrafts with greater SLWC in the mixed-phase region.

Carey and Buffalo (2007) analyzed data from 48 inflow proximity soundings from the International H_20 Project (Weckwerth et al. 2004) and data from the NLDN in and near the STEPS domain in four regions containing severe storms in which over 25% of CG flashes were +CG flashes and in five regions containing severe storms in which no more than 25% of CG flashes were +CG flashes. The storms occurred on six different days in May-June 2002. They then compared mean and median values of environmental parameters of the two sets of regions and tested for statistically significant differences using a combination of a Student's *t* test and the Wilcoxon-Mann-Whitney rank sum test (Wilks 2011) given the null hypothesis that both types of regions had identical environments.

The greatest environmental differences between the regions having over 25% +CG flashes and at most 25% +CG flashes were found in the following parameters: regions with larger +CG flash percentages tended to have a shallower WCD, higher CBH, lower mean mixing ratio in the lowest 100 hPa, greater lapse rate over 850-500 hPa, lower wet-bulb zero height, lower precipitable water (PWAT) in a layer from the surface to 400 hPa, lower dew point temperature (T_d) at the surface, and a greater surface dew point depression (DPD). P-values for the differences between the two sets of regions for each of the aforementioned parameters were $p \leq 0.001$. Out of all of these, the greatest difference was in WCD. Other environmental parameters were found to be significantly different in the two types of regions as well, with $0.001 < p \leq 0.1$:

regions with larger +CG flash percentages had greater 0-3 km above-ground-level (AGL) shear, greater 0-3 km storm-relative helicity (SRH), a lower freezing level, a warmer surface temperature, a larger 700-500 hPa lapse rate, less convective inhibition (CIN), a lower equilibrium level (EL), a shallower LFC-EL depth, smaller CAPE from the LFC to the -10°C level, higher CAPE between the -10°C and -40°C levels, greater normalized CAPE (NCAPE) from the LFC to the EL, greater NCAPE between the -10°C and -40°C levels, and higher NCAPE between the LFC and -40°C levels. (NCAPE is related to the average parcel acceleration, given by:

$$NCAPE = CAPE/\Delta h,$$

where Δh is the distance between the levels being considered.) There were not large differences in the environments of the two sets of cases for CAPE between the LFC and EL and between the LFC and -40°C, for NCAPE between the LFC and -10°C, equivalent potential temperature (θ_e), storm-relative wind speed at the EL, or 0-6 km AGL shear.

It seems counterintuitive that regions in which storms had larger +CG percentages were found to have a drier low-to-mid troposhere than the regions with lower +CG percentages, if the larger percentages were caused by storms having inverted-polarity charge structure, because larger SLWCs are thought to be needed to produce inverted-polarity storms. In fact, Carey and Buffalo (2007) found that the adiabatic liquid water content (the maximum available water content that could be realized through adiabatic ascent) in regions with larger +CG flash percentages was two-thirds that in regions with smaller +CG flash percentages at the -20°C level.

If a greater SLWC in the mixed-phase region were to somehow explain the

regions with larger +CG percentages, even though they had less adiabatic liquid water content, the *actual* liquid water content in their mixed-phase regions would have to be greater. Carey and Buffalo (2007) proposed that in regions of storms with larger +CG flash percentages, the higher CBH, shallower WCD, higher CAPE and NCAPE, and greater dynamical forcing of the updraft would increase the actual SLWC in the mixed-phase region by allowing enough of the actual liquid water content to survive into the mixed-phase region, as suggested Williams et al. (2005), that it more than compensated for the difference in adiabatic water content. They cautioned that no single environmental parameter could determine the polarity of a storm's charge distribution, but that a favorable combination could. Even though WCD and CBH were among the most important parameters for the mesoscale regions that they studied, high percentages of +CG flashes are not found in the desert southwest (where CBHs are highest and WCDs are shallow) perhaps due to insufficient CAPE.

Rather than analyze a limited number of specific soundings, as in Carey and Buffalo (2007), Lang and Rutledge (2011) automated the analysis of over 28,000 storm cells by ingesting data from the STEPS field project into the Colorado State University Lightning, Environment, Aerosol, and Radar (CLEAR) framework. In addition to analyzing environments of the storm cells, they used Lightning Mapping Array data to analyze the altitude of the peaks in the vertical distribution of mapped VHF sources, which correspond to the altitudes of the positive charge in lightning, for each storm cell. Cells in which CGs were mainly (at least 50%) +CG flashes had a midlevel positive charge between -10°C and -30°C (consistent with inverted-polarity charge structure), and cells in which CGs were mainly (over 50%) -CG flashes had an upper level and

lower positive charge near -40°C and near 0 to -10°C, respectively (consistent with normal-polarity tripolar charge structure).

Unlike Carey and Buffalo (2007), Lang and Rutledge (2011) found that the biggest difference in the environmental conditions for cells with at least 50% +CG flashes and cells with fewer than 50% +CG flashes was for CAPE. +CG-dominated cells had almost double the CAPE of -CG-dominated cells. The differences in WCD and CBH were minimal; in fact, the positive cells were found to have slightly lower CBHs and slightly deeper WCDs. They did not consider this a refutation of the shallower WCD hypothesis for inverted-polarity storms but instead claimed that differences in CBH and WCD may be more important when comparing storms across different regions having different environmental characteristics than when comparing storms within a given region. +CG-dominated cells were also associated with greater storm-relative helicity, more VHF sources, larger 30 and 40 dBZ echo volume above the freezing level, higher storm heights, and greater 0-3 km and 0-6 km environmental wind shear. The features of the +CG-dominated cells thus indicated more intense convection and stronger updrafts, which likely implies greater SLWCs and positive charging of graupel throughout the entire depth of the mixed-phase region (Lang and Rutledge 2011). The similarity in CBH and WCD and stark differences in other parameters between the +CG-dominated and -CG-dominated cells again suggest that the inversion of a storm's electrical structure is due to a favorable combination of environmental characteristics, rather than due to any single parameter.

Like Lang and Rutledge (2011), but unlike Carey and Buffalo (2007), Fuchs et al. (2015) used the CLEAR framework to analyze the vertical distribution of VHF

sources to infer normal- or inverted-polarity charge structure, but unlike that study, they analyzed environmental characteristics across different regions of the CONUS: near Oklahoma City, Oklahoma; Denver, Colorado; Washington, D.C.; and Huntsville, Alabama. They studied 4322 cell observations from storms that occurred from April to June 2012. They defined anomalous storms as having their principal VHF source mode, which was inferred to be centered on the main positive charge region, at or below -30°C. This definition includes inverted-polarity storms by virtue of their dominant midlevel positive charge, but could also include unusual cases in which most lightning in normal-polarity storms involved the lower positive charge. Normal-polarity storms in which the lower positive charge dominates lightning activity during a significant period appear to occur much less frequently than inverted-polarity storms, and so probably had little effect on their results. Most of the cases with a mode at lower altitudes probably had inverted-polarity charge structure, with graupel charging positively through greater depths, likely due to higher SLWCs in the mixed-phase region. Storms with a peak above the altitude of -30°C were considered to have a normal-polarity structure.

Fuchs et al. (2015) found no anomalous storms in Washington, D.C. or Alabama. The highest flash rates and densities were found in Colorado, followed by Oklahoma, Alabama, and Washington, D.C. Colorado was also found to have the highest reflectivities above the -25°C level and the lowest below that level. They proposed that the relative lack of precipitation (as noted by the reflectivity) below the freezing level indicated less warm-phase precipitation growth scavenging cloud liquid in the updraft below the mixed-phase region. Similarly, they proposed that the relative

abundance of hydrometeors above the -25°C isotherm indicated more robust mixed-phase microphysics and caused the observed higher flash rates. In general, the Colorado cells had the highest CBHs and shallowest WCDs. Values of NCAPE were similar in Oklahoma and Colorado, but tended to be lower in the other two regions.

Most of the anomalous Oklahoma storms had high NCAPE and moderate CBHs. All of the anomalous storms having high CBHs and moderate NCAPE values were in Colorado. This could suggest a compensatory effect whereby suboptimal CBHs (and therefore WCDs) are offset by very large NCAPE values and vice versa. Fuchs et al. (2015) suggested that the parameter allowing these two parameters to compensate for each other was warm cloud residence time, with anomalous charge structure being more likely when there is little residence time in updrafts at levels warmer than 0°C. Higher NCAPE would decrease the warm cloud residence time by allowing faster updrafts. Shallower WCD would also decrease the warm cloud residence time by shortening the distance traveled by an air parcel from the cloud base to the height of the freezing level.

Compensatory effects may exist among other environmental parameters as well. For example, Fuchs et al. (2015) suggested that greater aerosol concentrations could increase SLWC by allowing more numerous but smaller droplets below the mixed-phase region, which would suppress collision-coalescence processes and allow more cloud droplets to enter into the mixed-phase region. They found that the effects of increasing aerosol concentrations were most pronounced in regions where the WCD was deeper, implying that optimal aerosol concentrations could compensate for a suboptimal WCD in maximizing SLWC. Additionally, Fan et al. (2018) found that higher aerosol concentrations increased both updraft intensity and precipitation. Thus,

higher aerosol concentrations could also act to decrease the warm cloud residence time.

1.7 The Goals of this Study

This study combines 11 years of NLDN and North American Regional Reanalysis (NARR) data to compare the environments of storm cells with very high (at least 80%) and very low (at most 10%) percentages of +CG lightning across the whole CONUS. The cells with very high (low) percentages of +CG flashes are inferred to have vertical charge structure that is inverted (normal) in polarity. No other study of this scale has used threshold percentages this high and low to distinguish between cells producing mainly +CG flashes and those producing mainly -CG flashes, and no other study has analyzed differences between the environments of normal- and inverted-polarity cells within a given region for multiple regions spanning the entire CONUS. It is hoped that the larger difference in the percentage of +CG lightning will better elucidate any environmental differences leading to the anomalous inverted-polarity cells. Furthermore, comparing differences in the environments of normal- and inverted-polarity cells within each region, rather than across different regions, will allow the focus to be shifted away from climatological differences that would normally be expected from region to region, whether or not storms of a given polarity were to occur, and towards the those differences that affect vertical charge structure. The goals of this study are as follows:

1. To determine whether any regional environmental differences identified between normal- and inverted-polarity cells are consistent with the hypothesis that inverted-polarity storm cells tend to have larger SLWCs than normal-polarity storm

cells have, and specifically whether they are consistent with the various processes hypothesized to produce large SLWC in the literature.

2. To determine whether the differences found between the environments of normal- and inverted-polarity cells are consistent or vary from one region of the country to another.

2. Data and Methods

2.1 The National Lightning Detection Network

The NLDN, now owned by Vaisala, is composed of an array of detectors spanning the CONUS that detect electromagnetic radiation in the very low frequency (3-30 kHz) and low frequency (30-300 kHz) range. It has been in operation since the 1980s, and for the period of this study (2004-2014), the CG flash detection efficiency is estimated at 90-95% (Cummins and Murphy 2009). Data made available for analysis by Vaisala from the NLDN include the date, time, latitude, longitude, peak current, and multiplicity (i.e., the number of return strokes) of each flash. Each detector uses a combination of time-of-arrival and magnetic direction finding technology to detect both intracloud (IC) and cloud-to-ground (CG) flashes (Cummins and Murphy 2009).

Time-of-arrival techniques compare the time of arrival of the signal at three or more detecting stations to compute the location of a flash in real time. The locus of all flash origins for which a given difference in time of arrival between two stations is possible forms a hyperbola. With three detecting stations, the intersection of the hyperbolae from each of pair of stations marks the origin of the flash, shown in Figure 3a. More than three stations is desired to eliminate ambiguity, however, because the hyperbolae can occasionally intersect at two points when using only three (Cummins and Murphy 2009), as shown in Figure 3b.

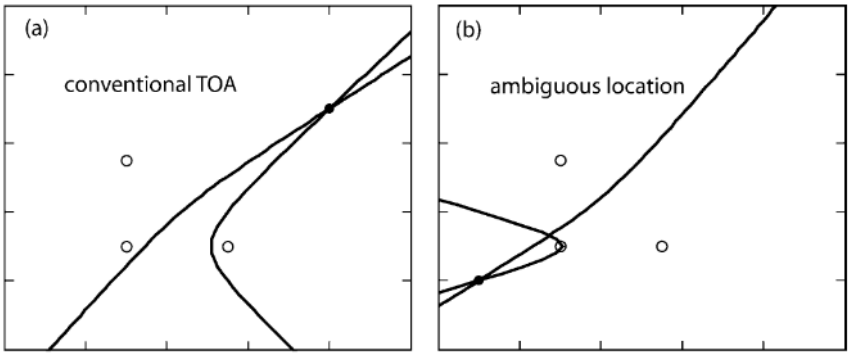

Figure 3: Illustration of the use of a time-of-arrival technique with three detecting stations (open circles). The location of the flash is marked by a filled circle. The single intersection of hyperbolae in (a) marks the location of the flash. The two intersections in (b) make the location of the flash ambiguous, and another detector is needed to eliminate this ambiguity. Adapted from Cummins and Murphy (2009).

A magnetic direction finding station uses two conducting loops placed perpendicular to one another to find the direction from which the cloud-to-ground return stroke signal came. Since a +CG return stroke in one direction has the same signal as a -CG return stroke 180° away, an electric field antenna is also used to eliminate the 180° ambiguity in the polarity of the magnetic signal (Cummins and Murphy 2009). The intersection of directions from two or more stations gives the location of the ground strike.

2.2 North American Regional Reanalysis Data

The NARR output provides over 13.5 TB of environmental data for the U.S., Canada, and Mexico from 1979 to the present. It uses observations in the National Centers for Environmental Prediction (NCEP) Eta 32-km model, NCEP-Department-of-

Energy Global Reanalysis, and the Noah Land-Surface Model (Mesinger et al. 2006). Output is provided at 32-km horizontal resolution, every three hours, and for 45 vertical layers, including 29 pressure levels (NCAR/UCAR 2018). Parameters available span a wide range of categories, from atmospheric moisture, dynamics, and thermodynamics to surface radiative properties to surface and sub-surface conditions. It should be noted that surface temperature and moisture are not ingested into the reanalysis, so environmental parameters related to these should be interpreted with some caution.

2.3 National Lightning Detection Network Methods of Analysis

Ground flashes from the NLDN were analyzed for the 11-year period from 2004-2014. This time period was chosen because it spanned a time between two major upgrades which changed detection efficiency and/or flash classification criteria. The upgrade preceding this analysis occurred from 2002-2003. Before the upgrade, the NLDN had merged with the Lightning Position and Tracking (LPATS) System, resulting in a mixture of station technologies, with some stations using only direction-finders and some using only time-of-arrival. During this period, the NLDN required detection by at least one direction-finder station so that criteria for discriminating between IC and CG signals would be uniform across the network. After the upgrade, the geographic configuration of the network was optimized and all stations were replaced with Improved Accuracy through Combined Technology (IMPACT) stations, each of which used both time-of-arrival and magnetic direction finding. This upgrade increased the stroke detection efficiency from 50% to 60-80% and the flash detection efficiency to 90-95% (Cummins and Murphy 2009). Our study analyzed only flashes, not the

individual strokes that compose the flashes.

Our analysis ended in 2014 because during August of 2015, the algorithm used by the Central Processor of the NLDN was upgraded to reduce time-of-arrival errors and to improve flash classification by analyzing the waveform characteristics of the incoming signal (Nag et al. 2016). Post-upgrade analysis was carried out by Nag et al. (2016) from August 20 to December 10, 2015. After the upgrade, fewer cloud pulses with peak currents < -50 kA and > 20 kA were reported because what had been identified as high-current cloud pulses were more likely to be classified as CG strokes. Preliminary analysis in our study of storms with very high percentages of +CG flashes found many more +CG flashes in 2016, the first full year after the upgrade, than in prior years. We therefore decided to not analyze data beyond 2014, for this study.

The size of the dataset was reduced by including only those flashes between 49.5°N and 24.5°N, and between -124.8°E and -66.8°E, a region which covered the entire CONUS. Additionally, all CG flashes with peak current magnitudes less than 15 kA were discarded. Based on network testing performed by the University of Arizona after the 2002-2003 upgrade, it is estimated that close to 90% of events with peak currents less than 10 kA interpreted as +CG flashes by the NLDN are actually cloud pulses; but only around 10% of events with peak currents greater than 20 kA interpreted as +CG flashes by the NLDN are actually cloud pulses (Cummins and Murphy 2009). A similar problem was found with IC flashes misidentified by the NLDN as -CG flashes in inverted-polarity storms (Fleenor et al. 2009; Calhoun et al. 2013). Because studying inverted-polarity storms was our goal, we chose a threshold of 15 kA with the goal of removing the majority of false CG flashes while not discarding too many real CG

flashes in those storms.

Since a goal of the analysis was to find areas with high flash counts and high percentages of +CG and -CG flashes, it was necessary to grid the lightning data onto a Cartesian grid. To this end, a Lambert Conformal Conic Projection (LCCP) was used. The LCCP slices a portion of the globe with a cone at two secant lines of constant latitude, called the standard parallels. The points on the globe are then projected onto the cone. No projection, including the LCCP, is perfect. While no distortion occurs along the standard parallels, both areal and linear distortion occur away from them. The LCCP works well for countries in the midlatitudes that have a greater east-west extent than north-south extent, making it an appropriate choice for the CONUS (Alpha and Snyder 1982).

For this study, we used a popular choice of the standard parallels, at 33°N and 45°N, because it ensures that the areal distortion across the CONUS is minimal and that the maximum linear scale error is 2.5% (Alpha and Snyder 1982). The origin of the Cartesian grid was chosen to be at 21.8719°N and -118.4547°E so that the entire CONUS would be in the first quadrant. The reference longitude, about which the grid was centered, was -95.8°E, the average of the two longitudes bounding our analysis region.

The lightning grid was constructed by first converting the origin to Cartesian coordinates. Then the latitude and longitude of every flash also was converted to Cartesian coordinates, and the coordinates of the origin were subtracted from them to obtain x and y coordinates relative to the origin. The conversion of a location from (latitude, longitude) to (x,y) coordinates can be accomplished in a few steps (Snyder

1987):

Step 1: $$\alpha = \frac{\ln(\sin(ptop_{comp})) - \ln(\sin(pbottom_{comp}))}{\ln\left(\tan\left(\frac{ptop_{comp}}{2}\right)\right) - \ln\left(\tan\left(\frac{pbottom_{comp}}{2}\right)\right)}$$

Step 2: $$\beta = \frac{R * \sin(ptop_{comp})}{\alpha * tan^{\alpha}\left(\frac{ptop_{comp}}{2}\right)}$$

Step 3: $$\gamma = \beta * \left(\frac{\sin(\text{lat}_{\text{comp}})}{1 + \cos(\text{lat}_{\text{comp}})}\right)^{\alpha}$$

Step 4: $$x = \gamma * \sin(\alpha * (lon - reflon))$$

Step 5: $$y = -\gamma * \cos(\alpha * (lon - reflon))$$

Here, $ptop_{comp}$ is the complement of the latitude (the latitude subtracted from 90 degrees) of the top standard parallel, $pbottom_{comp}$ is the complement of the latitude of the bottom standard parallel, R is the radius of the earth in kilometers (estimated to be 6371 km), lat_{comp} is the complement of the latitude of the point whose coordinates are to be converted, *lon* is the longitude of the point whose coordinates are to be converted, and *reflon* is the reference longitude. The coordinates of the origin are computed as above, and the conversion of a flash is done in the same way, except that the x_{origin} is subtracted from x in Step 4, and the y_{origin} is subtracted from y in Step 5. Once all of the flash locations were converted to Cartesian coordinates, flashes with x-coordinates less than zero and greater than 4680 km were discarded because they fell outside of the CONUS. The resulting dataset was inside the space bounded by the intersection of the two shapes shown in Figure 4.

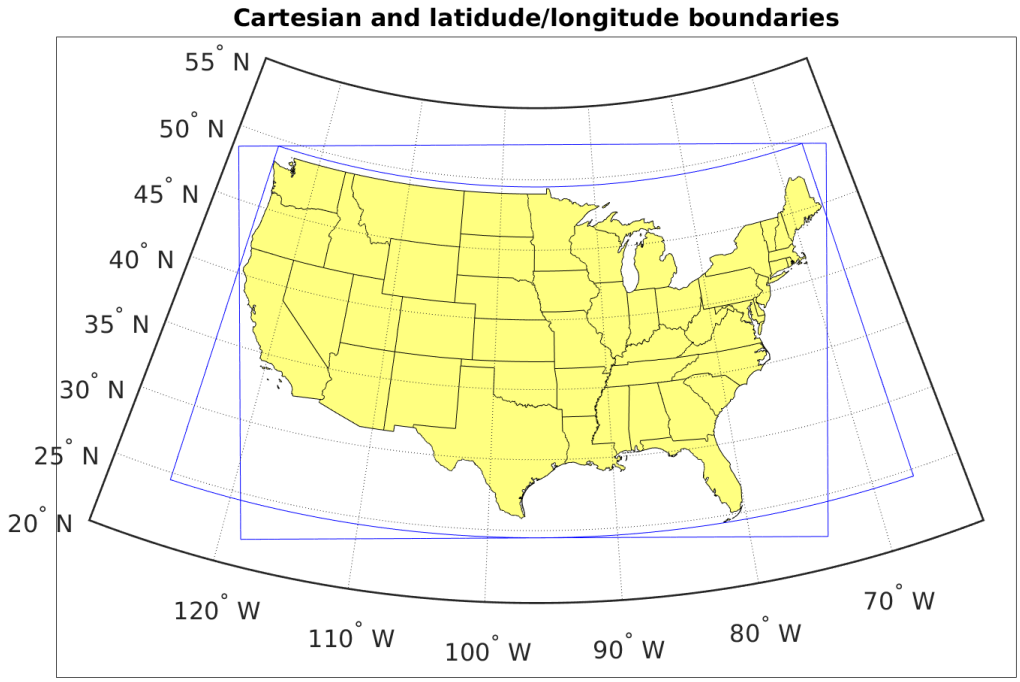

Figure 4: Strike data were kept only if they fell inside the intersection of the two spaces bounded by blue shapes.

The rectangle formed by the grid boundaries was then divided into grid squares 5 km along a side, and the flashes that occurred in each 5 km x 5 km grid cell were then tabulated every 5-minute period. For convenience, each 5 km x 5 km grid cell was identified by its integer grid number, given by:

$$(x', y') = \left(ceiling\left(\frac{x}{5}\right), ceiling\left(\frac{y}{5}\right)\right),$$

where "ceiling" gives the smallest integer that is greater than or equal to its argument, and x and y are given by Steps 4 and 5. Thus, by this point, the numbers of +CG and -CG flashes were counted in each grid square, for every 5-minute period spanning the 11-year period of the analysis.

The goal of gridding the data was to identify grid squares with frequent CG flash rates and either very high or very low percentages of +CG flashes. The assumption on

which this analysis was based is consistent with observations by Rust et al. (2005) and Weiss et al. (2008). Namely, grid squares with very low percentages of +CG flashes were associated with storm cells with normal vertical polarity of charge, and grid squares with very high percentages of +CG flashes were associated with inverted-polarity storm cells. However, since we estimated the typical timescale of an individual thunderstorm cell to be closer to 15 minutes than to 5 minutes, the grids were temporally aggregated. For every 5-minute period, the +CG and -CG flash counts in each grid square were added to the counts of the prior and subsequent 5-minute periods. Similarly, because the typical size of an individual thunderstorm cell is closer to 15 km across than to 5 km across, the grids were spatially aggregated into 15 km x 15 km grid squares every 5 km. Thus, maxima in 15 km x 15 km x 15 minute grid cells could be identified with 5 km and 5 minute resolution. Figure 5 shows an example of how the spatial and temporal aggregations were carried out. In the rest of this study, a 15 km x 15 km x 15 minute grid cell will be referred to as a storm cell. Although actual storm cells may well have a different size or duration, they are more likely to be larger and longer-lasting, rather than smaller and briefer.

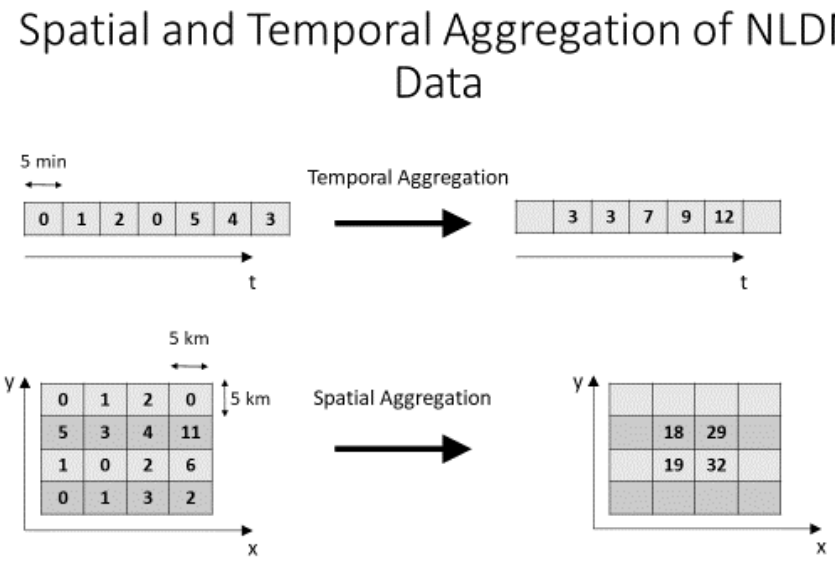

Figure 5: In the case of temporal aggregation (top), before aggregating, the value in each square represents the flash count for a given grid square for each 5-minute period. After the data are temporally aggregated, the value in each square represents the 15-minute running total of flash count, evaluated every 5 minutes. The spatial aggregation (bottom) was carried out in an analogous way. Before aggregating, the number in each 5 km by 5 km square represents its flash count in a given 15-minute period. After aggregation, the number in each square represents the total flash count in each grid square plus the count in each of its adjacent neighbors. Thus, the number is the flash count in the 15 km by 15 km area centered on that grid square, evaluated every 5 km in the x- and y-directions.

Once the grids cells were built and aggregated, storm cells with the following characteristics were identified:

- at least 10 flashes and a +CG flash percentage of 100%
- at least 10 flashes and a +CG flash percentage of at least 90%

- at least 10 flashes and a +CG flash percentage of at least 80%
- at least 20 flashes and a -CG flash percentage of at least 90%

The cells with a +CG flash percentage of at least 80%, at least 90%, and 100% were assumed to have a charge structure that was inverted in polarity, and those with a -CG flash percentage of at least 90% were assumed to have normal-polarity charge structure. Although this is typically true of deep convective cells, CG flash activity in the stratiform regions of mesoscale convective systems (MCSs) often are dominated by +CG flashes, although the deep convective regions typically are dominated by -CG flashes and have normal-polarity charge structure (e.g., Rutledge and MacGorman 1988; Rutledge et al. 1993; Makowski et al. 2013).

Since our intent in this study is to focus on the charge structure of deep convective cells, it was desirable to minimize contamination by MCS stratiform regions. The 10-flash threshold for +CG flashes eliminates most stratiform cases because +CG flashes in the stratiform region tend to be sparser and less frequent. In addition to the flash number and percentage filtering, storm cells were kept only if they occurred between 3pm and 11pm local solar time because MCSs are most common in late night and early morning, after upscale growth has occurred, while deep convection tends to occur from the time of maximum solar heating until around 11pm local time. Here, local solar time (LST) was given by:

$$LST = GMT - \left(\frac{abs(lon)}{180^o}\right)(12\ hours),$$

where *GMT* is the time that a given cell occurred in Greenwich Mean Time and *lon* is the cell's longitude.

CG flash activity in winter storms often is dominated by +CG flashes, but the

environmental characteristics responsible for this are thought to be much different from those responsible for producing inverted-polarity structure in deep convection. Thus, only cells in each region's warm season were kept in order to prevent winter storms with high percentages of +CG flashes (e.g., Rudlosky and Fuelberg 2011) from contaminating the analysis. The warm season for the northern regions and for the central-central region (shown in Figure 6) was defined to be from May through September, and that for the southern regions was defined to be April through October. Finally, in order to be able to carry out statistical analysis on the data, sample spatial and temporal independence was sought. For each cell, ordered from those with the most flashes to those with the least, all cells with a lower flash count that overlapped in space with it and occurred within 30 minutes of it were discarded. Since it is expected that the environmental conditions and flash characteristics of storm cells that are farther apart in space and time should be less correlated, this acted to make elements of the dataset less mutually dependent.

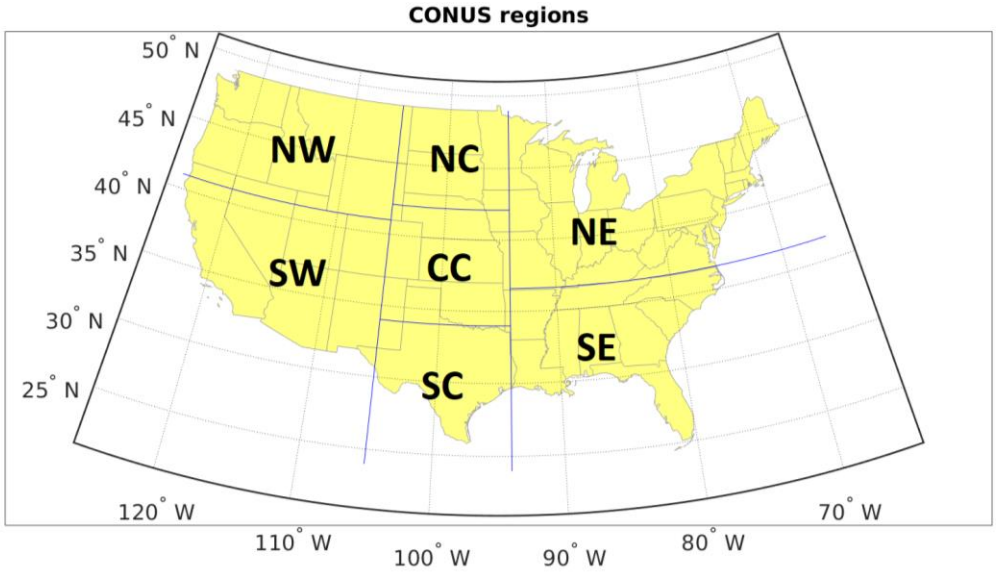

Figure 6: Partitioning of CONUS into the seven analyzed regions.

Because one goal of this study was to evaluate whether the same environmental properties were conducive to inverted-polarity storms in different climatological regions and, if not, to determine the differences, the CONUS was divided into seven regions, shown in Figure 6, based roughly on their different climates. The seven regions are the southwest (SW), northwest (NW), southcentral (SC), central-central (CC), northcentral (NC), southeast (SE), and northeast (NE) regions. Fuchs et al. (2015) compared environmental conditions of normal-polarity storms in two regions with those of inverted-polarity storms in two completely different regions of the CONUS. However, some environmental differences they found, such as in warm cloud depth, would likely have existed between the two pairs of regions, regardless of the vertical polarity of the storm charge distribution. Other studies (e.g., Carey and Buffalo 2007; Lang and Rutledge 2011) compared environmental differences between inverted- and normal-polarity storms for only one region of the CONUS. This is the first study attempting to compare the environments of normal- and inverted-polarity storms by analyzing all CG-producing storms occurring over a multiyear period of time for various regions spanning the entire CONUS.

2.4 North American Regional Reanalysis Methods of Analysis

The latitude and longitude of each of the gridpoints in the 32-km NARR grid were converted to Cartesian coordinates with the same origin as the one we used for gridding the CG flash data. Then, for every storm cell, the closest NARR gridpoint was found, and the environmental conditions were calculated at that gridpoint. Since the NARR data is provided only every 3 hours, and many cells existed between those times,

linear interpolation in time was required to estimate the values of the parameters at the time that each cell occurred.

In this study, we analyze 17 different parameters, which we have divided into three categories: dynamic parameters, thermodynamic parameters, and moisture parameters. The dynamic parameters are: 0-3 km shear, 0-6 km shear, 0-3 km storm-relative helicity (SRH), and storm-relative wind speed at the equilibrium level (EL). The thermodynamic parameters are: surface equivalent potential temperature (θ_e), convective available potential energy (CAPE) from the level of free convection (LFC) to the EL (LFC to EL CAPE), LFC to EL normalized CAPE (NCAPE, i.e., CAPE divided by the distance between these two levels), LFC to -20°C CAPE, LFC to -20°C NCAPE, 0°C to -20°C CAPE, 0°C to -20°C NCAPE, convective inhibition (CIN), and EL. The moisture parameters are: dew point depression at 2 m AGL (DPD), cloud base height (CBH), warm cloud depth (WCD), and precipitable water (PWAT). Most of the above parameters were not available directly from the NARR dataset and had to be calculated from parameters that were provided.

Parameters explicitly provided in the NARR data that were not calculated were: SRH, PWAT, and CBH. All heights provided were geopotential heights, which we estimated to be the actual height. "Hybrid level 1" in the NARR database was estimated to be the surface level. Since heights were given above mean sea level (MSL), to obtain AGL heights, the MSL heights were subtracted from the height of hybrid level 1.

The following is how we calculated parameters derived from NARR data. DPD was calculated by subtracting the 2 m AGL dew point temperature from the 2 m AGL dry bulb temperature. The WCD was obtained by subtracting the CBH from the height

of the freezing level. To calculate θ_e, the following formula was used (AMS 2015):

$$\theta_e = T\left(\frac{p_0}{p_d}\right)^{\frac{R_d}{c_p}} H^{-\frac{wR_v}{c_p}} e^{\frac{wL_v}{c_pT}},$$

where T is the surface dry bulb temperature, p_0 is a reference pressure equal to 1000 hPa, p_d is the partial pressure of dry air at the surface, R_d is the dry air gas constant and is equal to 287 J kg^{-1} K^{-1}, c_p is the specific heat of dry air at constant pressure and is equal to 1004 J kg^{-1} K^{-1}, H is the relative humidity at the surface, w is the mixing ratio at the surface, R_v is the water vapor gas constant and is equal to 461 J kg^{-1} K^{-1}, and L_v is the latent heat of vaporization of water at 0°C and is equal to 2.5x10^6 J kg^{-1}. Specific humidity (q) was provided in the NARR dataset, so w was calculated using:

$$w = \frac{q}{1-q}.$$

From w, water vapor partial pressure (p_v) was obtained from (Wallace and Hobbs 2006):

$$p_v = \frac{w}{w + \frac{R_d}{R_v}} p.$$

Here, p is surface pressure. Then, p_d was obtained as:

$$p_d = p - p_v.$$

Winds in the NARR dataset were given at constant pressure levels, along with the geopotential height of each pressure level. To obtain wind values at 0 km, 3 km, and 6 km, cubic spline interpolation was used. The 0-3 km and 0-6 km wind shear values were then calculated by subtracting the winds at the surface from the 3 km winds and from the 6 km winds, respectively.

To calculate CAPE, the following relationship was used:

$$CAPE = R_d \int_{EL}^{LFC} \frac{(T_{vpar} - T_{venv})}{p} dp,$$

where *EL* is again the equilibrium level, *LFC* is again the level of free convection, T_{vpar} is the virtual temperature of the ascending air parcel and T_{venv} is the virtual temperature of the environment (Wallace and Hobbs 2006). The pressure step (*dp*) used was 10 hPa. The height of each pressure level was found by linear interpolation with the natural logarithm of the pressure values. The CAPE in this analysis is approximately surface-based, since the air parcels were lifted from 1000 hPa or at most 10 hPa above hybrid level 1, whichever was higher. Virtual temperature was calculated using (Wallace and Hobbs 2006):

$$T_v = T\frac{\left(w+\frac{R_d}{R_v}\right)}{\left(\frac{R_d}{R_v}\right)(1+w)}.$$

Cubic splines interpolation was used to find *w* of the environment, and also *T* of the environment at every pressure level in 10 hPa increments. To find the *T* of the parcel, at every level below the lifted condensation level (LCL), the dry adiabatic lapse rate (-9.8 K km^{-1}) was assumed and *w* was conserved and equal to its value at the surface. At and above the LCL, the moist adiabatic lapse rate (Γ_m) was assumed, given by (AMS 2015):

$$\Gamma_m = g\frac{\left(1+\frac{L_v w_s}{R_d T_{par}}\right)}{c_p+L_v^2 w_s/(R_v T_{par}^2)},$$

where the subscript *s* denotes "saturation" and the subscript *par* denotes "parcel." The LCL was defined as the lowest layer where the relative humidity of the parcel,

$$H_{par} = \frac{w_{par}}{w_{spar}},$$

was at least 100%. At each layer,

$$w_{spar} = \frac{e_s R_d}{R_v(p-e_s)},$$

where e_s is the saturation vapor pressure, given by the Clausius-Clapeyron equation

(Rogers and Yau 1989):

$$e_s = (611.2\ Pa)\exp\left(19.83 - \frac{5417}{T_{par}}\right).$$

CIN was calculated by summing the CAPE of all negative-CAPE-bearing layers below the highest positive-CAPE-bearing layer. At NARR gridpoints at which the CAPE was 0 J kg^{-1}, the CIN was defined to be 0 J kg^{-1} as well. The height of the EL was defined to be the highest height at which T_{venv}=T_{vpar}, or the 100-hPa level, whichever was lower.

Storm-relative wind speed at the EL was found by subtracting the mean storm motion from the wind at the EL. Wind at the EL was found using cubic splines interpolation. Mean storm motion was estimated by taking the non-pressure-weighted average of the winds from the surface to 6 km.

Some adjustments were made, occasionally, when environmental values seemed unphysical. At locations at which CBH was very low and hybrid level 1 was likely slightly above the true ground level, the calculated value for CBH was at times slightly negative. To correct this, negative CBHs were set to 0 m. Also, due to the coarse resolution of the NARR data and the interpolation in time required to calculate environmental parameters, sometimes the characteristics of the environment did not match characteristics that would be expected to be required to produce a cell with vigorous electrical activity. For example, some cells occurred at NARR grid points with 0 J kg^{-1} of LFC to EL CAPE. This could have also been the result of the storm's effect on its nearby environment. To preserve only those cases in which the environment seemed less affected by nearby storm cells or in which interpolation did not lead to counterintuitive values, only those cells with an EL of at least 7 km were kept.

Table 1 shows the number of measurements of each parameter for each region for the +CG-dominated cells with at least 10 flashes, 80% or more of them being +CG flashes. Table 2 shows the same information for the -CG-dominated cells (with at least 20 flashes, 90% or more of them being -CG flashes). The bulk of the analysis of the +CG-dominated cells is focused on the 80%, 10-flash threshold rather than higher percentages because for some regions, using the higher thresholds would not have provided a large enough sample size.

Table 1: Sample sizes for each parameter and each region for the +CG-dominated cells with at least 10 flashes and at least 80% +CG flashes.

	SW	NW	SC	CC	NC	SE	NE
WCD	1494	528	1321	14006	11170	1148	4287
CBH	1494	528	1321	14006	11170	1148	4287
CIN	1581	639	1644	16640	13580	1207	4812
DPD	1581	639	1644	16640	13580	1207	4812
SRH	1581	639	1644	16640	13580	1207	4812
PWAT	1581	639	1644	16640	13580	1207	4812
θ_e	1581	639	1644	16640	13580	1207	4812
LFC to EL CAPE	1581	639	1644	16640	13580	1207	4812
LFC to EL NCAPE	1581	639	1644	16640	13580	1207	4812
LFC to -20°C CAPE	1581	639	1644	16640	13580	1207	4812
LFC to -20°C NCAPE	1581	639	1644	16640	13580	1207	4812
0°C to -20°C CAPE	1581	639	1644	16640	13580	1207	4812
0°C to -20°C NCAPE	1581	639	1644	16640	13580	1207	4812
EL height	1581	639	1644	16640	13580	1207	4812
0-3 km shear	1581	639	1644	16640	13580	1207	4812
0-6 km shear	1581	639	1644	16640	13580	1207	4812
storm-relative speed at EL	1581	639	1644	16640	13580	1207	4812

Table 2: Sample sizes for each parameter and each region for the -CG-dominated cells with at least 20 flashes and at least 90% -CG flashes.							
	SW	**NW**	**SC**	**CC**	**NC**	**SE**	**NE**
WCD	39891	5112	58380	45909	7874	205020	116150
CBH	39891	5112	58380	45909	7874	205020	116150
CIN	41472	6254	62023	50098	9473	207640	119460
DPD	41472	6254	62023	50098	9473	207640	119460
SRH	41472	6254	62023	50098	9473	207640	119460
PWAT	41472	6254	62023	50098	9473	207640	119460
θ_e	41472	6254	62023	50098	9473	207640	119460
LFC to EL CAPE	41472	6254	62023	50098	9473	207640	119460
LFC to EL NCAPE	41472	6254	62023	50098	9473	207640	119460
LFC to -20°C CAPE	41472	6254	62023	50098	9473	207640	119460
LFC to -20°C NCAPE	41472	6254	62023	50098	9473	207640	119460
0°C to -20°C CAPE	41472	6254	62023	50098	9473	207640	119460
0°C to -20°C NCAPE	41472	6254	62023	50098	9473	207640	119460
EL height	41472	6254	62023	50098	9473	207640	119460
0-3 km shear	41472	6254	62023	50098	9473	207640	119460
0-6 km shear	41472	6254	62023	50098	9473	207640	119460
storm-relative speed at EL	41472	6254	62023	50098	9473	207640	119460

3. Results

3.1 Geographic Distribution of Cells Dominated by +CG and -CG Flashes

We analyzed the spatial distributions of storm cells containing +CG flashes for the four different thresholds used: at least 20 CG flashes, 100% of which were +CG flashes; at least 10 CG flashes, 100% of which were +CG flashes; at least 10 CG flashes, 90% of which were +CG flashes; and at least 10 CG flashes, 80% of which were +CG flashes. The spatial distributions of storm cells meeting the four different thresholding criteria are shown for 2004 in Figures 7-10. The location of each storm cell meeting the specified criteria is marked with a red "+".

Figures 7-10 represent storm cells for the whole year of 2004, not just the warm season, and for all hours of the day, not just 3pm to 11pm local solar time. Due to the spatial and temporal overlap, a single CG flash would count, as appropriate, towards the +CG, -CG, and total CG flash count of adjoining cells and, therefore, would affect the +CG percentage in multiple cells. Furthermore, multiple instances of the same 15 km x 15 km geographic cell at multiple times are overplotted and so appear only once. Thus, the distribution of cells meeting specified criteria of flash rate and percentage of +CG flashes in these figures does not give quantitative counts of +CG and -CG flashes, or even of cells, but provides only a qualitative impression of the distribution of these cells and of the effect of increasing the total and +CG percentage thresholds. By increasing the percentage threshold of +CG flashes and the flash count threshold, we are able to hone in on the storms that are the most active producers of +CG flashes, which are

mainly in the Texas panhandle, eastern Colorado, western and central Kansas, Nebraska, Iowa, and stretching farther north and northeast into the Dakotas and Minnesota (mainly in the CC and NC regions).

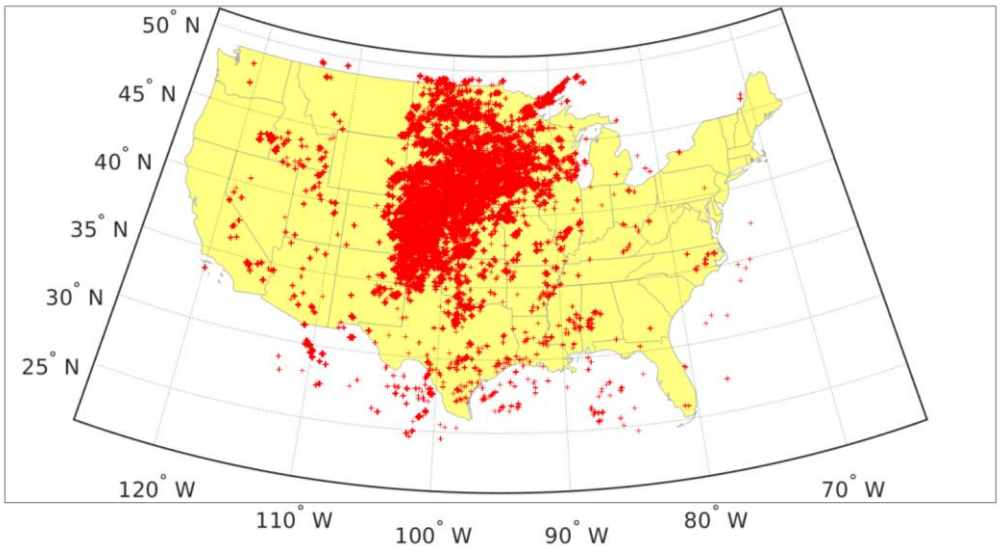

Figure 7: Locations of cells with at least 10 flashes, at least 80% of which are +CG flashes, for the year 2004.

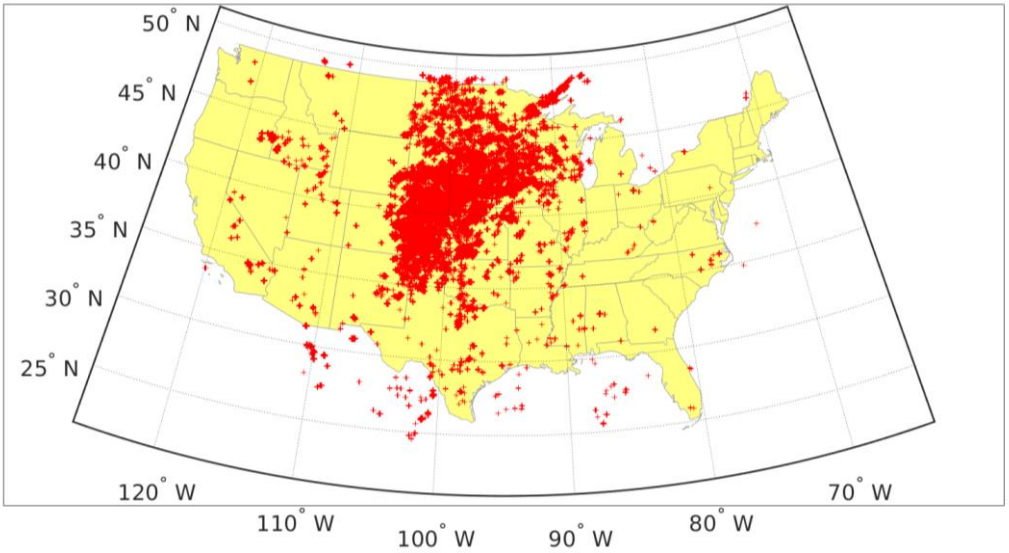

Figure 8: Locations of cells with at least 10 flashes, at least 90% of which are +CG flashes, for the year 2004.

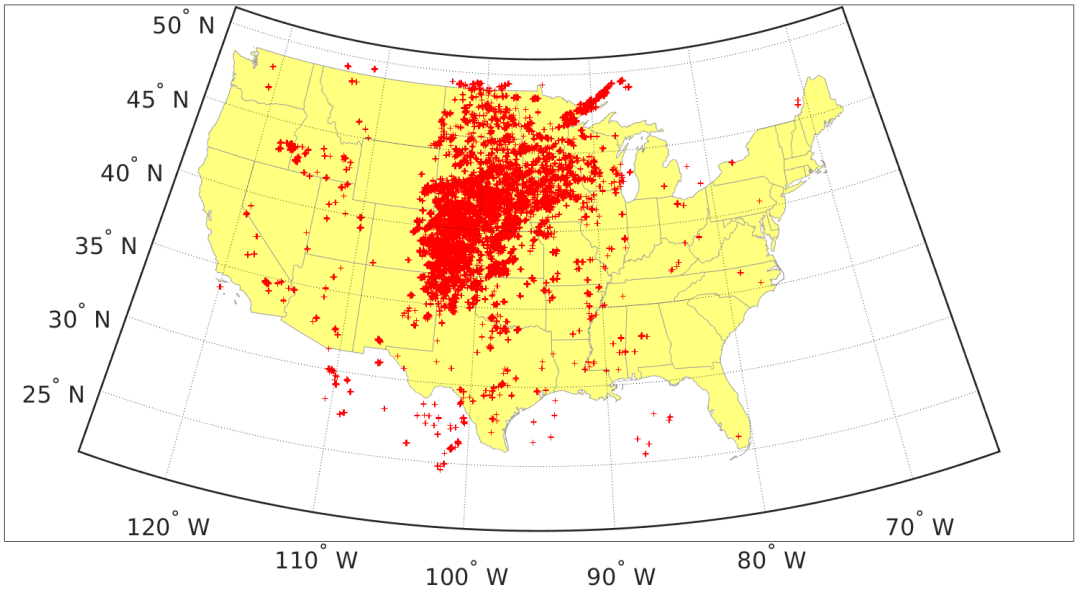

Figure 9: Locations of cells with at least 10 flashes, 100% of which are +CG flashes, for the year 2004.

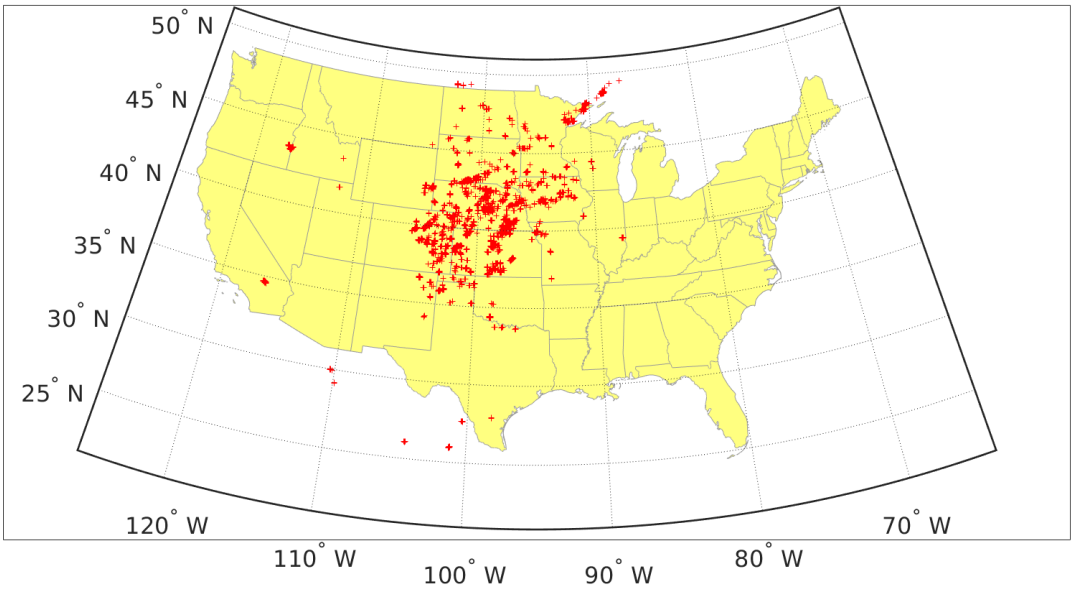

Figure 10: Locations of cells with at least 20 flashes, 100% of which are +CG flashes, for the year 2004.

Figures 11-20 show the same information as in Figure 10, but for the remaining analyzed years (2005-2014). There is some year-to-year variability, but the

overwhelming majority of cells with a very high flash rate and a very high percentage of +CG flashes are in the central and north-central CONUS.

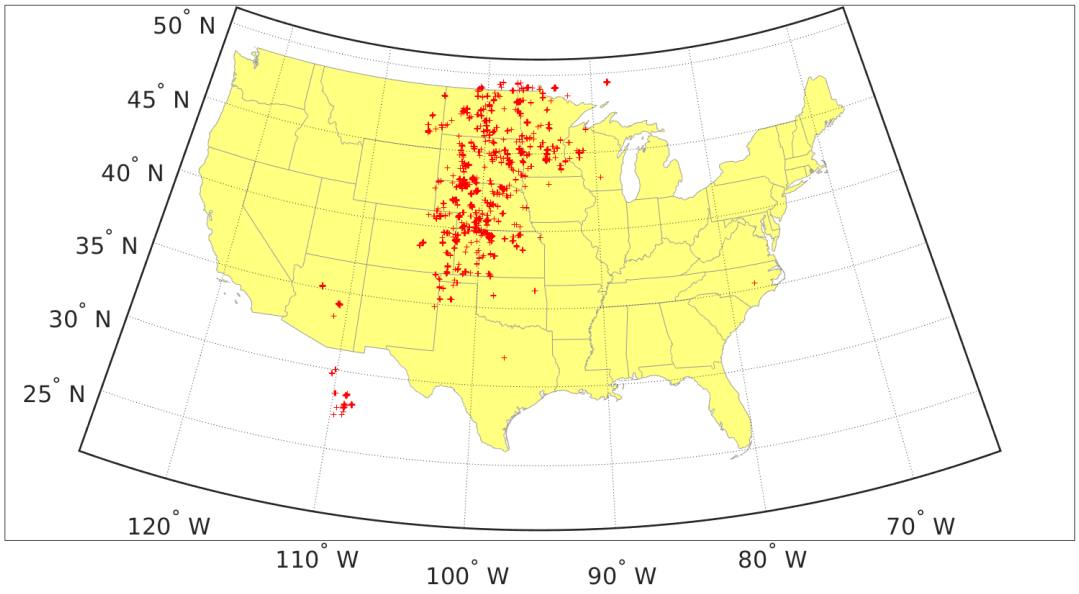

Figure 11: Same as Figure 10, but for the year 2005.

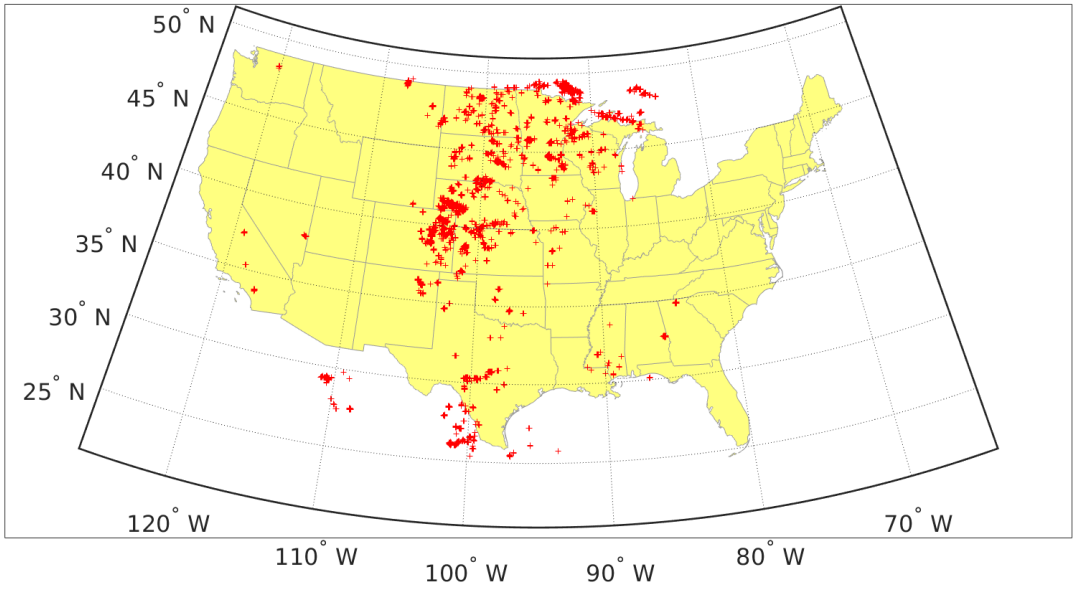

Figure 12: Same as Figure 10, but for the year 2006.

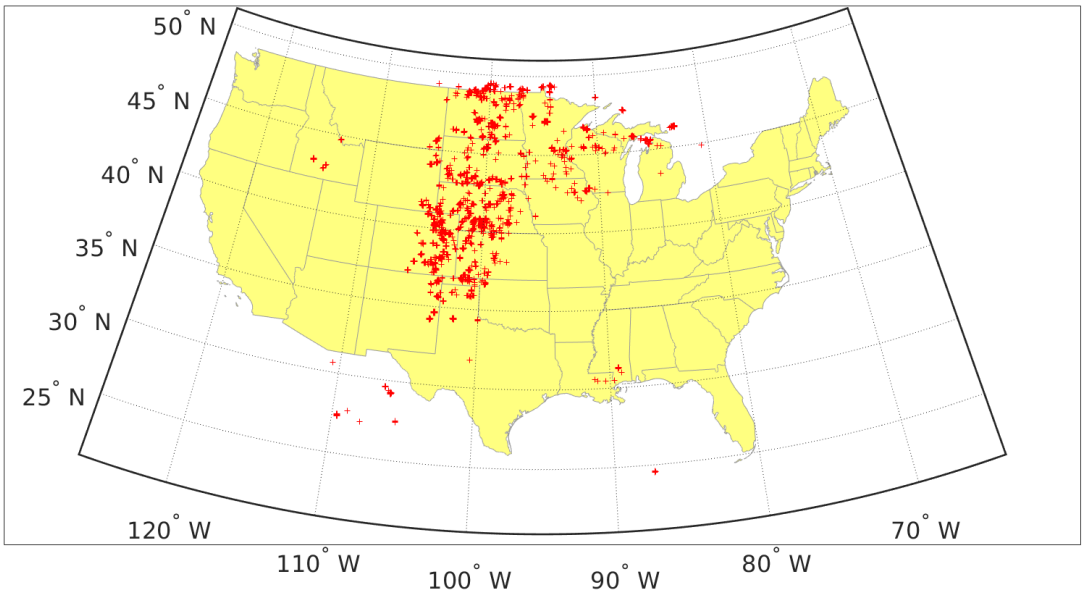

Figure 13: Same as Figure 10, but for the year 2007.

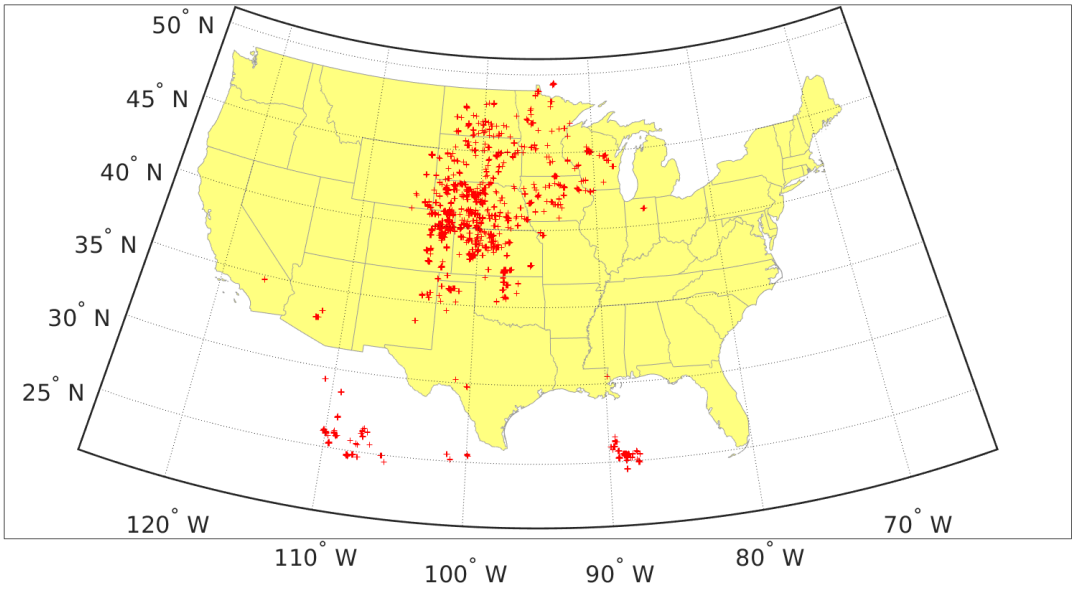

Figure 14: Same as Figure 10, but for the year 2008.

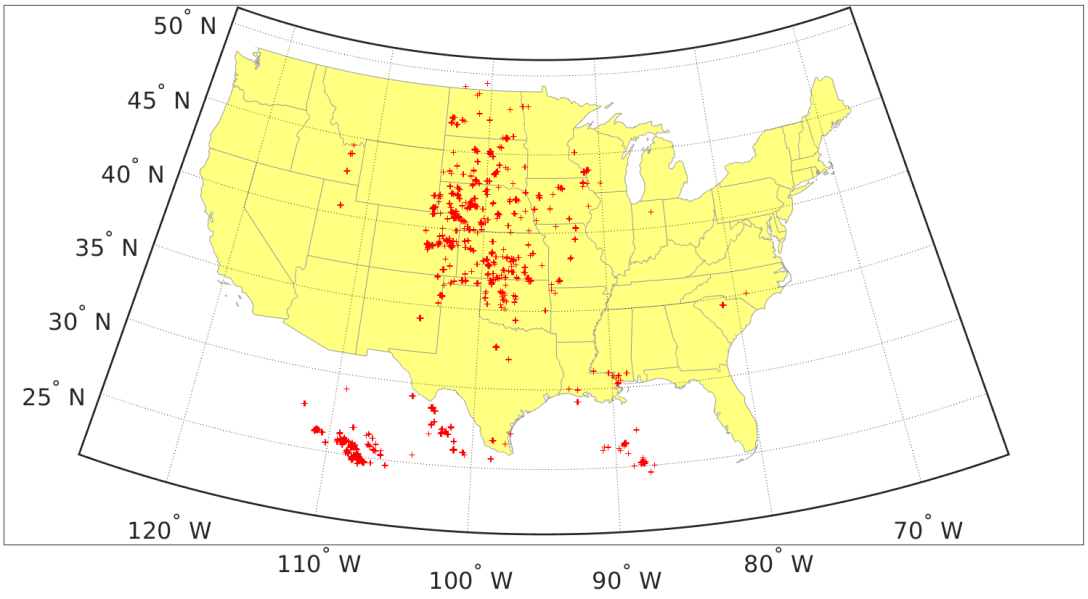

Figure 15: Same as Figure 10, but for the year 2009.

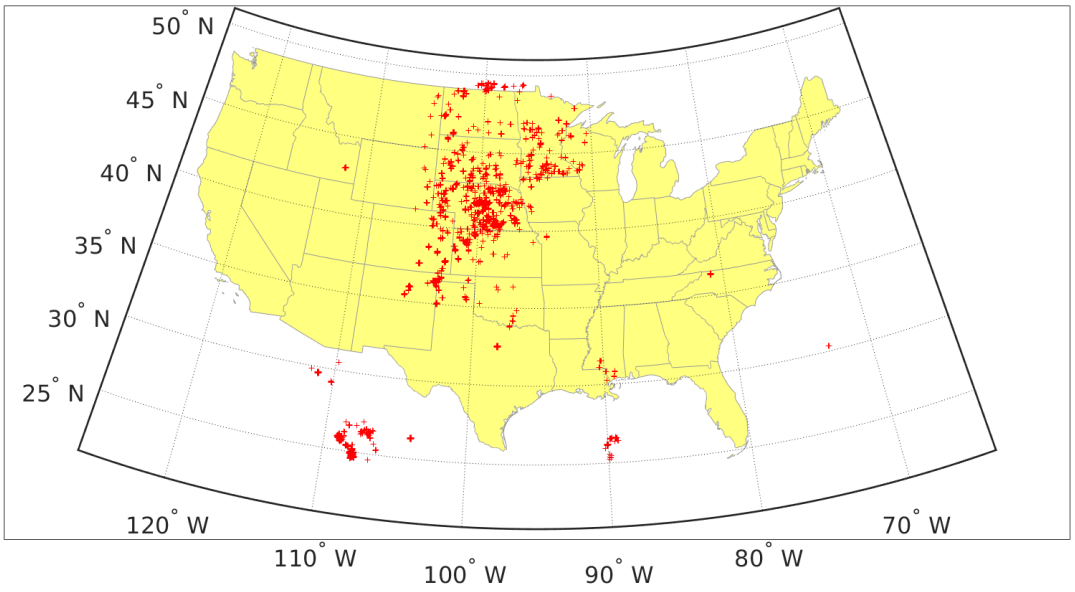

Figure 16: Same as Figure 10, but for the year 2010.

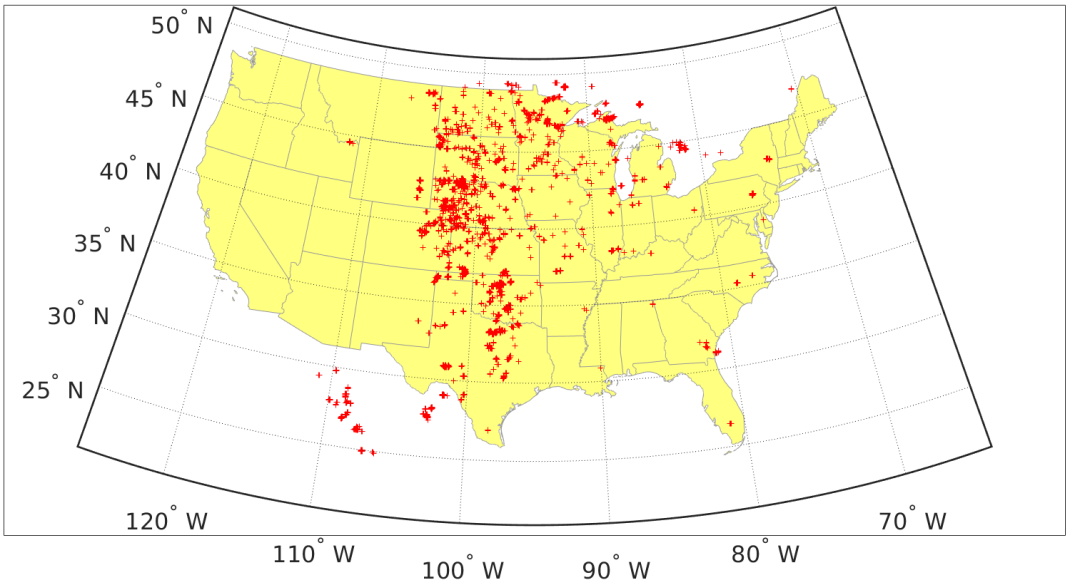

Figure 17: Same as Figure 10, but for the year 2011.

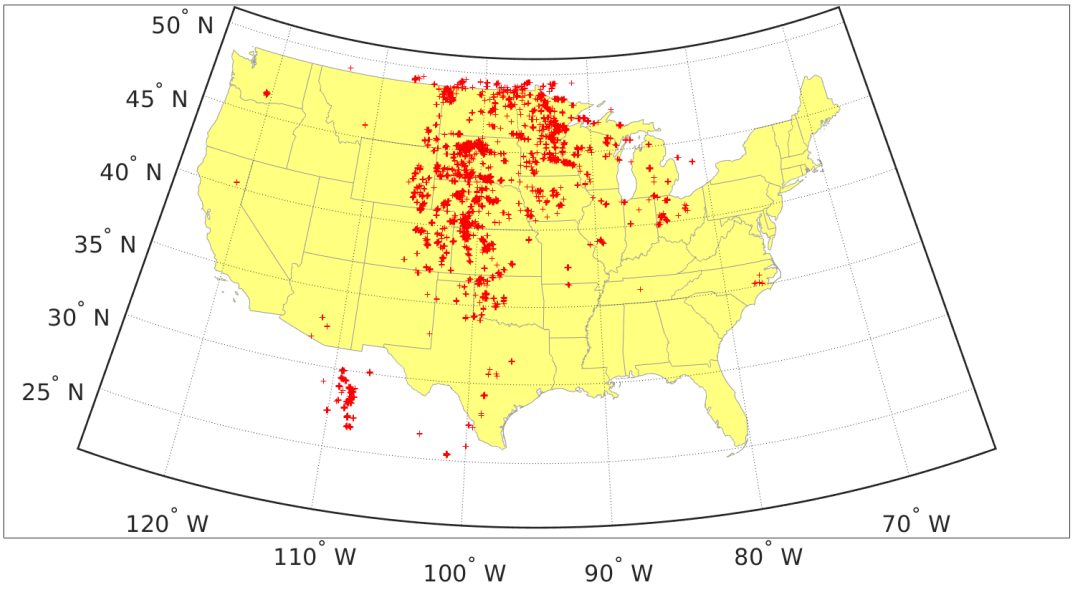

Figure 18: Same as Figure 10, but for the year 2012.

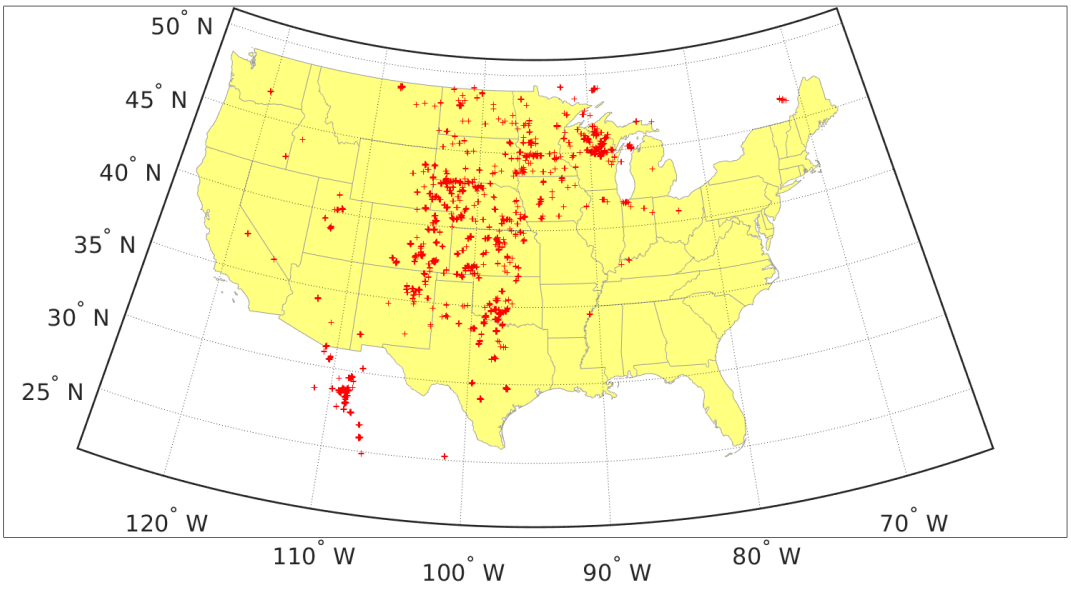

Figure 19: Same as Figure 10, but for the year 2013.

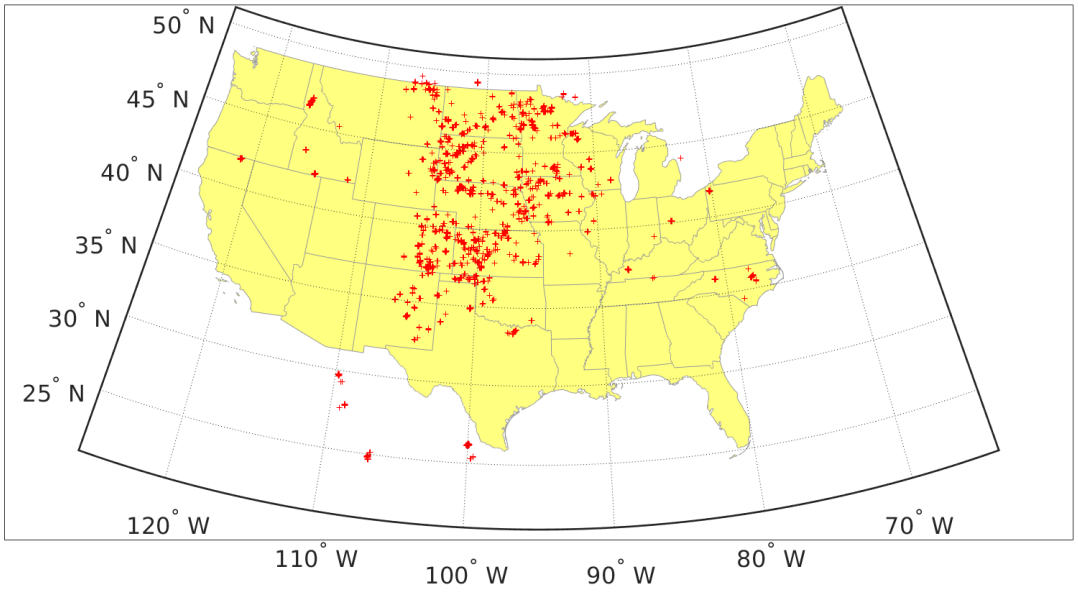

Figure 20: Same as Figure 10, but for the year 2014.

Figure 21 shows a contour plot of the number of storm cells with at least 10 flashes, at least 80% of them being +CG flashes, for all years. As in Figures 7-20, these counts are of cells from all seasons and all hours of the day, without removing the spatial or temporal overlap between cells. The bulk of +CG flash activity lies in the CC

and NC regions.

Figure 22 shows a contour plot of the number of storm cells having at least 20 flashes, at least 90% of which are -CG flashes, for all years. As in Figures 7-20, these counts are of cells from all seasons and all hours of the day, without removing the spatial or temporal overlap between cells. The majority of storms dominated by -CG flash activity occurs south of a diagonal line extending from the northeast to the southwest corners of the CONUS. The regions with the largest density of storms dominated by -CG flashes are in southern Louisiana and Mississippi, as well as in Florida. Because the largest densities of storms dominated by -CG flashes are so much larger than the largest densities of storms dominated by +CG flashes, the largest densities of storms with large total CG flash rates would be essentially the same as the largest densities of storms dominated by -CG flashes.

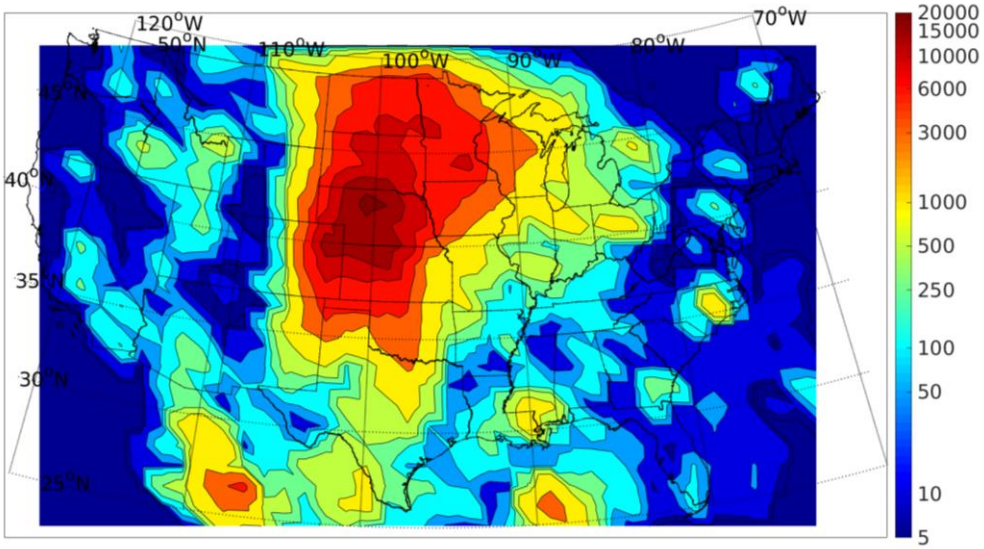

Figure 21: Counts of the number of cells with at least 10 flashes, at least 80% of them being +CGs, for the years 2004-2014. Each color in the map corresponds to a label on the colorbar.

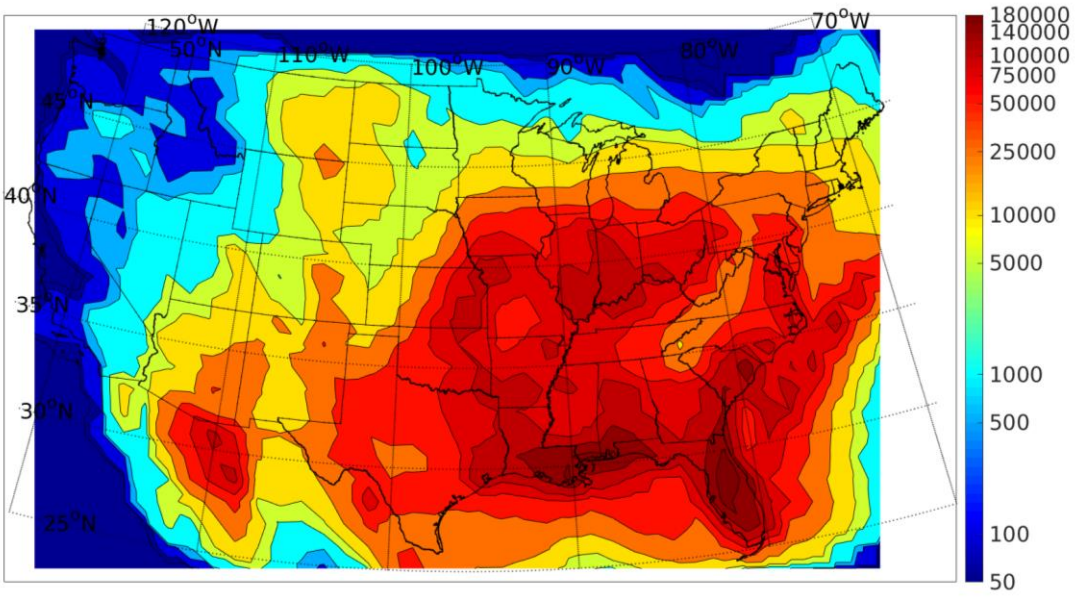

Figure 22: Counts of the number of cells with at least 20 flashes, at least 90% of them being -CGs, for the years 2004-2014. Each color in the map corresponds to a label on the colorbar.

Figures 23 and 24 are similar to Figures 21 and 22, except they show only the reduced dataset used in this study. In other words, they contain only those cells that occurred from 3pm-11pm local time, during the warm season, and that remained after the spatial and temporal overlapping was removed by the algorithm described in Section 2.3. Note that the pattern in Figure 23 (24) is roughly the same as that in Figure 21 (22), even though the datasets have been reduced. The environmental parameters analyzed in the next section are for the environments of the cells shown in Figures 23 and 24.

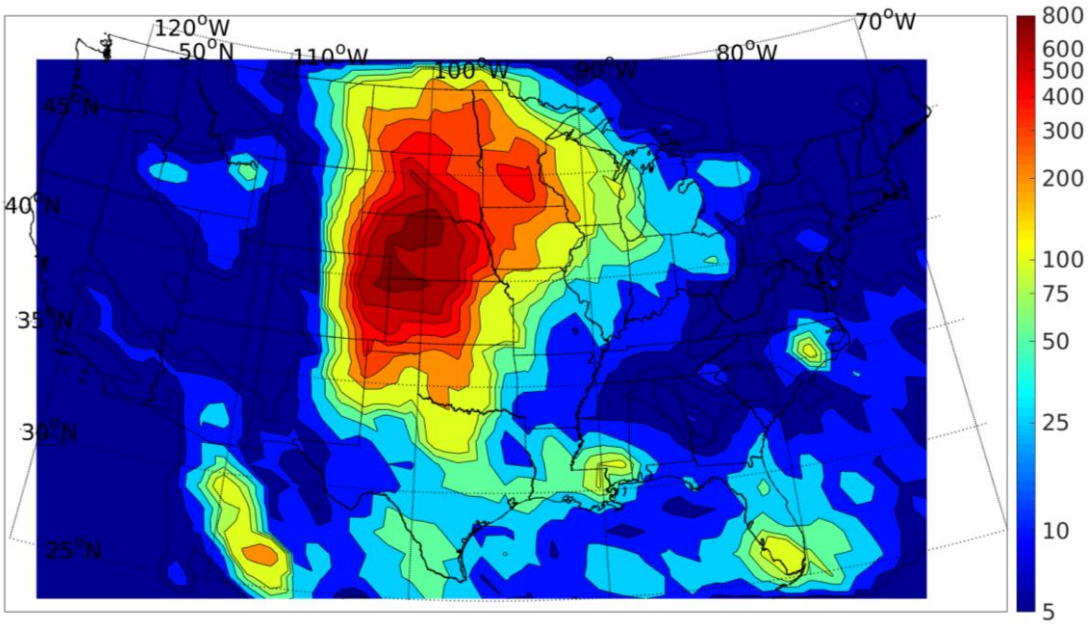

Figure 23: Same as Figure 21, except counts are for the reduced dataset used in this study.

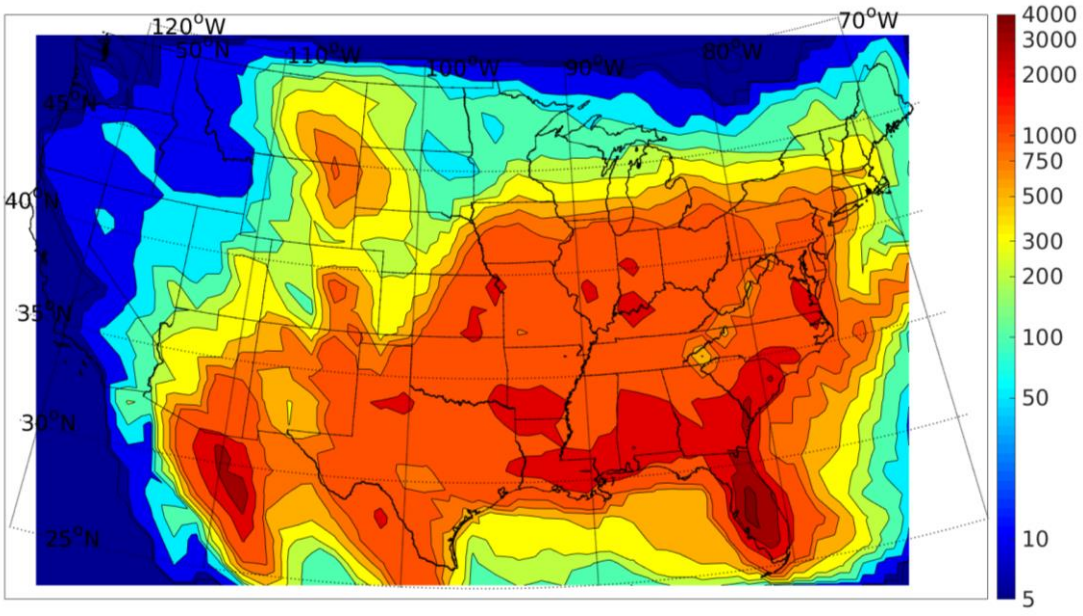

Figure 24: Same as Figure 22, except counts are for the reduced dataset used in this study.

Most previous studies of regions containing the larger +CG percentages or containing storms with significant, but smaller, +CG thresholds have found cases mainly in the central CONUS, and regions containing large -CG percentages have been found mainly in Gulf Coast states (e.g., Knapp 1994; Boccippio et al. 2001; Orville et al. 2002; Carey and Buffalo 2007). The storms with large CG flash rates and large -CG percentages in Figures 22 and 24 are consistent with the larger -CG percentages, -CG densities, and total CG densities found in Gulf Coast states by these previous studies and by many others, including Cooray (2015). Figures 7-21 and 23 show that storm cells with high flash rates and high percentages of +CG flashes can also occur well outside of the central CONUS identified, for example, by Knapp (1994), Boccippio et al. (2001), and Carey and Buffalo (2007), as they occur even in parts of Mexico, Canada, and well into the Gulf of Mexico, as found also by Orville et al. (2002). The high +CG to total CG ratios found by some previous studies along the west coast are not present in our analyses, likely because storm cells there that produced higher percentages of +CG flashes had low flash rates that fall below the thresholds used in this study.

3.2 Presentation Format of Results

The results of the environmental studies of the 17 parameters listed in Section 2.4 will be presented in the same format as in Figure 25, which shows violin plots of cloud base height (CBH) values for -CG- and +CG-dominated cells for each region. Violin plots show the quartile values, much like box-and-whisker plots, but are scaled so that their areas are all equal, and the proportion of storm cells having a given range

value of CBH values is depicted by the relative width of the violin plot in that range.

Below the violin plots, the percent difference in median CBH values between the -CG- and +CG-dominated cells is given. The percent difference here is defined as:

$$\%Difference = 100(CBH_{+} - CBH\_)/CBH\_,$$

where CBH_{+} is the median CBH of the +CG-dominated cells, and CBH_{-} is the median CBH of the -CG-dominated cells, so a positive percent difference means that the +CG-dominated cells had a higher median value of CBH. The significance level of the difference in medians is also shown in Figure 25. Significance levels were calculated from two-tailed permutation tests (Wilks 2011). The null hypothesis for these tests was that the given parameter (here, CHB) of the +CG- and -CG-dominated cells had the same probability distribution function, (i.e., there was no difference in CBH between -CG- and +CG-dominated cells).

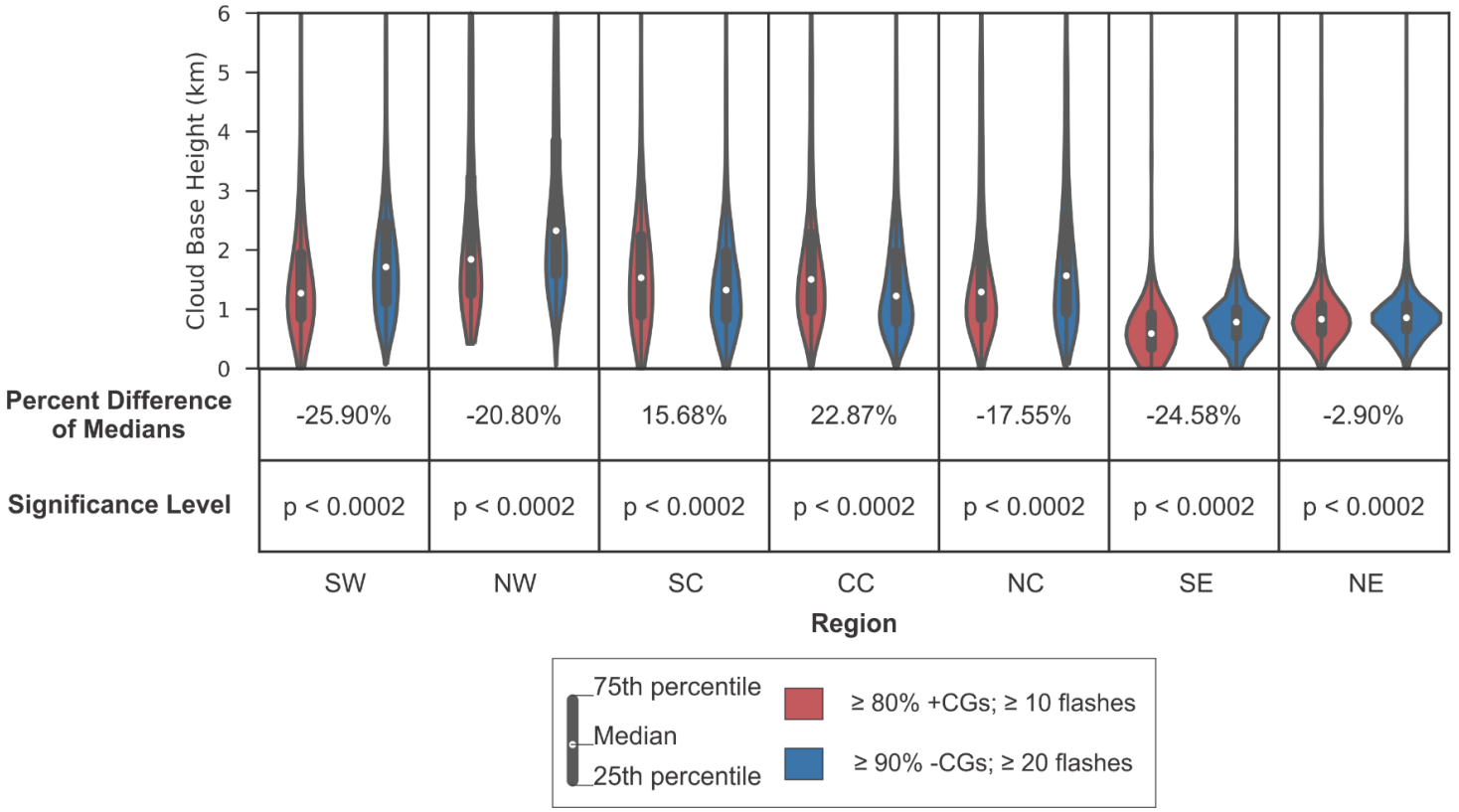

Figure 25: Violin plots of cloud base height in all seven regions are shown. The plots for the +CG-dominated cells are colored in red, and those for the -CG-dominated cells are colored in blue. The percent differences in the median cloud base height of the +CG- and -CG-dominated cells is shown, along with the significance level of those differences.

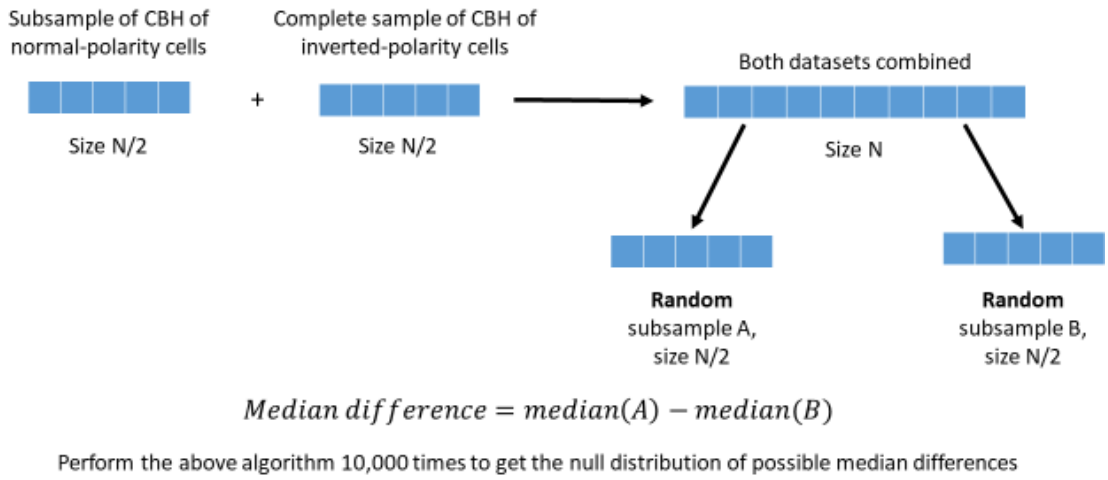

Figure 26: Procedure to construct the two random distributions and compute the difference in their two median values for a single trial. The distribution of differences from many trials is then compared with the difference in medians of the two original distributions to test the null hypothesis that the two original distributions are statistically the same, to the level of significance determined by the number of trials.

Permutation tests are valid when the principle of exchangeability applies, namely, that under the null hypothesis, data labels (i.e., "-CG-dominated" and "+CG-dominated") are arbitrary (Wilks 2011). In this case, the first step in producing a distribution for testing the null hypothesis is to produce a combined data set containing equal numbers of samples from both original distributions. (The number of cells in the smaller of the two distributions was the number used in our analysis, and it was usually the number of +CG-dominated cells). This combined data set is then randomly resampled without replacement to produce two new distributions with equal numbers of ensemble members, and the difference in the medians of these two new distributions is computed. The resampling was done 10,000 times, and the difference in the medians of

the original two ensembles is then compared with the distribution of differences in the two medians from all the trials. Figure 26 demonstrates the procedure involved in constructing the null distribution.

The significance level for the test is related to the p-value for the comparison between the actual difference in means and the distribution of differences from the trials. A p-value of $p < \alpha$ in a two-tailed permutation test meant that the actual value of the median difference of CBH fell outside of the range bounded by the n^{th} and $(100-n)^{th}$ percentiles of the null distribution, where $n = 100(\alpha/2)$. In other words, a p-value of $p < \alpha$ meant that if the null hypothesis were true that the CBHs of -CG- and +CG-dominated cells had the same probability distribution, there would be a 100α percent chance of obtaining an actual difference in median CBH at least as large as the one measured. It can then be said that the difference in median CBHs is significant at the $100(1-\alpha)$ percent level. In this study, a difference in medians is not considered statistically significant unless it is significant at the 90% level or higher. Figure 27 shows the actual difference in median CBH for the +CG-dominated and -CG-dominated cells in the central-central (CC) region, marked by the vertical red line. Note that it falls outside every single one of the 10,000 values in the null distribution. Its p-value is thus $p < 0.0002$, which means that if there truly were no difference in the CBHs of the -CG- and +CG-dominated storm cells, there would be a 0.02% chance of obtaining the measured difference in median CBH. It can therefore be said that the CBHs in the -CG-dominated cells are significantly different from those in the +CG-dominated cells.

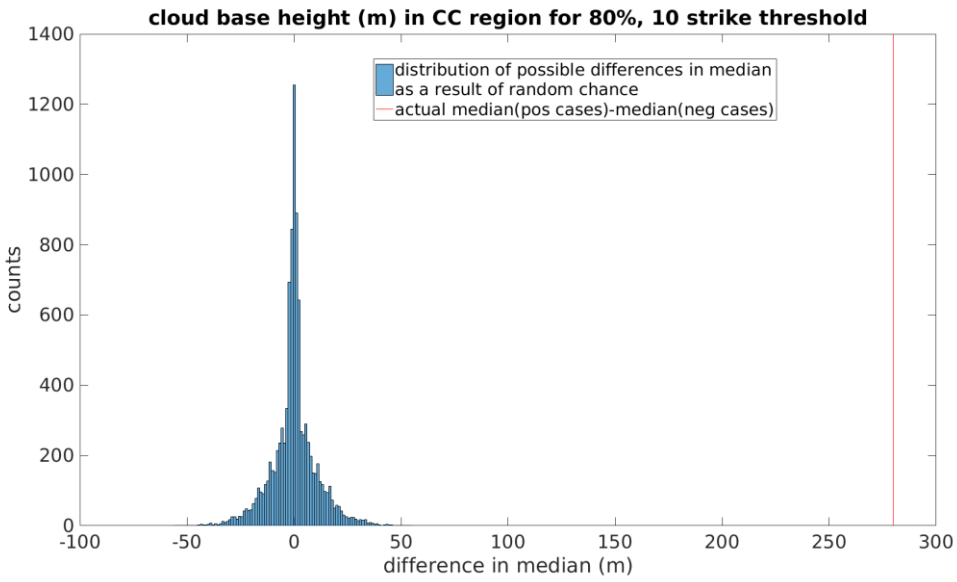

Figure 27: Actual difference in median CBH in the CC region between -CG- and +CG-dominated storm cells shown as red line and compared to the null distribution (histogram plot) of differences in median CBH arising from random chance.

Note that not all of the parameters analyzed have statistically significant differences in median values for all of the regions analyzed. For example, 0-3 km wind shear in the NW region falls well within the null distribution with a p-value of $p < 0.6904$, shown in Figure 28. This means that if there were no statistical difference in 0-3 km shear in -CG- and +CG-dominated cells in the NW region, there would be a 69.04% chance of measuring a difference in medians at least as large as the one found. Thus, the measured difference in medians suggests that there is not a statistical difference in 0-3 km shear between the environments of -CG-dominated cells and those of +CG-dominated cells in the NW region.

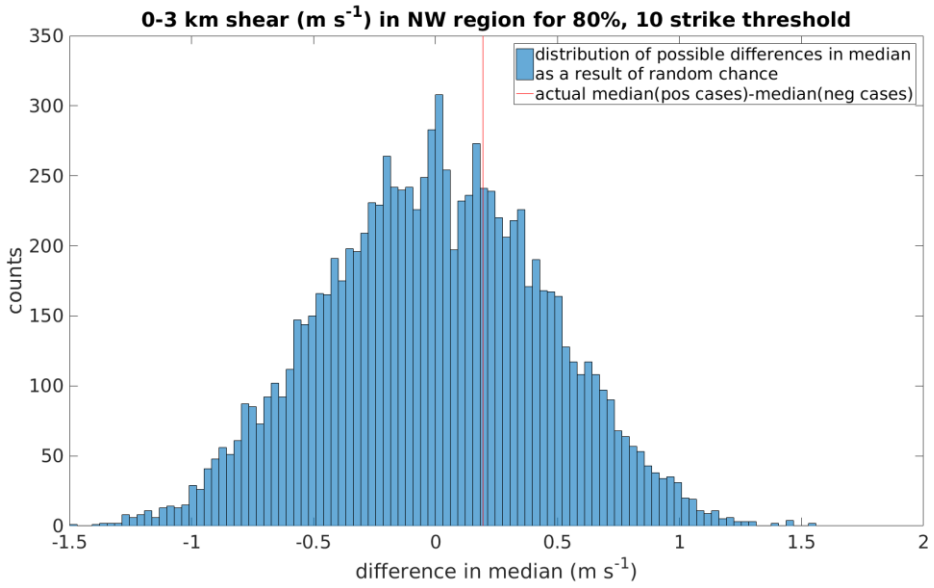

Figure 28: Same as Figure 27, except for 0-3 km shear the NW region.

3.3 Difference in Moisture Parameters between -CG- and +CG-Dominated Storms

The four moisture parameters analyzed in this study are cloud base height (CBH), warm cloud depth (WCD), dew point depression (DPD), and precipitable water (PWAT). Their characteristics in different regions and for +CG- and -CG-dominated cells are discussed in the following subsections. Most previous studies of the environments conducive to inverted-polarity storms have focused on the CC region (e.g., MacGorman et al. 2005; Lang and Rutledge 2011) because that is the region in which Lightning Mapping Array observations and electric field soundings had identified these storms. We and other studies hypothesize that a higher cloud base height, shallower warm cloud depth, greater dew point depression, and lower precipitable water allow greater supercooled liquid water contents (SLWCs) in the

thunderstorm updraft, making conditions more favorable for the formation of inverted-polarity storms. This study will focus on both the CC region and the NC region because these regions contain the majority of +CG-dominated cell observations although other regions also will be analyzed.

3.3.1 Cloud Base Height

CBH is believed to increase SLWC in the updraft by decreasing the WCD (and therefore the warm cloud residence time) and also allowing broader, stronger updrafts. Since the water content is less diluted by dry-air entrainment in the updraft core of broader updrafts, more water content is able to be transported to the mixed-phase region. Figure 25 shows the distribution of CBHs in each region and for -CG- and +CG-dominated storm cells. It also shows the percent difference in median CBH between -CG- and +CG-dominated storm cells and its accompanying significance level, for all regions. For all regions, CBH took on a unimodal distribution that was right-skewed (the longest tail contained the highest values). The mode of the distribution was below the median in all regions except for the SE and NE regions, where it was approximately at the median level. In the CC region, +CG-dominated cells had a median CBH that was 23% higher than that for the -CG-dominated cells, consistent with the hypothesis that higher CBHs lead to higher SLWCs. The SC region is similar to the CC region in that its +CG-dominated cells had a median CBH that was 16% higher than that in its -CG-dominated cells.

However, the SC and CC regions were the only regions with higher median CBHs in the +CG-dominated storms than in the -CG-dominated storms. It is

particularly significant that this relationship did not hold in the NC region, which had the second-highest sample size of high-flash-rate, high-percentage +CG flash cells. There, +CG-dominated cells actually had a median CBH that was 18% lower. The region containing cells with the highest median CBH was the NW region, where the +CG-dominated cells had a median CBH 21% lower than that of the -CG-dominated cells. The region in which the median CBHs for -CG- and +CG-dominated cells had the largest percent difference from one another was the SW region (+CG-dominated cells had a 26% lower median value). The fact that CBH was not higher in +CG-dominated storms in so many regions suggests that CBH is not the only important factor in determining a storm's polarity. All regions had significant differences in median CBH with $p < 0.0002$ and were thus significant at the 99.98% level.

3.3.2 Warm Cloud Depth

A shallower WCD is believed to be important for allowing higher SLWCs by decreasing the warm cloud residence time of parcels ascending in the updraft. Figure 29 shows the characteristics of WCD in -CG- and +CG-dominated cells for all regions. A negative value of WCD meant that the cloud base was above the freezing level. The distribution of WCD was left-skewed (the longest tail contained the lowest values).

The regions in which +CG-dominated cells had shallower WCDs are the SC, CC, and NE regions although the percent difference in the NE was very small. +CG-dominated cells in the CC region were found to have a median WCD that was 28% shallower than the region's -CG-dominated cells. This relationship also held for the SC region, where +CG-dominated cells had a median WCD that was 17% shallower than

that in the -CG-dominated cells.

In the remaining regions, median WCD was greater, although by very little in the SE. In all regions except for the NW region, the difference in median WCD was significant at the 99.98% level, and it was significant at the 94.1% level in the NW region. Again in the NC region, which contained many of the +CG-dominated storm cells, +CG-dominated cells had a median WCD that was 19% deeper than -CG-dominated cells. The NW region, which had the shallowest median WCDs for +CG-dominated storms, also had even shallower median WCDs for -CG-dominated storms. The SW region was the region in which WCD served as the best discriminator between -CG- and +CG-dominated cells, and +CG-dominated cells had a median WCD that was 34% deeper than that in -CG-dominated cells. The fact that median WCDs for +CG-dominated storms was greater than the median for -CG-dominated storms in a majority of regions suggests that WCD is not the only factor that is important in determining the polarity of storm charge distributions.

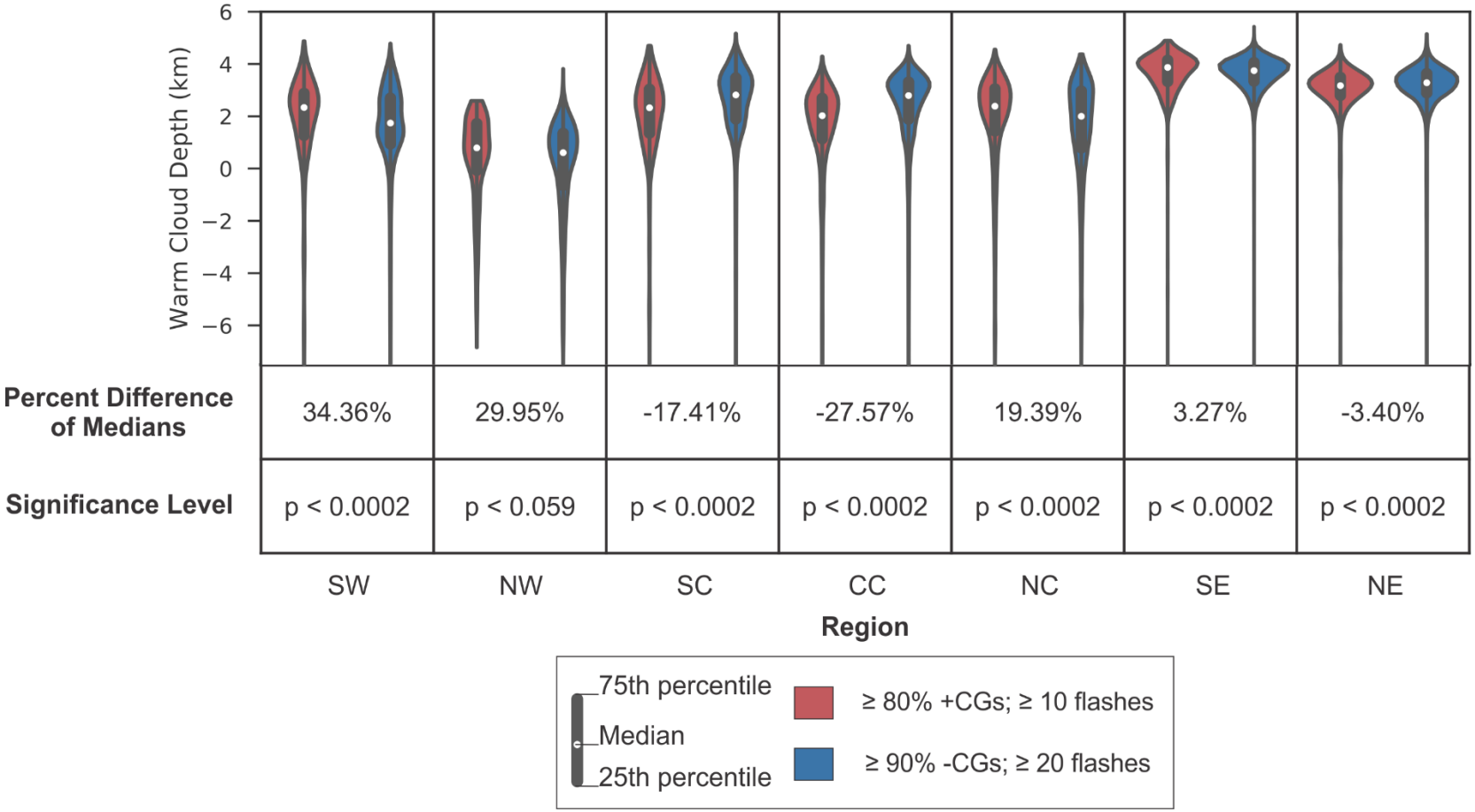

Figure 29: Same as Figure 25, but for warm cloud depth.

3.3.3 Dew Point Depression

Several early studies found that supercell storms dominated by +CG flashes tended to occur in drier subcloud regions with larger DPDs (Macgorman and Burgess 1994; Knapp 1994; Smith et al. 2000), so our environmental analysis of DPD was intended to test whether this is generally true. Figure 30 shows the characteristics DPD measured 2 m above ground level in the environments of -CG- and +CG-dominated cells for all regions. The difference between the median DPD of +CG-dominated cells and that of -CG-dominated cells was significant at the 96.34% level in the NW region, at the 99.86% level in the SC region, and at the 99.98% level in all other regions. All the distributions were skewed toward larger values.

As for WCD, the only regions in which the percent difference in median DPD was consistent with the above hypothesized relationship of DPD between the two types of cells were the CC, SC, and NE regions, and the percent difference in the NE region was small. The maximum percent difference was for the CC region (35%). In all other regions, DPD was larger in -CG-dominated storm cells, a fact which argues against larger DPD being essential for producing +CG-dominated storms. The environments of cells in the SE and the NE regions tended to have the lowest DPDs overall, likely because of strong moisture flux from the Gulf of Mexico and the Atlantic Ocean.

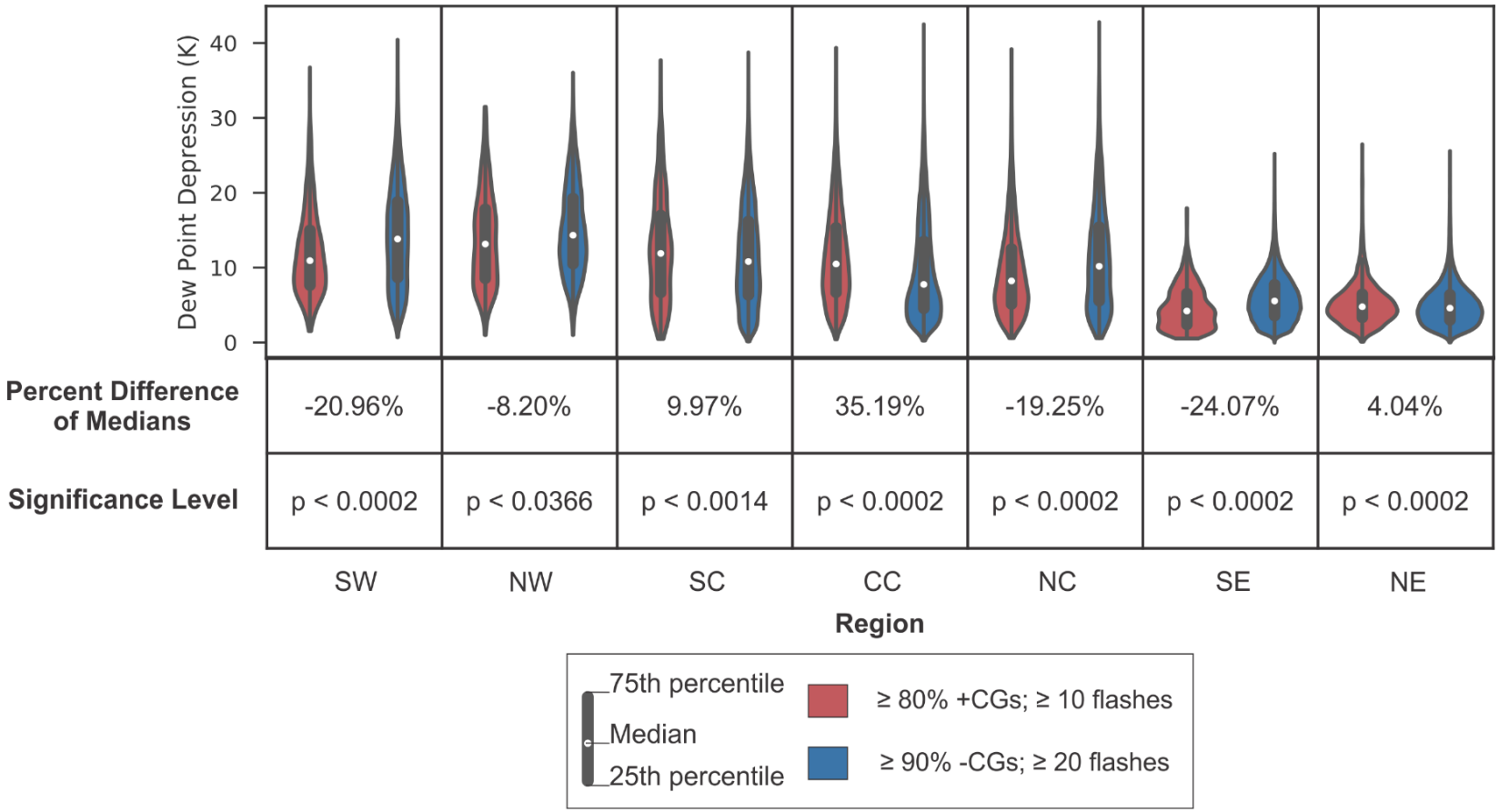

Figure 30: Same as Figure 25, but for dew point depression.

3.3.4 Precipitable Water

As for the other moisture parameters, we analyzed PWAT because Carey and Buffalo (2007) suggested that lower PWAT maximizes SLWC by reducing water loading in the updraft, which would suppress the collision-coalescence processes that act to deplete the smaller cloud droplets that contribute to the SLWC and reduce the entrainment of dry air, allowing more liquid water to ascend into the mixed-phase region. We would thus expect a tendency for +CG-dominated cells to have lower PWAT. Figure 31 shows the characteristics of PWAT in -CG- and +CG-dominated cells for all regions.

Unlike the distributions of the other moisture parameters, the distributions of PWAT didn't show a marked preference towards being right-skewed or left-skewed. Overall, the percent differences in the median PWATs between +CG-dominated cells and -CG-dominated cells tended to be smaller than for the other moisture parameters, but the differences in the medians themselves were significant at the 99.98% level in all regions except the SW region, in which the difference was significant at the 98.24% level, and in the NW region, in which the medians were not significantly different. Of those regions with significant differences, the medians of all but two regions had less PWAT for +CG-dominated storms than for -CG-dominated storms, with the CC region and SC region having the largest magnitude of percent difference (22% and 16%, respectively). Thus, unlike the other moisture parameters, the median PWAT values in the majority of regions were consistent with the hypothesis that lesser amounts of PWAT tend to favor inverted-polarity cells through larger SLWCs. The only exceptions in which median PWATs were larger for +CG-dominated storms were the NC region

and the SW region, with percent differences of 6.6% and 3.4%, respectively. However, the fact that there were exceptions suggests that PWAT, like the other moisture variables, is not the only control on cell polarity. Since in the NC region, none of the four moisture parameters were able to explain the large number of +CG-dominated storm cells there, other types of environmental parameters (i.e., thermodynamic and dynamic) must be important there.

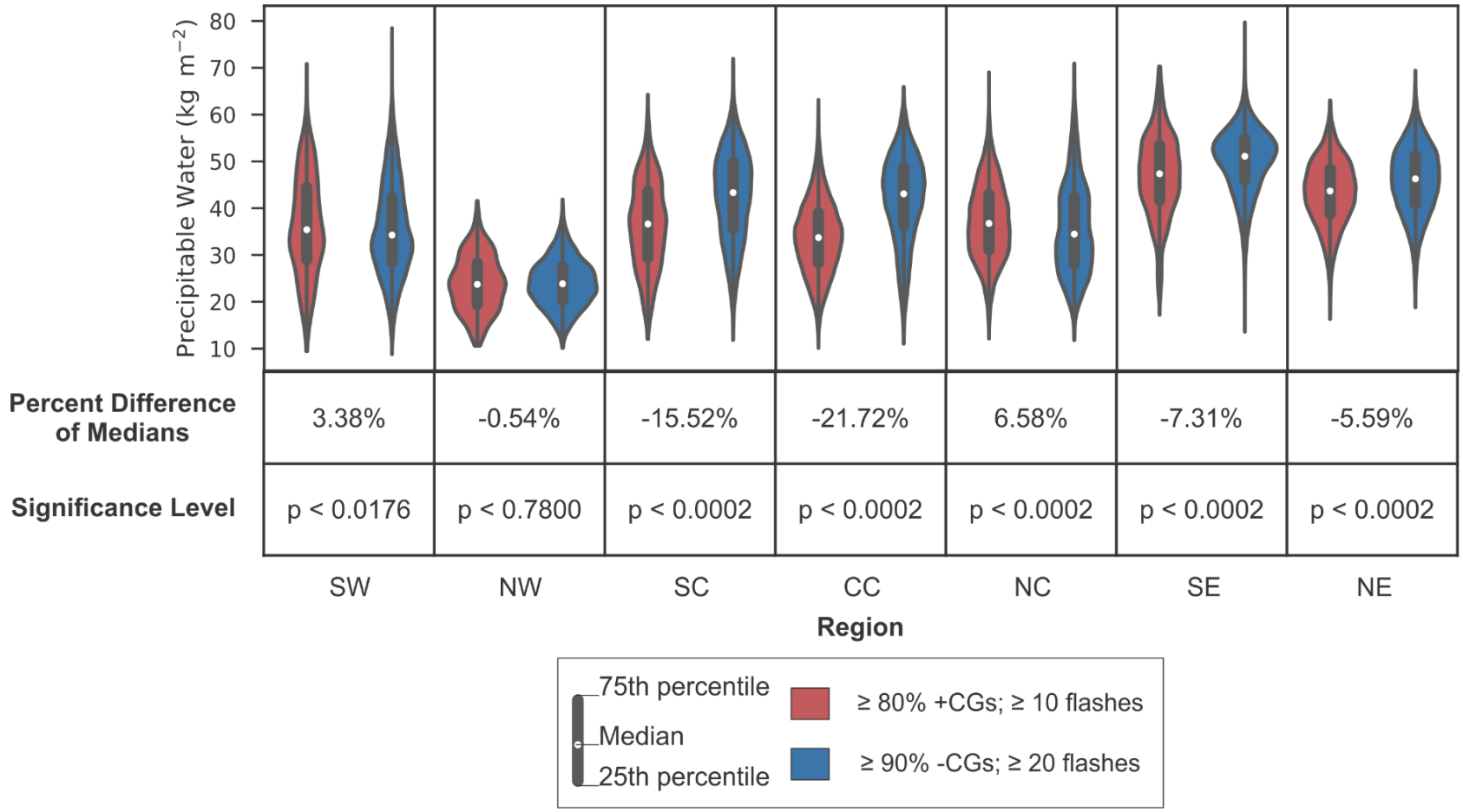

Figure 31: Same as Figure 25, but for precipitable water.

3.4 Difference in Thermodynamic Parameters between -CG- and +CG-Dominated Storms

The nine thermodynamic parameters studied are: surface equivalent potential temperature (θ_e), CAPE from the level of free convection (LFC) to the equilibrium level (EL), normalized CAPE (NCAPE) from the LFC to the EL, CAPE from the LFC to -20°C level, NCAPE from the LFC to -20°C level, CAPE from the 0°C to the -20°C level, NCAPE from the 0°C to the -20°C level, CIN, and EL. We and other studies hypothesize that higher values of CAPE, NCAPE, CIN, and EL tend to increase SLWC in the updraft region, allowing the formation of inverted-polarity cells. It is not known a priori how θ_e could affect SLWC. The characteristics of these parameters in different regions and for +CG- and -CG-dominated cells are discussed in the following subsections. Again, special focus will be placed on the CC region and NC regions.

3.4.1 Surface Equivalent Potential Temperature

Smith et al. (2000) found on the days they analyzed that θ_e was smaller in the environment of +CG-dominated storms than in the environment of -CG-dominated storms. We analyze θ_e without knowing a priori how it could potentially influence the SLWC in the mixed-phase region. Figure 32 shows the characteristics of surface θ_e in -CG- and +CG-dominated cells for all regions. There was no obvious, consistent skewing of the distributions to either side.

Compared to all of the other variables analyzed in this study, θ_e was the worst discriminator between environments conducive to +CG-dominated cells and those conducive to -CG-dominated cells. Although the difference in medians was statistically

significant at the 99.98% level in all regions except the NW region, the magnitude of the percent difference was at most 1.1% for all regions. To the extent the differences have meaning, the percent differences in medians for the CC, SC, and SE regions were consistent with the observations by Smith et al. (2000), but that was not true of most of the other regions. High significance levels were possible here even though the percent differences in medians were very small because the distributions tended to have a larger fraction of their values close to the median.

3.4.2 CAPE from the LFC to EL

The hypothesis being tested here is that, even if warm cloud depths were larger than optimal values, greater updraft speeds would reduce the warm cloud residence time of an ascending air parcel and so might enhance the amount of SLWC enough to produce an inverted-polarity charge distribution. Additionally, greater updraft speeds could allow higher supersaturation, which could activate a greater number of smaller droplets. This would suppress collision-coalescence, allowing more cloud droplets and therefore more SLWC in the mixed-phase region. Figure 33 shows the characteristics of LFC to EL CAPE in -CG- and +CG-dominated cells for all regions. Note that most of the distributions were unimodal or approximately unimodal, and all were skewed to the right, with tails toward larger values of LFC to EL CAPE. The difference in medians was significant at the 99.98% level in all regions, except in the NW region (significant at the 92.84% level), and in the SE region, where it was not significant.

In all regions except the CC and SE regions, the +CG-dominated cells storms had significantly larger median values of LFC to EL CAPE than the -CG-dominated

cells had, consistent with the above hypothesis. The percent difference in medians was especially large in the SW and NC regions, which had the largest percent differences in median values (88% and 77%, respectively). Thus, this parameter was a better predictor of the polarity of a given storm cell than the moisture parameters presented in previous sections, which mostly had an unfavorable impact on SLWC outside of the CC and SC regions, according to the hypothesized role of those moisture properties. The reverse was true of the CC region: its environment had among the most favorable moisture properties, but it tended to have unfavorable LFC to EL CAPE, as the median value in +CG-dominated cells was less than that in -CG-dominated storms.

For the parameters considered so far at least, the distribution of no one environmental parameter was sufficient to discriminate between +CG-dominated and -CG-dominated cells (which are likely inverted- and normal-polarity cells, respectively) in all regions, and the distributions had considerable overlap between them for all the parameters. However, it appears that favorable LFC to EL CAPE can compensate for unfavorable microphysics and vice versa. The additional LFC to EL CAPE needed to produce +CG-dominated storms appeared to be especially great in the SW and NC regions. The environment of cells in the NW region tended to have the lowest LFC to EL CAPE, and this may explain why the NW region had the fewest observations of cells dominated by either polarity of CGs. +CG-dominated cells in the NE region had the highest median LFC to EL CAPE of all of the regions.

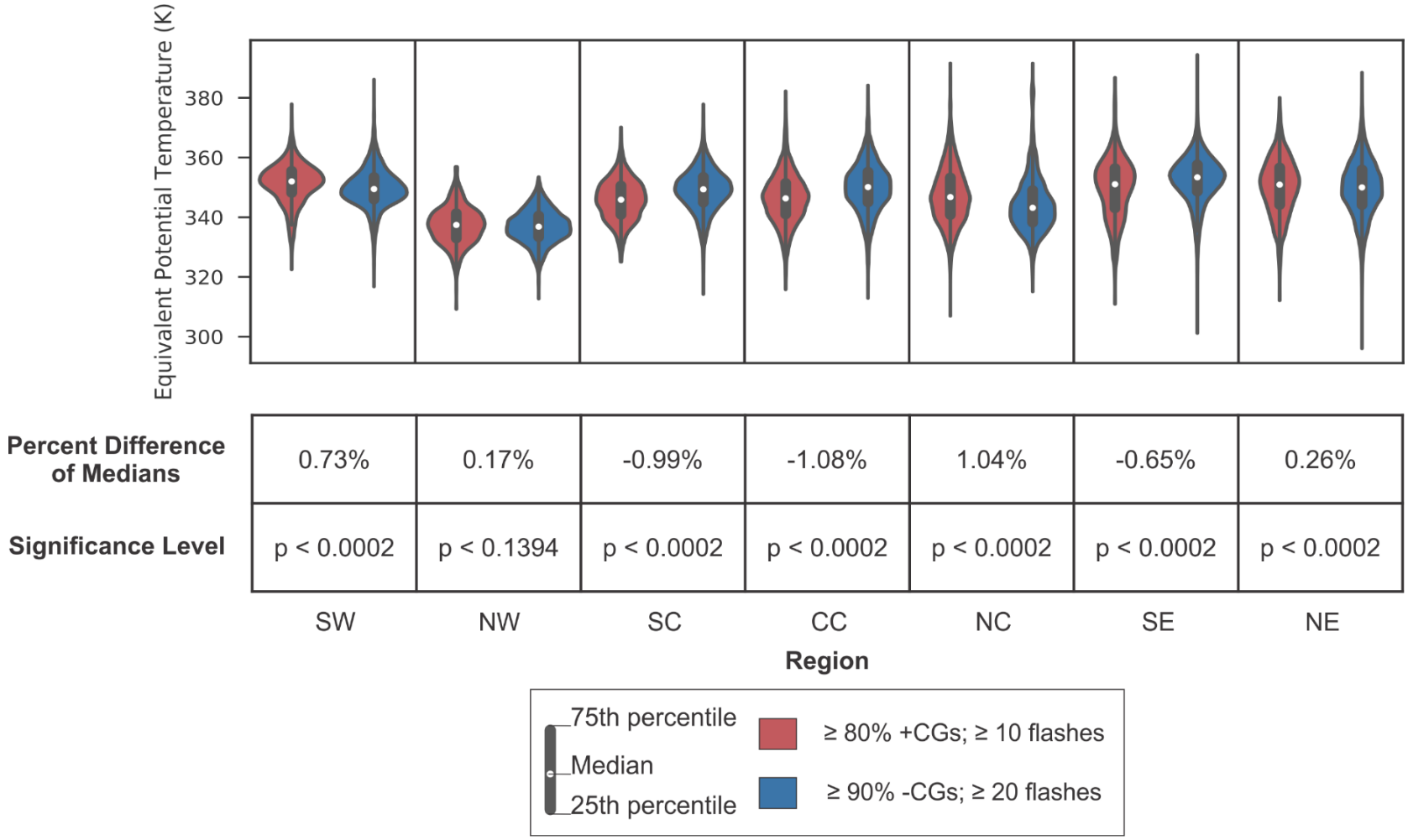

Figure 32: Same as Figure 25, but for θ_e.

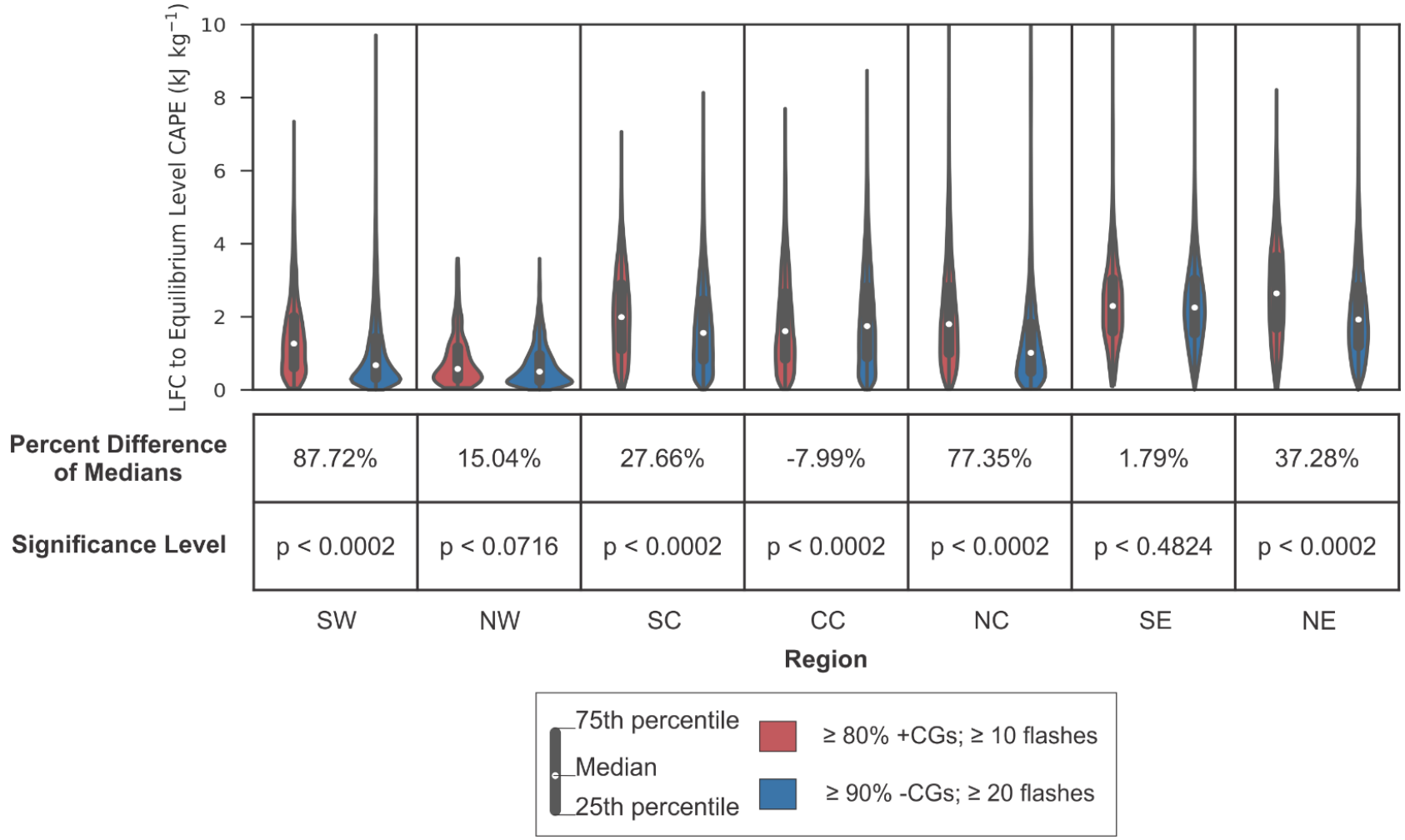

Figure 33: Same as Figure 25, but for LFC to EL CAPE.

3.4.3 NCAPE from the LFC to EL

As in the case of LFC to EL CAPE, higher values of LFC to EL NCAPE are believed to lead to higher SLWCs by increasing updraft speeds, which would shorten the warm cloud residence time and increase supersaturation. Additionally, we analyze NCAPE to determine whether or not updraft acceleration may play a role. Figure 34 shows the characteristics of LFC to EL NCAPE in -CG-dominated and +CG-dominated cells for all regions. All of the distributions were right-skewed, and all the differences in medians were significant at the 99.28% level or higher, except in the NW region, where the difference in medians was not significant. In all regions, LFC to EL NCAPE for +CG-dominated storm cells was larger than that for -CG-dominated storm cells.

For all regions except the CC region, the same storm class was favored as for LFC to EL CAPE although the percent differences were smaller for the majority of regions. In the CC region, the favored dominant polarity actually switched, with median LFC to EL CAPE being larger for -CG-dominated cells and median LFC to EL NCAPE being larger for +CG-dominated cells. However, the percent difference for the medians of both parameters was relatively small. The region in which LFC to EL NCAPE had the largest percent difference between the two types of cells was the SW region (57%), as it was in the case of LFC to EL CAPE. As in the case of LFC to EL CAPE, LFC to EL NCAPE is the largest for the +CG-dominated cells in the NE region.

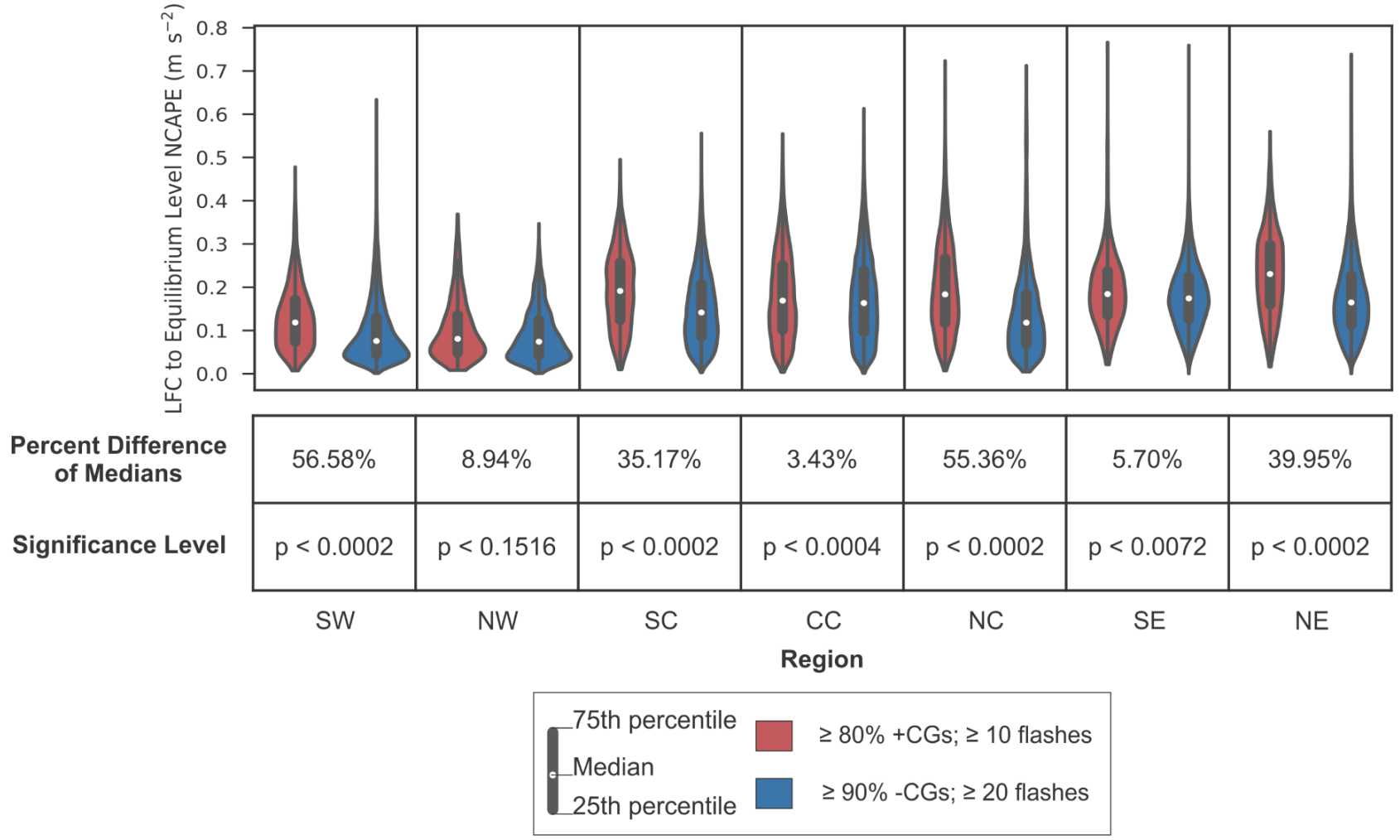

Figure 34: Same as Figure 25, but for LFC to EL NCAPE.

3.4.4 CAPE from the LFC to -20°C

By studying CAPE over the layer from the LFC to -20°C, we sought to analyze the effect of updraft speed in the middle of the mixed-phase region on SLWC, and therefore, storm cell polarity. Figure 35 shows the characteristics of LFC to -20°C CAPE in -CG- and +CG-dominated cells for all regions. As in the case of LFC to EL CAPE and NCAPE, the distributions for LFC to -20°C CAPE were all right-skewed. . All the medians were statistically different at the 99.98% level except in the NW region, in which the level of statistical significance was 98.78%, and in the SE region, in which the median differences were not statistically different. The LFC to -20°C CAPE was larger for +CG-dominated cells in all regions except for the CC and SE regions. In the CC region, the median LFC to -20°C CAPE for +CG-dominated cells was 17% smaller than that for -CG-dominated cells.

Once again, it appears clear that no one environmental parameter clearly leads to +CG-dominated or -CG-dominated cells (and therefore, normal- or inverted-polarity cells). In the CC region, LFC to -20°C CAPE was unfavorable, but the moisture parameters considered in previous sections tended to be favorable. On the other hand, the percent difference in median LFC to -20°C CAPE was largest by far for the NC and SW regions, so this parameter was a good discriminator between the two categories of cells there, but the median moisture parameters in those regions tended to be unfavorable for +CG-dominated cells. Furthermore, the magnitude of the median LFC to -20°C CAPE was insufficient in itself, as the largest median values of both categories of storms occurred in the NE and SE regions, but these regions did not have the greatest number of +CG-dominated cells.

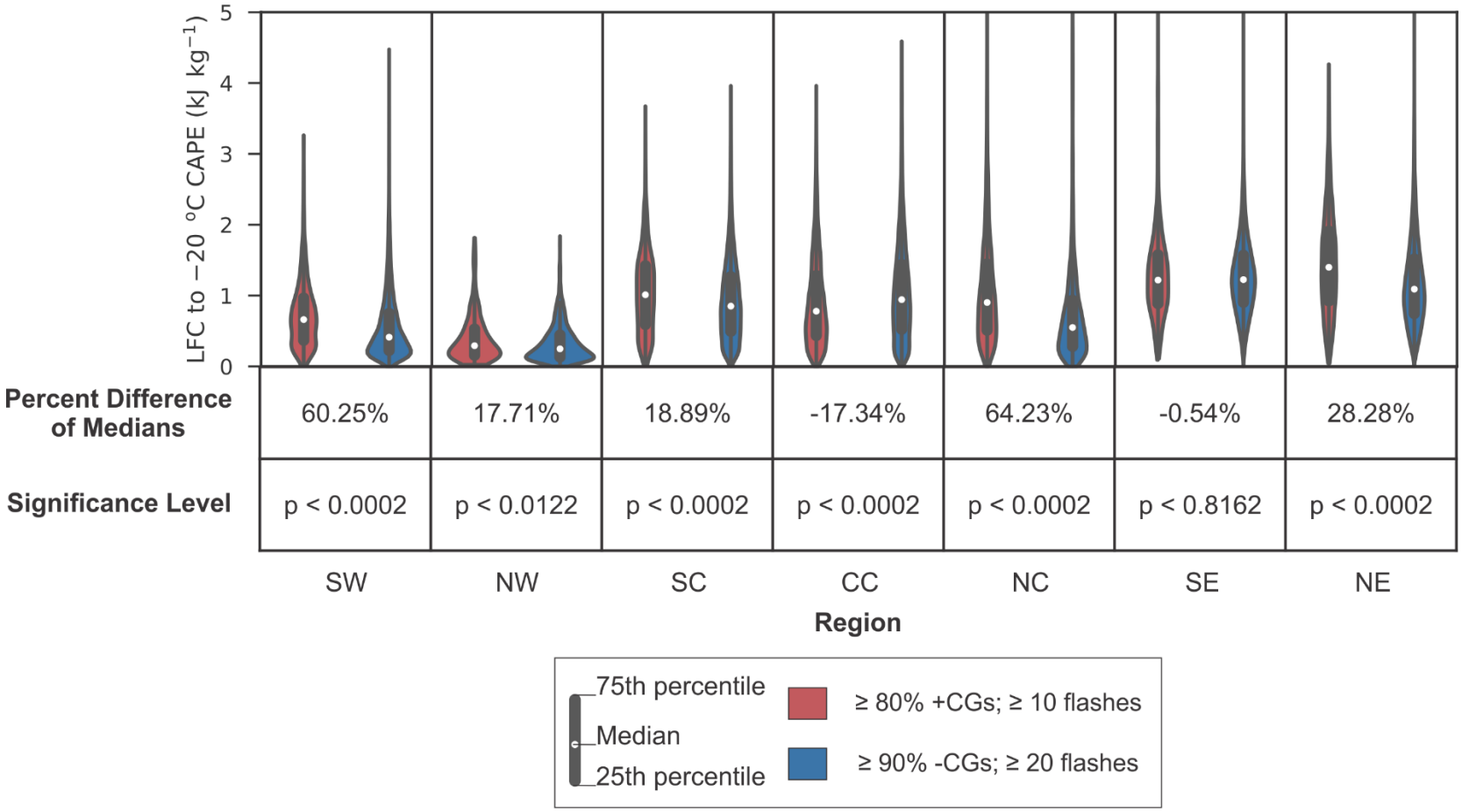

Figure 35: Same as Figure 25, but for LFC to -20°C CAPE.

3.4.5 NCAPE from the LFC to -20°C

We analyzed NCAPE over the layer from the LFC to -20°C because we sought to analyze the effect of updraft acceleration from the lower levels up through the middle of the mixed-phase region. We hypothesized that greater LFC to -20°C NCAPE would allow greater updraft accelerations and therefore faster updrafts, decreasing the warm cloud residence time and increasing supersaturation, thereby increasing the SLWC in the updraft. Figure 36 shows the characteristics of LFC to -20°C NCAPE in +CG-dominated and -CG-dominated cells for all regions. As was the case for the other CAPE variables presented above, all of the distributions were right-skewed. The difference in medians was statistically significant only in the SW, SC, NC, and NE regions, and the median values were larger for +CG-dominated storms in all of these regions.

The largest percent differences in median LFC to -20°C NCAPE were in the NC and SW regions (45% and 44%, respectively), where moisture parameters were typically unfavorable for +CG-dominated storms. The regions in which the difference in medians was not statistically significant included the CC region, which had the largest number of storms in which +CGs dominated frequent CG flash activity. The fact that the SE and NE regions had among the largest median values of LFC to -20°C NCAPE, but did not have the greatest number of +CG-dominated storms, again suggests that it is not the value of this parameter itself that is important, but rather its role as part of the mixture of important environmental parameters affecting CG flash production (and likely, storm polarity).

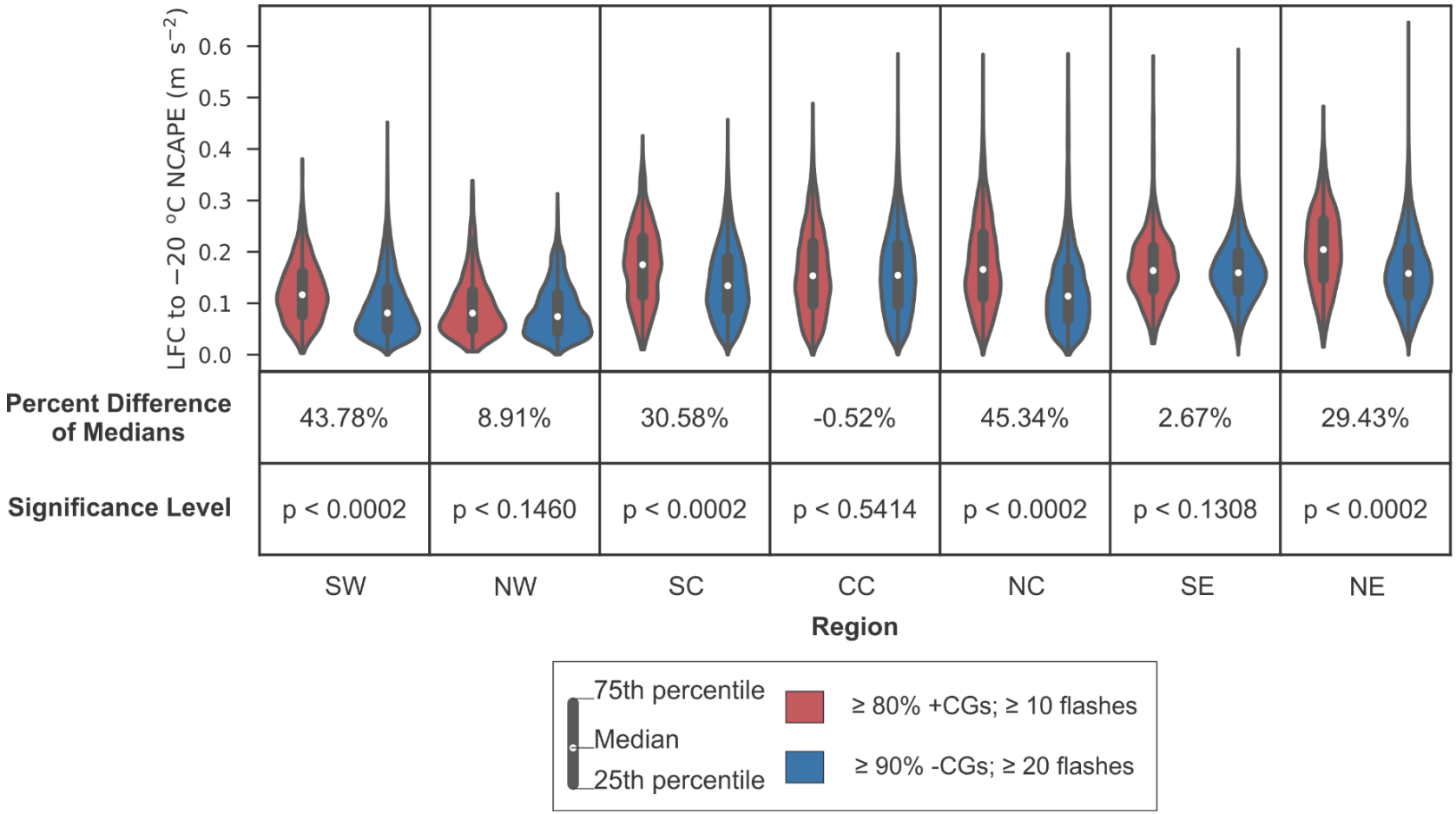

Figure 36: Same as Figure 25, but for LFC to -20°C NCAPE.

3.4.6 CAPE from 0°C to -20°C

We chose to analyze 0°C to -20°C CAPE in order to evaluate the importance of CAPE solely in the lower part of the mixed-phase region, where the most collisional charging occurs. As for the other CAPE parameters, we hypothesized that greater 0°C to -20°C CAPE would tend to support stronger updrafts, increasing the SLWC in the mixed-phase region of the updraft by decreasing the warm cloud residence time and increasing supersaturation. Figure 37 shows the characteristics of 0°C to -20°C CAPE in -CG- and +CG-dominated cells for all regions. As was the case for the other CAPE variables presented above, all of the distributions were right-skewed. All the differences in median values were significant at the 99.98% level, except for the difference in the NW region, which was significant at the 98.84% level, and that in the SE region, which was significant at the 99.38% level.

As was true of CAPE from the LFC to the EL, +CG-dominated cells in all regions except the CC region were associated with higher median values of CAPE in the 0°C to -20°C layer, consistent with the above hypothesis. In the CC region, -CG-dominated cells had a larger median value of CAPE in this layer, contrary to what this hypothesis predicts, so again, it suggests that 0°C to -20°C CAPE is not the only parameter affecting storm cell polarity. However the percent difference was small, only -4.0%. The largest percent difference in medians again occurred in the NC region. The highest median value of 0°C to -20°C CAPE was for +CG-dominated cells in the NE region, and the smallest median value was in the NW region.

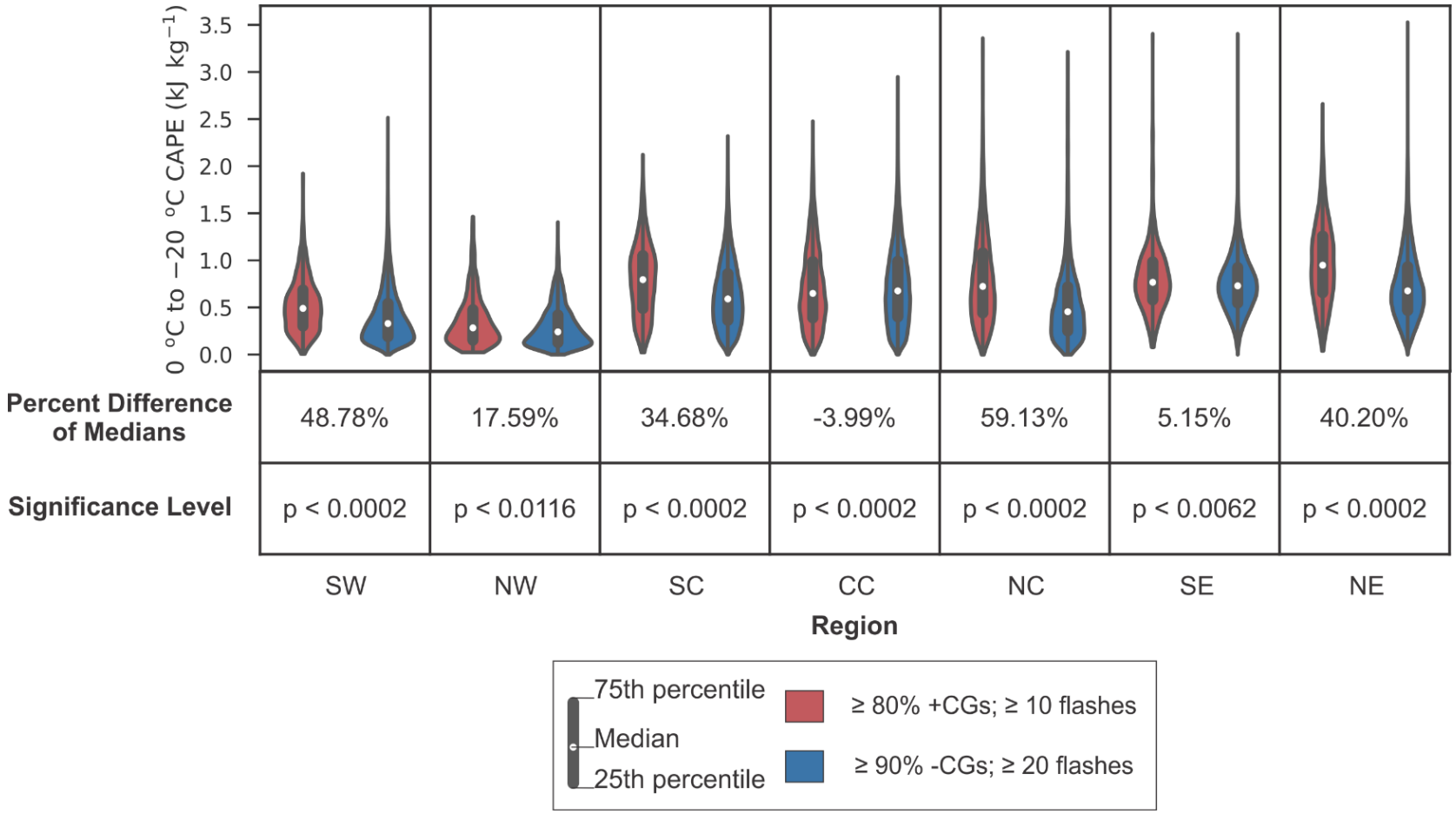

Figure 37: Same as Figure 25, but for 0°C to -20°C CAPE.

3.4.7 NCAPE from 0°C to -20°C

We chose to analyze 0°C to -20°C NCAPE in order to evaluate the effect of updraft acceleration in the lower part of the mixed-phase region on charge structure. We hypothesized that greater updraft accelerations in the lower part of the mixed-phase region, where most collisional charging occurs, would allow faster updrafts, decreasing the warm cloud residence time and increasing supersaturation, which would increase the SLWC in the mixed-phase region. Figure 38 shows the characteristics of 0°C to -20°C NCAPE in -CG- and +CG-dominated cells for all regions. All the differences in median values between +CG-dominated and -CG-dominated cells were significant to at least the 98.98% level. The values of percent difference and the pattern in relative values from one region to another for NCAPE in this layer were very similar to those made in the previous section for CAPE in this layer, so the statements and inferences made in the previous section apply equally well to this section and will not be repeated here.

3.4.8 CIN

We analyzed the magnitude of CIN because environments with higher |CIN| require air parcels near the surface to be heated more before they are able to ascend than those in environments with lower |CIN|. Assuming the same temperature profile higher up in both cases, the hotter air parcels will ascend faster, thereby allowing faster updrafts, shorter warm cloud residence times, and greater supersaturations. As explained in Section 1.6, this could allow for higher SLWC in the mixed-phase region.

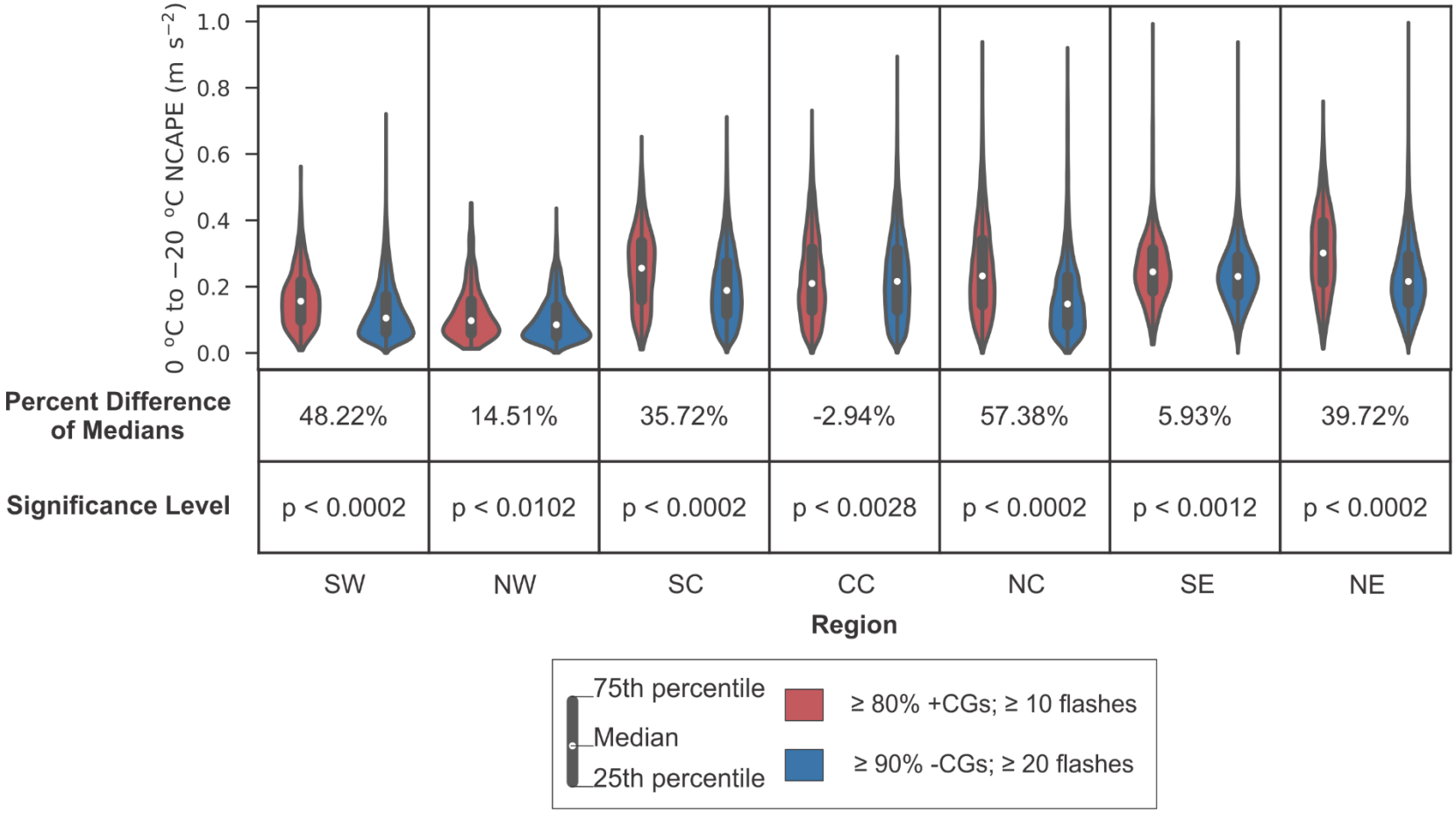

Figure 38: Same as Figure 25, but for 0°C to -20°C NCAPE.

Figure 39 shows the characteristics of the magnitude of CIN in -CG- and +CG-dominated cells for all regions. The median values of |CIN| for +CG-dominated and -CG-dominated cells were significantly different in all regions at the 99.96% level or higher except in the SW region, where they were not significantly different. All the distributions in all regions were unimodal and right-skewed. The median |CIN| of +CG-dominated cells was greater than that for -CG-dominated cells in the SC, CC, SE, and NE regions, with percent differences of 68%, 44%, 31%, and 32%, respectively. Thus, |CIN| in these regions was consistent with its hypothesized contribution to producing +CG-dominated (and therefore, inverted-polarity) cells. However, the hypothesis failed in the SW, NW, and NC regions, where the differences were either not significant or median |CIN| was greater for -CG-dominated cells, so other environmental parameters were needed to produce +CG-dominated (and therefore, likely inverted-polarity) cells in those regions.

3.4.9 Equilibrium Level

We analyzed the EL because of its influence on updraft speed. Storm cells with higher ELs provide a greater depth for integrating potential buoyant energy and parcel acceleration caused by the amount by which the temperature along the moist adiabat exceeds the environmental temperature. Because it provides only a greater depth over which to accumulate CAPE, which depends also on the amount of temperature excess, EL likely will have a subtler influence on updraft speed than CAPE itself, but analyzing this parameter is useful in isolating one of the influences on CAPE. As noted in Section 1.6, stronger updrafts would decrease the warm cloud residence time, which would

allow for higher SLWC in the mixed-phase region.

Figure 40 shows the characteristics of the EL in -CG-dominated and +CG-dominated cells for all regions. The direction of skew varied more for this parameter than for other parameters we have considered thus far. The differences in median were significant at the 99.98% level in all regions except for the NW and NE regions, where the differences were not significant. Overall, the percent differences in medians of +CG-dominated and -CG-dominated cells were relatively small, consistent with it having a more subtle influence on updraft speed than the various layers of CAPE. The only regions in which +CG-dominated cells had statistically significantly higher median ELs than -CG-dominated cells were the SW and NC regions. In the CC, SC, and SE regions, the median ELs were lower for +CG-dominated cells than for -CG-dominated cells, so to the extent EL affects the dominant CG polarity (and therefore, charge structure), the effect was negative in these regions, and other environmental parameters likely compensated for it. As for several of the CAPE-related parameters, the NW region had the smallest median EL, due to its tendency to have a drier subcloud environment than the regions farther east and a lower tropopause than the regions farther south. The SE had the largest median ELs, due to its tendency to have a more moist subcloud layer than regions farther west and a higher tropopause than regions farther north.

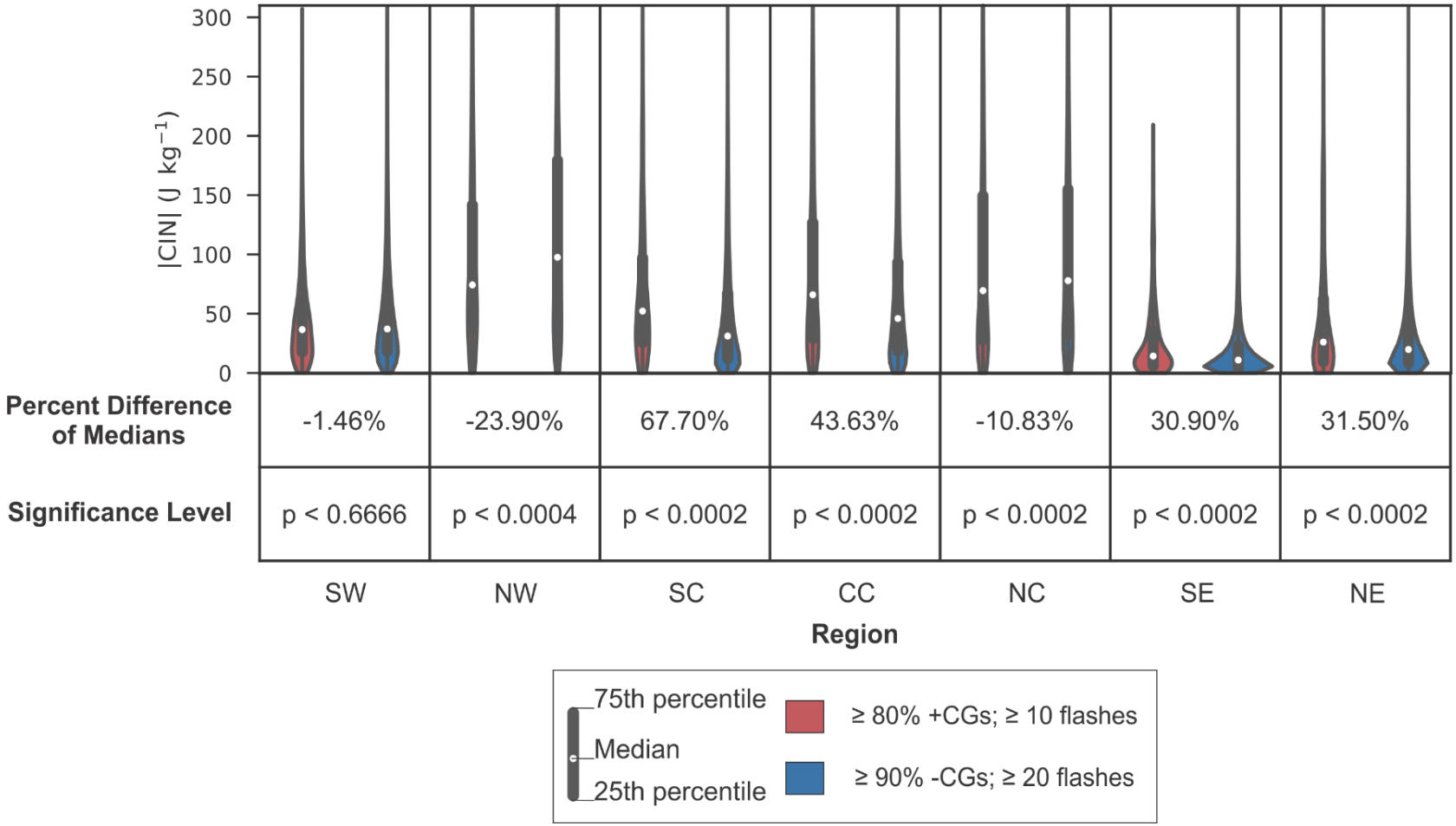

Figure 39: Same as Figure 25, but for |CIN|.

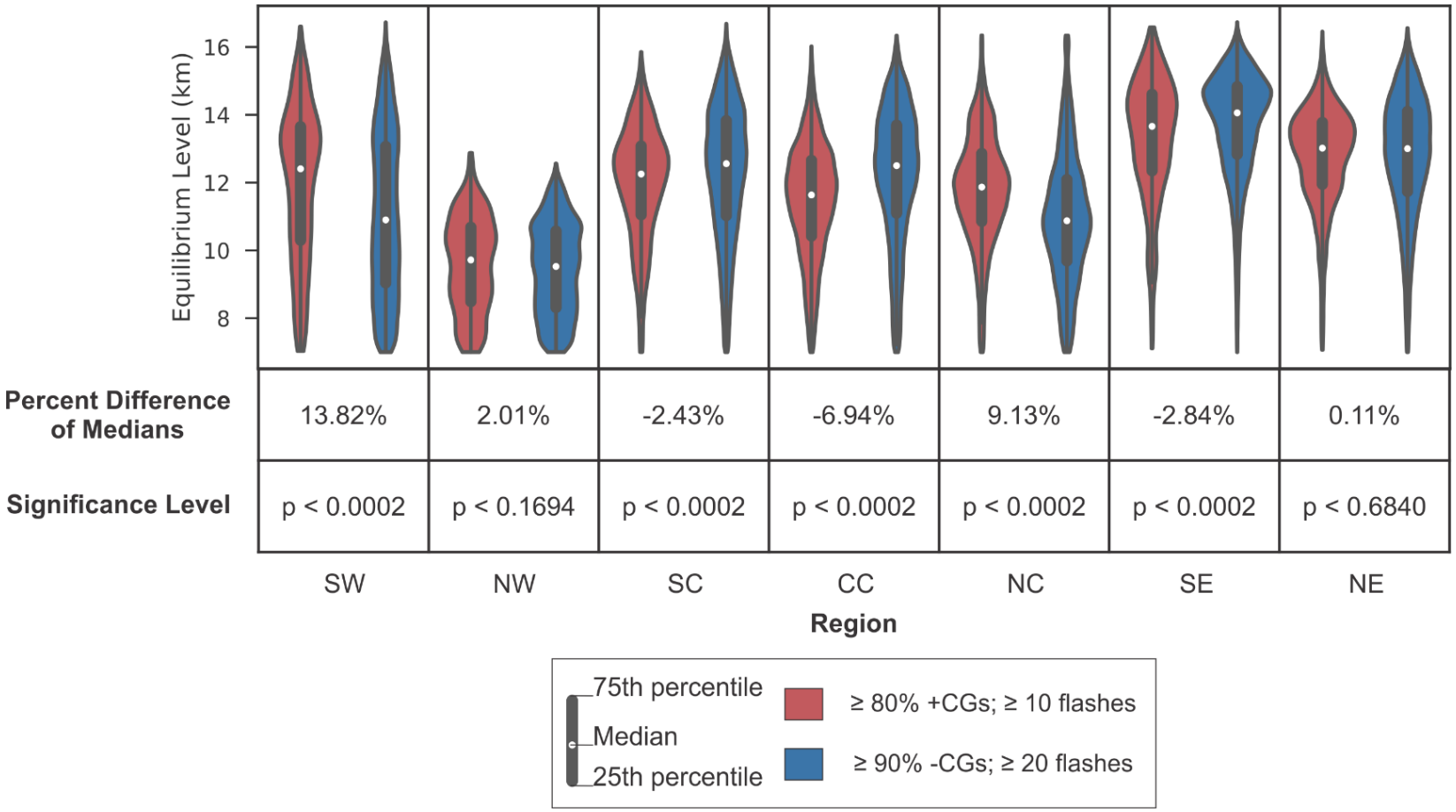

Figure 40: Same as Figure 25, but for Equilibrium Level.

3.5 Difference in Dynamic Parameters between -CG- and +CG-Dominated Storms

The four dynamic parameters studied are: 0-3 km shear, 0-6 km shear, storm-relative wind speed at the equilibrium level, and storm-relative helicity (SRH). Their characteristics in different regions and for +CG- and -CG-dominated cells are shown below. We hypothesized that greater 0-3 and 0-6 km shear, greater storm-relative wind speed at the EL, and greater SRH would allow greater SLWCs in the mixed-phase region, which is conducive to the formation of inverted-polarity storms. As noted in the Introduction, the CC region is the most studied region with regard to environmental differences between -CG- and +CG-dominated storm cells. Special focus will be placed on the CC region and also on the NC region, since they are the regions in which the majority of +CG-dominated cells are found.

3.5.1 0-3 km shear

We analyzed 0-3 km shear because greater 0-3 km shear could allow for greater dynamical forcing of the updraft (Carey and Buffalo 2007), potentially increasing updraft speeds and reducing the warm cloud residence time. As explained in Section 1.6, a shorter warm cloud residence time is conducive to realizing higher SLWC in the mixed-phase region. Figure 41 shows the characteristics of 0-3 km shear in environments containing -CG-dominated and +CG-dominated storm cells for all regions. All of the distributions were right-skewed. The differences in median 0-3 km shear were significantly different at the 99.98% level in all regions except for the NW region, where the difference was not statistically significant. For all regions, +CG-

dominated cells had greater median 0-3 km shear than -CG-dominated cells had. The percent difference in each of the three southern regions was greater than the percent difference in the adjoining region north of it and was greatest in the SE region.

3.5.2 0-6 km shear

Since stronger 0-6 km shear is more conducive to rotating updrafts, and updraft rotation causes dynamic pressure gradient forces that can strengthen the updraft, we hypothesized that environments supporting greater 0-6 km shear could form storms with faster updrafts and therefore shorter warm cloud residence times. Thus, environments with greater 0-6 km shear may allow greater SLWCs in the mixed-phase region.

Figure 42 shows the characteristics of 0-6 km shear in environments containing -CG- and +CG-dominated cells for all regions. As was true of 0-3 km shear, all the distributions were right-skewed, and the differences in median were significant at the 99.98% level in all regions except the NW region, where the difference in medians was not statistically significant. The median value for 0-6 km shear in every region having statistically significant differences was larger for +CG-dominated cells than for -CG-dominated cells. In all regions except in the SW and NW regions, the percent differences in median 0-6 km shear were larger than they were for 0-3 km shear. As for 0-3 km shear, the percent difference in median 0-6 km shear in each of the three southern regions was larger than the percent difference in each adjoining region north of it, and the largest percent difference was in the SE region.

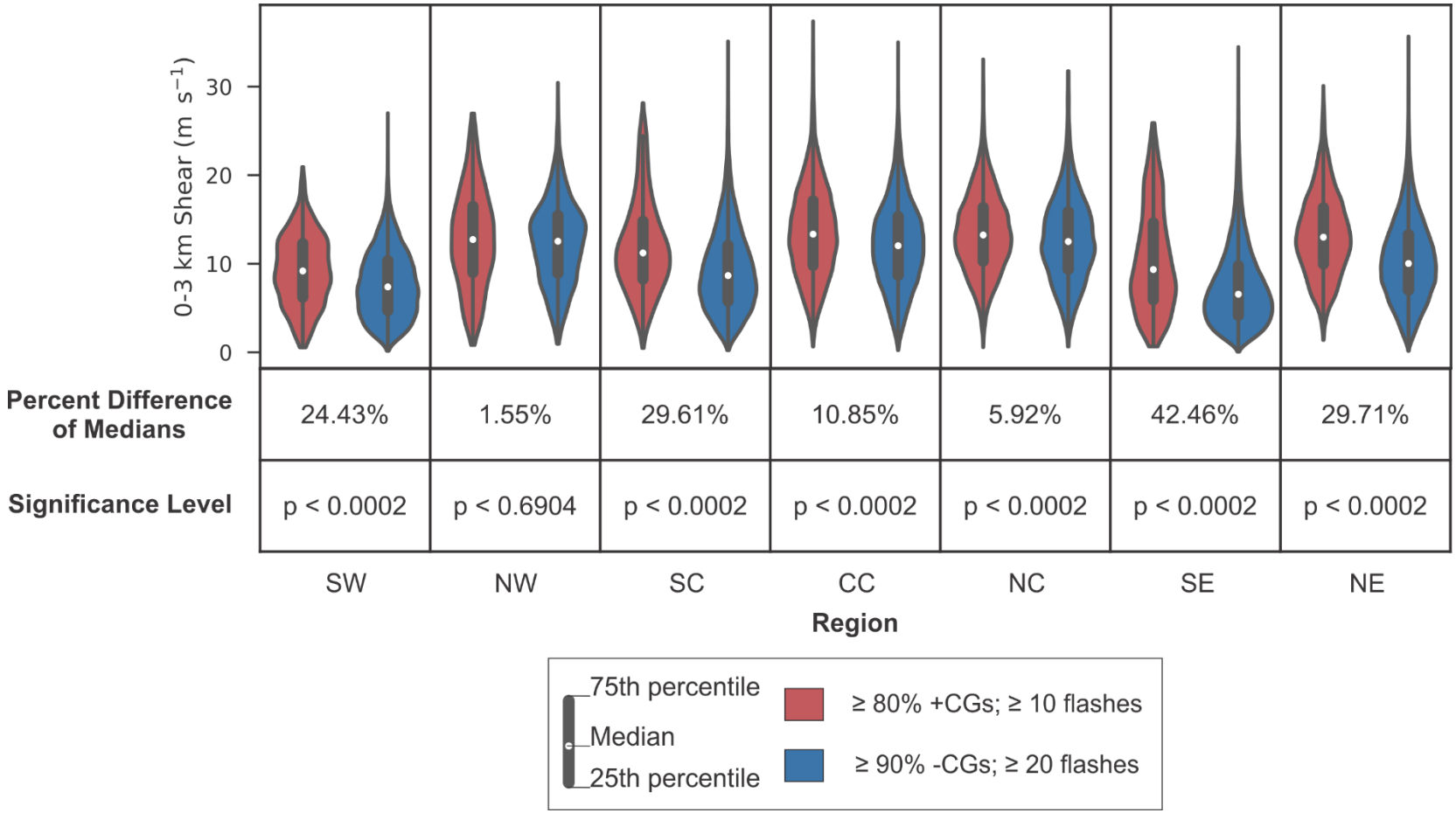

Figure 41: Same as Figure 25, but for 0-3 km shear.

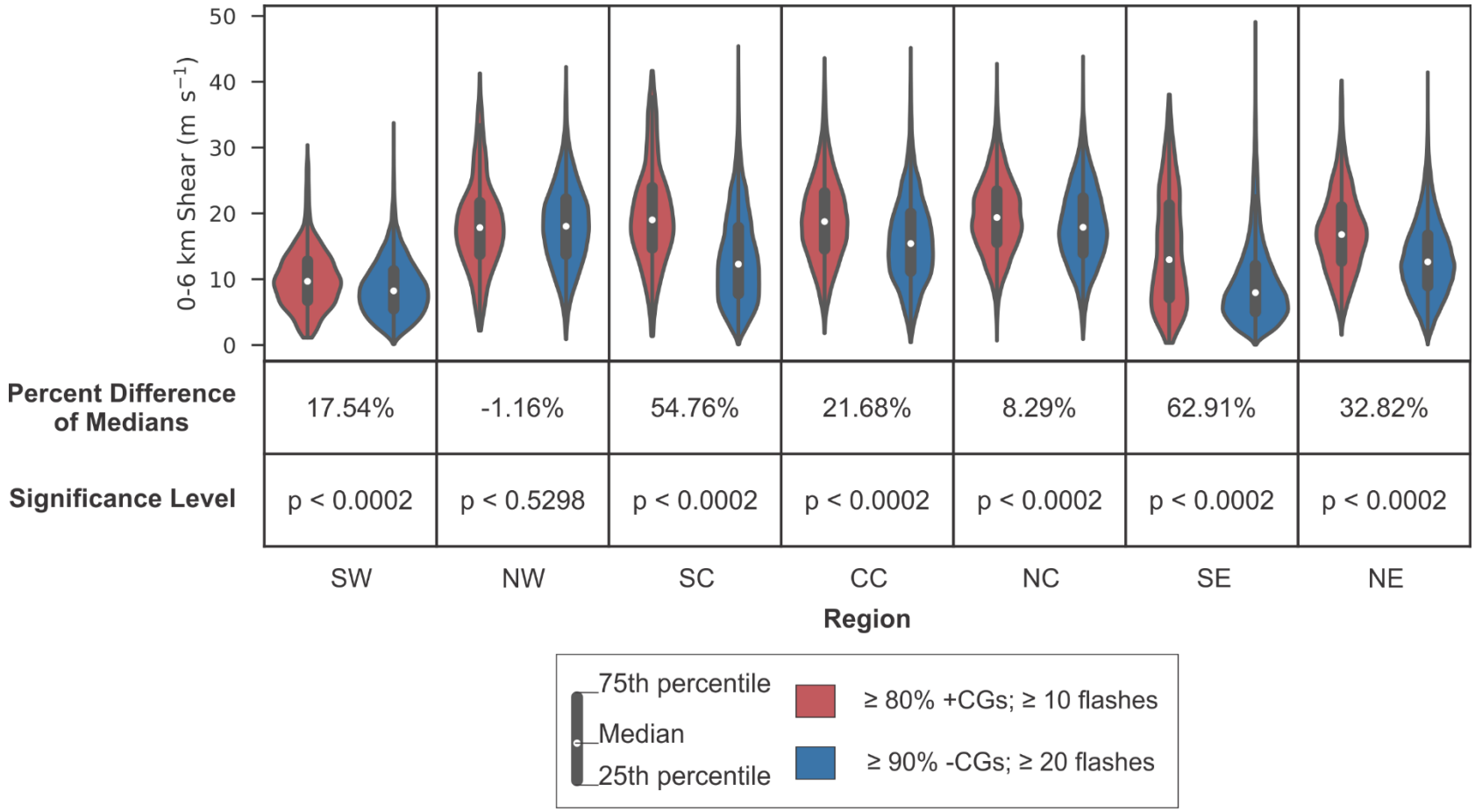

Figure 42: Same as Figure 25, but for 0-6 km shear.

3.5.3 Storm-Relative Wind Speed at the Equilibrium Level

We chose to analyze storm-relative wind speed at the EL because (MacGorman et al. 2011, 2017) hypothesized that storms with stronger storm-relative wind speed at the EL would loft more of the precipitation from near the top of updrafts to far enough distances from the storm that it would not be recirculated into the updraft. Fewer precipitation-sized particles in the updraft below the freezing level would lead to higher concentrations of small cloud droplets and larger values of SLWC in the mixed-phase region because fewer precipitation-sized particles would be available to scavenge cloud droplets through warm-cloud collision-coalescence processes.

Figure 43 shows the distribution of storm-relative wind speed at the EL in environments containing either +CG-dominated or -CG-dominated cells for all regions. All of the distributions were right-skewed, and the differences in median were significant in all regions at the 99.98% level, except in the SW region, where it was significant at the 96.42% level, and the NW region, where it was significant at the 93.68% level. Storm-relative wind speed at the EL was larger for +CG-dominated cells than for -CG-dominated cells in all regions except the NW region, but the percent differences were small or modest except in the SC region, where it was 61%. The fact that the median storm-relative wind speed at the EL in the NW region was greater for -CG-dominated storms and was no greater than 6.3% in two other regions suggests, again, that it is not the only important environmental parameter for producing +CG-dominated (and therefore, inverted-polarity) storms although it appears to play a role in at least some regions.

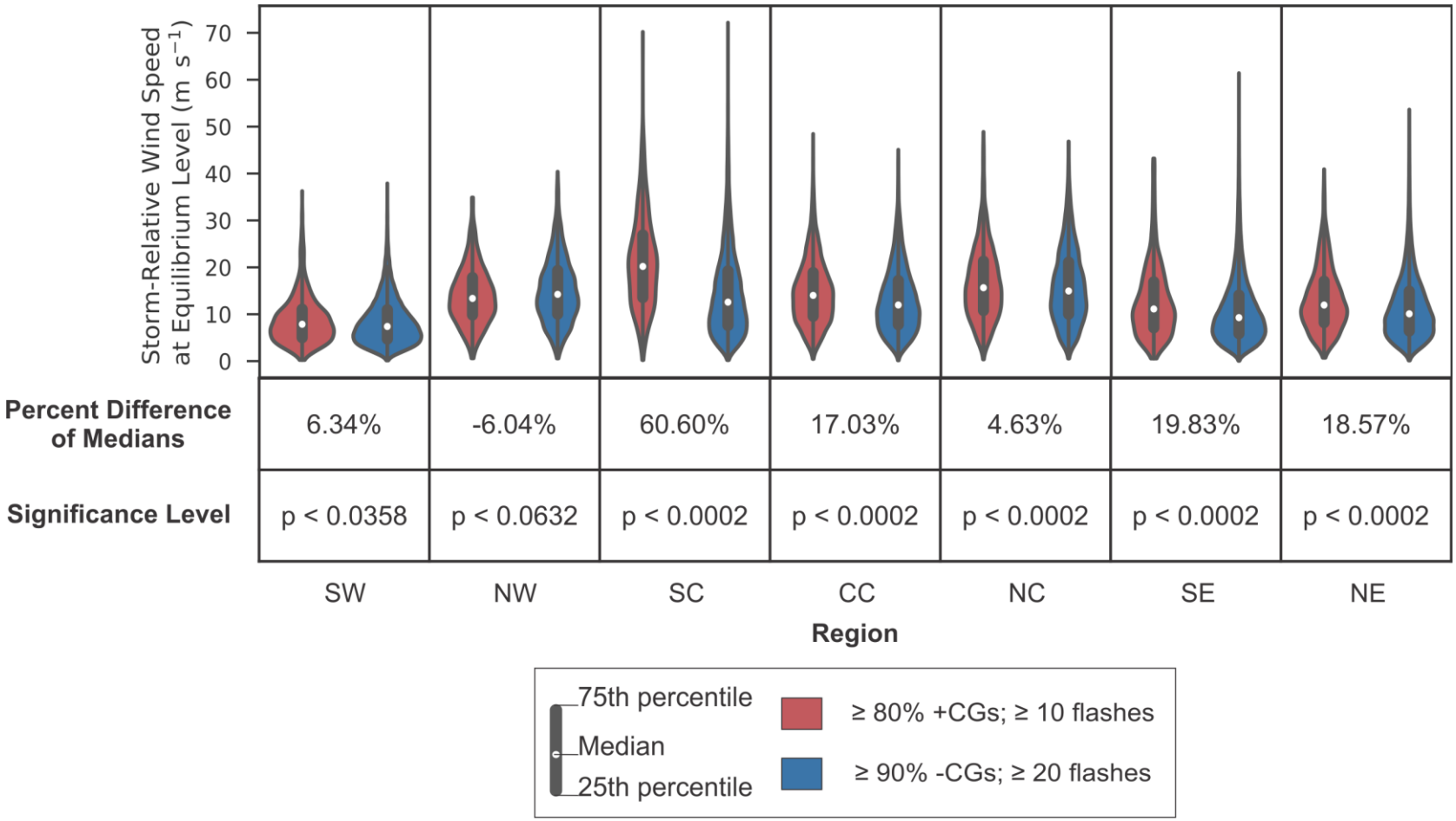

Figure 43: Same as Figure 25, but for storm-relative wind speed at the equilibrium level.

3.5.4 0-3 km Storm-Relative Helicity

We chose to analyze SRH because greater SRH provides greater dynamical forcing to the updraft (Carey and Buffalo 2007) by causing it to rotate, potentially increasing updraft speed due to the dynamic pressure perturbations associated with rotation. Faster updrafts allow shorter warm cloud residence times, which increases SLWC by the methods described in Section 1.6. Furthermore, centrifugal force from the rotation tends to inhibit entrainment into the inner core of the updraft, and so reduces or prevents dilution of the SLWC there.

Figure 44 shows the distribution of SRH in environments containing +CG-dominated or -CG-dominated cells in every region. All of the distributions were right-skewed, and the differences in median between +CG-dominated and -CG-dominated cells were significant at the 99.98% level in all regions except in the NW region, where the difference was not statistically significant. Median SRH was larger for +CG-dominated cells than for -CG-dominated cells in every region. As for the wind shear parameters, the percent difference in each southern region was considerably larger than the percent difference in the adjoining region north of it. Furthermore, the largest percent differences were in the easternmost regions, the largest (66%) being in the SE, and the second largest (50%) being in the NE. Again, the fact that the difference was not statistically significant in the NW and that the percent difference was relatively small in the CC and NC regions suggests that this parameter is not the only one affecting the dominant polarity of frequent CG flashes (and therefore, charge structure).

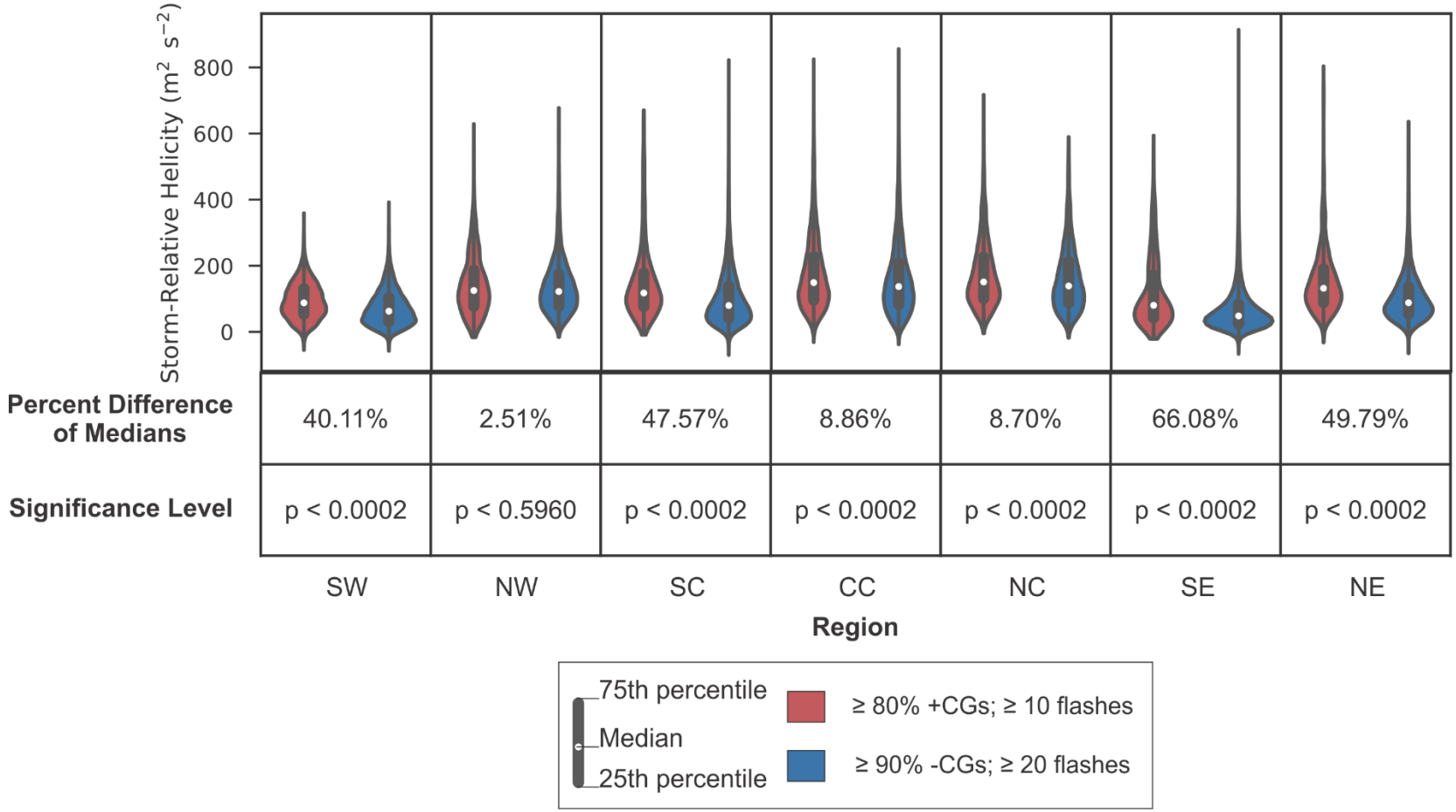

Figure 44: Same as Figure 25, but for 0-3 km storm-relative helicity.

4. Conclusion

The goal of this study was to compare the environments of storms that had inverted polarity electrical structure (midlevel positive charge and upper level negative charge) with the environments of storms having normal electrical structure (midlevel negative charge and upper level positive charge) over the whole CONUS for multiple years. Direct observations of electrical structure are unavailable over most of that domain. Because storms having frequent CG flashes dominated by +CG flashes have been found to have inverted-polarity charge structure (e.g., Rust and MacGorman 2002; MacGorman et al. 2005; Rust et al. 2005; Wiens et al. 2005; Tessendorf et al. 2007; Lang and Rutledge 2011; Fuchs et al. 2015), we inferred storm cells with high flash rates and predominantly +CG flashes to be inverted-polarity storm cells. The analyzed data, therefore, consisted of gridded CG data from the National Lightning Detection Network (Cummins and Murphy 2009) between 2004 and 2014. To minimize contamination from +CG flashes that occur in other scenarios, such as in MCS stratiform regions and winter storms, we analyzed storms only during the warm season between 1500 and 2300 Local Time. Furthermore, we imposed a threshold on each 15 km x 15 km grid cell used as a proxy for an inverted- or normal-polarity storm cell: for +CG flashes (inverted polarity), ≥10 CG flashes per 15 min period, 80% of which were +CG; for -CG flashes (normal polarity), ≥20 CG flashes per 15 min period, 90% of which were -CG. To minimize contamination from intracloud flashes, we required peak currents of both polarities to be ≥15 kA.

Note that we did not try to prune the data to ensure that the storm cells included in our analysis were completely statistically independent of each other because

observations have shown that the dominant CG polarity can be different in adjoining storms and can change in a given storm relatively quickly (e.g., Macgorman and Burgess 1994; Weiss et al. 2008), and we did not want to destroy those gradients. However, we wanted to avoid counting the same cell every 5 min or every 5 km, which was the spacing we preserved in our grid. Therefore, we ordered the grid cells from largest to smallest CG flash rate, and starting from the cell with the largest rate, we eliminated all cells that both overlapped with it and occurred within 30 minutes of it.

We analyzed seventeen environmental parameters that we thought might influence the SLWC in the mixed-phase region. SLWC is thought to be important to the polarity of a storm's charge distribution because laboratory experiments have found that unusually large values of SLWC cause graupel (small ice particles) to gain positive (negative) charge, instead of the usual negative (positive) charge, during rebounding collisions (Takahashi 1978; Saunders et al. 1991; Saunders and Peck 1998). Thus, large SLWC would cause the vertical polarity of the charge distribution in the updraft to be inverted from the usual polarity. We divided the CONUS into seven regions and analyzed which of these parameters were more likely to increase SLWC for +CG-dominated storms, rather than for -CG-dominated storms, in each region.

What we found was that, in every region, at least one environmental parameter that we expected to favor producing larger SLWC in the updraft was more likely to be favorable for storm cells dominated not by frequent +CG flashes, but by frequent -CG flashes, which typically are associated with normal-polarity storms. However, in every region, any environmental parameters that were inconsistent with the high-SLWC hypothesis had multiple parameters that were consistent with the hypothesis that large

SLWC values cause inverted-polarity storms. Furthermore, the combination of favorable parameters varied from one region to another with, for example, moisture parameters being more important in some regions than others. However, the dynamic parameters were associated with +CG-dominated cells in the greatest number of regions – all regions except the NW.

Tables 3 and 4 summarize the results of our analysis of the relationship of environmental parameters to +CG-dominated cells and -CG-dominated cells. Table 3 shows the percent difference between the medians for +CG-dominated cells and -CG-dominated cells for all environmental variables in all regions, taken from Figure 25 and Figures 29-44. A superscript asterisk (*) is placed next to percentages that are not statistically significant at the 90% level. Table 4 presents the results in a more qualitative manner by showing whether the relationship of a variable between the two dominant CG polarities of storm cells (1) was supported by the high-SLWC hypothesis ("yes"), (2) was not ("no"), or (3) the significance level of the difference in medians was less than 90%, so the null hypothesis that the medians of the parameter for +CG- and -CG-dominated storm cells were statistically the same was not disproven ("-").

Table 3: Percent differences in median for all variables in all regions, given as before in Figure 25 and in Figures 29-44. Cell boxes in the table for moisture parameters have green shading, those for thermodynamic parameters have orange shading, and those for dynamic parameters have yellow shading.

	SW	NW	SC	CC	NC	SE	NE
WCD	34	30.	-17	-28	19	3.3	-3.4
CBH	-26	-21	16	23	-18	-25	-2.9
DPD	-21	-8.2	10.	35	-19	-24	4.0
PWAT	3.4	-0.54*	-16	-22	6.6	-7.3	-5.6
θ_e	0.73	0.17*	-1.0	-1.1	1.0	-0.65	0.26
LFC to EL CAPE	88	15	28	-8.0	77	1.8*	37
LFC to EL NCAPE	57	8.9*	35	3.4	55	5.7	40.
LFC to -20°C CAPE	60.	18	19	-17	64	-0.54*	28
LFC to -20°C NCAPE	44	8.9*	31	-0.52*	45	2.7*	29
0°C to -20°C CAPE	49	18	35	-4.0	59	5.2	40.
0°C to -20°C NCAPE	48	15	36	-2.9	57	5.9	40.
|CIN|	-1.5*	-24	68	44	-11	31	32
EL height	14	2.0*	-2.4	-6.9	9.1	-2.8	0.11*
0-3 km shear	24	1.6*	30.	11	5.9	42	30.
0-6 km shear	18	-1.2*	55	22	8.3	63	33
storm-relative wind speed at EL	6.3	-6.0	61	17	4.6	20.	19
SRH	40.	2.5*	48	8.9	8.7	66	50.

Table 4: Our evaluation whether or not the percent differences in Table 3 support the high-SLWC hypothesis. The colors of shading for cell boxes in the table are the same as in Table 3.

	SW	NW	SC	CC	NC	SE	NE
WCD	no	no	yes	yes	no	no	yes
CBH	no	no	yes	yes	no	no	no
DPD	no	no	yes	yes	no	no	yes
PWAT	no	-	yes	yes	no	yes	yes
θ_e	no	-	yes	yes	no	yes	no
LFC to EL CAPE	yes	yes	yes	no	yes	-	yes
LFC to EL NCAPE	yes	-	yes	yes	yes	yes	yes
LFC to -20°C CAPE	yes	yes	yes	no	yes	-	yes
LFC to -20°C NCAPE	yes	-	yes	-	yes	-	yes
0°C to -20°C CAPE	yes	yes	yes	no	yes	yes	yes
0°C to -20°C NCAPE	yes	yes	yes	no	yes	yes	yes
|CIN|	-	no	yes	yes	no	yes	yes
EL height	yes	-	no	no	yes	no	-
0-3 km shear	yes	-	yes	yes	yes	yes	yes
0-6 km shear	yes	-	yes	yes	yes	yes	yes
storm-relative wind speed at EL	yes	no	yes	yes	yes	yes	yes
SRH	yes	-	yes	yes	yes	yes	yes

As discussed in the Introduction section, most previous studies of the environment of inverted-polarity storms and of +CG-dominated storms have analyzed storms in the CC region. In the CC region, our analyses found that the median values of all of the moisture and dynamic parameters were more favorable for +CG-dominated cells than for -CG-dominated cells, consistent with the high-SLWC hypothesis, but median values of most of the thermodynamic parameters were not consistent with the high-SLWC hypothesis. The only strongly favorable thermodynamic parameter was |CIN|. The percent differences between medians for the two dominant CG polarities

were greater for the moisture parameters in the CC region than in any other region.

The data that Carey and Buffalo (2007) analyzed came mainly from the CC region and showed that the storm cells suspected of having inverted-polarity charge structure had a shallower WCD, higher CBH, lower PWAT, greater DPD, greater 0-3 km shear, greater 0-3 km SRH, a lower EL, and greater LFC to EL NCAPE, as found in the present study. However, unlike this study, Carey and Buffalo (2007) found that storms inferred to have inverted-polarity charge structure had less |CIN|, and they did not find significant differences for LFC to EL CAPE, storm-relative wind speed at the EL, or 0-6 km shear. The threshold percentage of +CG flashes that they used to distinguish between potentially normal- and inverted-polarity storms was 25%, while we used a threshold of at least 80% +CG flashes to classify a cell's charge structure as inverted and no more than 10% +CG flashes to classify it as normal. The different values of the thresholds and the large separation between +CG and -CG thresholds in our study may explain the differences in the results for the two studies.

Lang and Rutledge (2011) analyzed data taken from the STEPS field campaign, in the CC region. They compared storm cells with at least 50% +CG flashes to those with less than 50% and found that the former tended to be inverted in polarity. As in our study, they found that inverted-polarity storms existed in environments with greater 0-3 km shear, greater 0-6 km shear, and greater 0-3 km SRH. However, unlike in our study, they found that inverted-polarity storm cells had much more LFC to EL CAPE, slightly lower CBHs, slightly deeper WCDs, and higher storm heights (inferred here as also meaning a higher EL).

The storms studied in the Oklahoma region and in the Colorado region by Fuchs

et al. (2015) were within the CC region of our study. Their findings were similar to ours in that they found that inverted-polarity or anomalously-charged storm cells had greater LFC to EL NCAPE and higher CBHs.

The NC region was the only region in which more cells satisfied our threshold for +CG flashes than satisfied our threshold for -CG flashes. In the NC region, which had the second largest number of +CG-dominated cells, the combination of environmental parameters thought to be consistent with the high-SLWC hypothesis was quite different than in the CC region. The medians for all the moisture parameters appeared more likely to enhance SLWC for -CG-dominated storms than for +CG-dominated storms, contrary to our hypothesis. However, the medians of all of the thermodynamic (except for |CIN| and θ_e) and dynamic parameters were more favorable for enhanced SLWC for +CG-dominated cells than for -CG-dominated cells. The percent differences for most of the thermodynamic variables were larger for the NC region than for any of the other regions, while those for the dynamic parameters were smaller for the NC region than for the majority of other regions.

In the SC region, the median values for the moisture parameters favored enhanced SLWC for those cells only slightly less than in the CC region. The medians of the dynamic parameters also appeared more favorable for +CG-dominated cells. Unlike the CC region, however, the medians of most of the thermodynamic parameters appeared more favorable for enhanced SLWC for +CG-dominated cells than for -CG-dominated cells. The percent differences for |CIN| and for the dynamic parameters thought to enhance SLWC were either the largest, or among the largest, differences favoring +CG-dominated cells of any of the regions.

The NE region was the only other region in which the median values of the most of the moisture parameters were more favorable for enhanced SLWC for +CG-dominated cells than for -CG-dominated cells, although the percent differences were much smaller in magnitude than for the CC and SC regions. Like the SC region, the median values of most of the thermodynamic and dynamic parameters appeared to favor enhanced SLWC in +CG-dominated cells more than in -CG-dominated cells.

The SE region had yet another combination of parameters favoring enhanced SLWC in +CG-dominated storms. Here the median values for most moisture parameters appeared to be less favorable for enhanced SLWC in +CG-dominated cells than in -CG-dominated cells, contrary to what was found in the SC, CC, and NE regions. Furthermore, the percent differences of medians for most of the thermodynamic parameters were relatively small, often too small for the differences to be statistically significant; only |CIN| had a moderately large percent difference favoring +CG-dominated cells. However, the SE region had either the largest, or among the largest, percent differences of median values of dynamic parameters favoring enhanced SLWC for +CG-dominated cells.

The combination of favorable parameters in the SW region was most similar to the combination in the NC region. Again, the moisture parameters were unfavorable, but were somewhat more unfavorable than in the NC region. Also, most of the thermodynamic parameters were strongly favorable, having among the largest percent differences relative to the other regions. The dynamic parameters were favorable, but with smaller percent differences than for most of the thermodynamic parameters. The percent differences for dynamic parameters in the SW region were somewhat larger

than those in the NC region.

The relationships with environmental parameters in the NW region are different in some respects from those of all other regions. Note that the NW region tends to have less CG lightning and had the smallest number of +CG-dominated cells and of -CG-dominated cells. As in several regions, the difference in median values of WCD and CBH the NW region were opposite to what would be consistent from their hypothesized role in producing inverted-polarity storms. Unlike what was found for most of the other regions, the median differences in dynamic parameters between +CG-dominated and -CG-dominated cells were mostly not statistically significant; the one dynamic parameter having a small, but significant difference was upper level, storm-relative wind, but that difference was opposite to what would be considered favorable for +CG-dominated cells according to the parameter's hypothesized role. Furthermore, the differences in medians for several of the thermodynamic parameters were not statistically significant. The largest positive percent differences for thermodynamic parameters were for the various CAPE parameters and for 0°C to -20°C NCAPE, and these indicated greater instability and updrafts for +CG-dominated cells, consistent with their hypothesized role in producing enhanced SLWC. The fact that environmental differences between +CG-dominated cells and -CG-dominated cells were mostly smaller in the NW region than elsewhere makes that region of particular interest for further study, to examine whether the characteristics of the storms themselves differed systematically in some way. Unfortunately, routinely collected data that would be useful for such a study are sparse or nonexistent in that region.

It is interesting to note the relative importance of CAPE and NCAPE in different

layers of the atmosphere. In general, for all 3 layers, CAPE tends to have larger percent differences than NCAPE, making CAPE a slightly better discriminator between the two types of cells. In the SW and NC regions, LFC to EL CAPE is the best discriminator between the two types of storms among the CAPE and NCAPE variables, suggesting that in those regions average parcel velocity throughout the whole storm could be more important than parcel acceleration in determining a storm cell's polarity. However, in the SC and SE regions, 0°C to -20°C NCAPE is the best discriminator, suggesting that in those regions parcel accelerations in the lower portion of the mixed-phase region are more important than accelerations elsewhere in determining a storm cell's polarity.

The primary conclusion of this study is that there is not one environmental variable that can determine the dominant polarity of frequent CG flashes in a storm, and by inference, that can determine the vertical polarity of a storm's charge distribution. Rather, it is a combination of moisture, thermodynamic, and dynamic parameters that work together. The various combinations are consistent with the hypothesis that inverted-polarity cells have higher SLWCs than normal-polarity cells.

Although we believe our conclusions are valid, there are a couple of caveats:

1. The storm cells used in our analysis were not necessarily statistically independent although we did restrict how close one storm cell could be to another in time and space. Any lack of independence of the analyzed cells would act to artificially inflate significance levels. Because most of the analyzed differences had a very high significance levels, however, it is likely that most of the differences would remain statistically significant if all the cells were independent.

2. Although our goal was to analyze the environments of storms whose charge distribution had inverted vertical polarity, we actually inferred storm polarity from the polarity and frequency of CG flashes. It is quite possible that the vertical polarity of the charge distribution of some of the storm cells we analyzed were not inverted, although we imposed seasonal and time-of-day constraints on our data set to try to minimize contamination.

Future studies would do well to supplement this dataset with observations of charge distributions inferred from balloon soundings of the electric field or from a VHF Lightning Mapping Array for at least some subset of the analyzed storms, in order to ensure that their charge structures are indeed inverted in polarity, as well as to begin analyzing the storm morphologies and moisture characteristics associated with the anomalous charge distributions. Additionally, there is clearly redundancy in many of the analyzed environmental parameters, such as between the CAPE and NCAPE parameters. Future work will involve using principal component analysis techniques to find the predictors of storm cell polarity that are most important and to eliminate redundancy therein. Multiple linear regression may also be used to quantitatively estimate the relative importance of each variable and to predict the polarity of a storm cell given the characteristics of its environment.

References

Alpha, T. R., and J. P. Snyder, 1982: United States Geological Survey: The Properties and Uses of Selected Map Projections. https://pubs.usgs.gov/pp/1395/plate-1.pdf.

AMS, 2015: American Meteorological Society Glossary of Meteorology. http://glossary.ametsoc.org (Accessed February 3, 2018).

Boccippio, D. J., K. L. Cummins, H. J. Christian, and S. J. Goodman, 2001: Combined Satellite- and Surface-Based Estimation of the Intracloud–Cloud-to-Ground Lightning Ratio over the Continental United States. *Mon. Weather Rev.*, **129**, 108–122, doi:10.1175/1520-0493(2001)129<0108:CSASBE>2.0.CO;2.

Brook, M., M. Nakano, P. Krehbiel, and T. Takeuti, 1982: The Electrical Structure of the Hokuriku Winter Thunderstorms. *J. Geophys. Res.*, **87**, 1207–1215, doi:10.1029/JC087iC02p01207.

Bruning, E. C., S. A. Weiss, and K. M. Calhoun, 2014: Continuous variability in thunderstorm primary electrification and an evaluation of inverted-polarity terminology. *Atmos. Res.*, **135**–**136**, 274–284, doi:10.1016/j.atmosres.2012.10.009.

Calhoun, K. M., D. R. Macgorman, C. L. Ziegler, and M. I. Biggerstaff, 2013: Evolution of lightning activity and storm charge relative to dual-Doppler analysis of a high-precipitation supercell storm. *Mon. Weather Rev.*, **141**, 2199–2223, doi:10.1175/MWR-D-12-00258.1.

Carey, L. D., and K. M. Buffalo, 2007: Environmental Control of Cloud-to-Ground Lightning Polarity in Severe Storms. *Mon. Weather Rev.*, **135**, 1327–1353, doi:10.1175/MWR3361.1.

——, S. A. Rutledge, W. A. Petersen, and L. D. Carey, 2003: The Relationship between Severe Storm Reports and Cloud-to-Ground Lightning Polarity in the Contiguous United States from 1989 to 1998. *Mon. Weather Rev.*, **131**, 1211–1228, doi:10.1175/1520-0493(2003)131<1211:TRBSSR>2.0.CO;2.

Clarence, N. D., and D. J. Malan, 1957: Preliminary discharge processes in lightning flashes to ground. *Q. J. R. Meteorol. Soc.*, **83**, 161–172, doi:10.1002/qj.49708335603.

Cooray, V., 2015: *An introduction to lightning*. Springer.

Cummins, K. L., and M. J. Murphy, 2009: An overview of lightning locating systems: History, techniques, and data uses, with an in-depth look at the U.S. NLDN. *IEEE Trans. Electromagn. Compat.*, **51**, 499–518, doi:10.1109/TEMC.2009.2023450.

Fan, J., and Coauthors, 2018: Substantial convection and precipitation enhancements by ultrafine aerosol particles. *Science (80-.).*, **359**, 411–418, doi:10.1126/science.aan8461.

Fleenor, S. A., C. J. Biagi, K. L. Cummins, E. P. Krider, and X. M. Shao, 2009: Characteristics of cloud-to-ground lightning in warm-season thunderstorms in the Central Great Plains. *Atmos. Res.*, **91**, 333–352, doi:10.1016/j.atmosres.2008.08.011.

Fuchs, B. R., and Coauthors, 2015: Environmental controls on storm intensity and charge structure in multiple regions of the continental United States. *J. Geophys. Res. Atmos.*, **120**, 6575–6596, doi:10.1002/2015JD023271.

Fuquay, D. M., 1982: Positive cloud-to-ground lightning in summer thunderstorms. *J. Geophys. Res.*, **87**, 7131–7140, doi:10.1029/JC087iC09p07131.

Gilmore, M. S., and L. J. Wicker, 2002: Influences of the Local Environment on Supercell Cloud-to-Ground Lightning, Radar Characteristics, and Severe Weather on 2 June 1995*. *Mon. Weather Rev.*, **130**, 2349–2372, doi:10.1175/1520-0493(2002)130<2349:IOTLEO>2.0.CO;2.

Jayaratne, E. R., and C. P. R. Saunders, 1984: The "rain gush", lightning, and the lower positive charge center in thunderstorms. *J. Geophys. Res. Atmos.*, **89**, 11816–11818, doi:10.1029/JD089iD07p11816.

Jayaratne, E. R., C. P. R. Saunders, and J. Hallett, 1983: Laboratory studies of the charging of soft-hail during ice crystal interactions. *Q. J. R. Meteorol. Soc.*, **109**, 609–630, doi:10.1002/qj.49710946111.

Knapp, D. I., 1994: *Using Cloud-to-Ground Lightning Data to Identify Tornadic Thunderstorm Signatures and Nowcast Severe Weather*.

Lang, T. J., and S. A. Rutledge, 2002: Relationships between Convective Storm Kinematics, Precipitation, and Lightning. *Mon. Weather Rev.*, **130**, 2492–2506, doi:10.1175/1520-0493(2002)130<2492:RBCSKP>2.0.CO;2.

——, and ——, 2011: A Framework for the Statistical Analysis of Large Radar and Lightning Datasets: Results from STEPS 2000. *Mon. Weather Rev.*, **139**, 2536–2551, doi:10.1175/MWR-D-10-05000.1.

——, and Coauthors, 2004: The severe thunderstorm electrification and precipitation study. *Bull. Am. Meteorol. Soc.*, **85**, 1107–1125, doi:10.1175/BAMS-85-8-1107.

Macgorman, D. R., and D. W. Burgess, 1994: Positive Cloud-to-Ground Lightning in Tornadic Storms and Hailstorms. *Mon. Weather Rev.*, **122**, 1671–1697, doi:10.1175/1520-0493(1994)122<1671:PCTGLI>2.0.CO;2.

MacGorman, D. R., and K. E. Nielsen, 1991: Cloud-to-Ground Lightning in a Tornadic Storm on 8 May 1986. *Mon. Weather Rev.*, **119**, 1557–1574, doi:10.1175/1520-0493(1991)119<1557:CTGLIA>2.0.CO;2.

——, and W. D. Rust, 1998: *The Electrical Nature of Storms*. Oxford University Press.

——, D. W. Burgess, V. Mazur, W. D. Rust, W. L. Taylor, and B. C. Johnson, 1989: Lightning Rates Relative to Tornadic Storm Evolution on 22 May 1981. *J. Atmos. Sci.*, **46**, 221–251, doi:10.1175/1520-0469(1989)046<0221:LRRTTS>2.0.CO;2.

——, W. D. Rust, P. Krehbiel, W. Rison, E. Bruning, and K. Wiens, 2005: The Electrical Structure of Two Supercell Storms during STEPS. *Mon. Weather Rev.*, **133**, 2583–2607, doi:10.1175/MWR2994.1.

——, I. R. Apostolakopoulos, N. R. Lund, N. W. S. Demetriades, M. J. Murphy, and P. R. Krehbiel, 2011: The Timing of Cloud-to-Ground Lightning Relative to Total Lightning Activity. *Mon. Weather Rev.*, **139**, 3871–3886, doi:10.1175/MWR-D-11-00047.1.

——, M. S. Elliott, and E. DiGangi, 2017: Electrical discharges in the overshooting tops of thunderstorms. *J. Geophys. Res. Atmos.*, **122**, 2929–2957, doi:10.1002/2016JD025933.

Makowski, J. A., D. R. MacGorman, M. I. Biggerstaff, and W. H. Beasley, 2013: Total Lightning Characteristics Relative to Radar and Satellite Observations of Oklahoma Mesoscale Convective Systems. *Mon. Weather Rev.*, **141**, 1593–1611, doi:10.1175/MWR-D-11-00268.1.

Mansell, E. R., D. R. MacGorman, C. L. Ziegler, and J. M. Straka, 2002: Simulated three-dimensional branched lightning in a numerical thunderstorm model. *J. Geophys. Res. Atmos.*, **107**, doi:10.1029/2000JD000244.

Marshall, T. C., W. D. Rust, and M. Stolzenburg, 1995: Electrical structure and updraft speeds in thunderstorms over the southern Great Plains. *J. Geophys. Res.*, **100**, 1001–1015, doi:10.1029/94JD02607.

Medici, G., K. L. Cummins, D. J. Cecil, W. J. Koshak, and S. D. Rudlosky, 2017: The Intracloud Lightning Fraction in the Contiguous United States. *Mon. Weather Rev.*, **145**, 4481–4499, doi:10.1175/MWR-D-16-0426.1.

Mesinger, F., and Coauthors, 2006: North American regional reanalysis. *Bull. Am. Meteorol. Soc.*, **87**, 343–360, doi:10.1175/BAMS-87-3-343.

Nag, A., M. J. Murphy, and J. A. Cramer, 2016: Update to the U.S. National Lightning Detection Network. *24th International Lightning Detection Conference (ILDC)*.

NCAR/UCAR, Research Data Archive: Computational & Information Systems Lab. rda.ucar.edu (Accessed February 3, 2018).

Orville, R. E., and G. R. Huffines, 2001: Cloud-to-ground lightning in the United States: NLDN results in the first decade, 1989–98. *Mon. Weather Rev.*, **129**, 1179–1193.

——, R. A. Weisman, R. B. Pyle, R. W. Henderson, and R. E. Orville, 1987: Cloud-to-ground lightning flash characteristics from June 1984 through May 1985. *J. Geophys. Res.*, **92**, 5640–5644, doi:10.1029/JD092iD05p05640.

——, G. R. Huffines, W. R. Burrows, R. L. Holle, and K. L. Cummins, 2002: The North American Lightning Detection Network (NALDN)—First Results: 1998–2000. *Mon. Weather Rev.*, **130**, 2098–2109, doi:10.1175/1520-0493(2002)130<2098:TNALDN>2.0.CO;2.

Pawar, S. D., and A. K. Kamra, 2009: Maxwell current density characteristics below isolated thunderstorms in tropics. *J. Geophys. Res. Atmos.*, **114**, doi:10.1029/2008JD010348.

Qie, X., T. Zhang, C. Chen, G. Zhang, T. Zhang, and W. Wei, 2005: The lower positive charge center and its effect on lightning discharges on the Tibetan Plateau. *Geophys. Res. Lett.*, **32**, 1–4, doi:10.1029/2004GL022162.

Rogers, R. R., and M. K. Yau, 1989: *A Short Course in Cloud Physics*. 3rd ed. Elsevier Inc.

Rudlosky, S. D., and H. E. Fuelberg, 2011: Seasonal, Regional, and Storm-Scale Variability of Cloud-to-Ground Lightning Characteristics in Florida. *Mon. Weather Rev.*, **139**, 1826–1843, doi:10.1175/2010MWR3585.1.

Rust, W. D., and D. MacGorman, 2002: Possibly inverted-polarity electrical structures in thunderstorms during STEPS. *Geophys. Res. Lett.*, **29**, doi:10.1029/2001GL014303.

——, D. R. MacGorman, and R. T. Arnold, 1981a: Positive cloud-to-ground lightning flashes in severe storms. *Geophys. Res. Lett.*, **8**, 791–794, doi:10.1029/GL008i007p00791.

——, W. L. Taylor, D. R. MacGorman, and R. T. Arnold, 1981b: Research on Electrical Properties of Severe Thunderstorms in the Great Plains. *Bull. Am. Meteorol. Soc.*, **62**, 1286–1293, doi:10.1175/1520-0477(1981)062<1286:ROEPOS>2.0.CO;2.

——, and Coauthors, 2005: Inverted-polarity electrical structures in thunderstorms in the Severe Thunderstorm Electrification and Precipitation Study (STEPS). *Atmos. Res.*, **76**, 247–271, doi:10.1016/j.atmosres.2004.11.029.

Rutledge, S. A., and D. R. MacGorman, 1988: Cloud-to-Ground Lightning Activity in the 10–11 June 1985 Mesoscale Convective System Observed during the Oklahoma–Kansas PRE-STORM Project. *Mon. Weather Rev.*, **116**, 1393–1408, doi:10.1175/1520-

0493(1988)116<1393:CTGLAI>2.0.CO;2.

——, E. R. Williams, and W. A. Petersen, 1993: Lightning and electrical structure of mesoscale convective systems. *Atmos. Res.*, **29**, 27–53, doi:10.1016/0169-8095(93)90036-N.

Saunders, C. P. R., and S. L. Peck, 1998: Laboratory studies of the influence of the rime accretion rate on charge transfer during crystal/graupel collisions. *J. Geophys. Res. Atmos.*, **103**, 13949–13956.

——, W. D. Keith, and R. P. Mitzeva, 1991: The effect of liquid water on thunderstorm charging. *J. Geophys. Res. Atmos.*, **96**, 11007–11017.

Simpson, G., and G. D. Robinson, 1941: The Distribution of Electricity in Thunderclouds, II. *Proceedings of the Royal Society A: Mathematical, Physical and Engineering Sciences*, Vol. 177 of, The Royal Society, 281–329.

Smith, S. B., J. G. LaDue, and D. R. MacGorman, 2000: The Relationship between Cloud-to-Ground Lightning Polarity and Surface Equivalent Potential Temperature during Three Tornadic Outbreaks. *Mon. Weather Rev.*, **128**, 3320–3328, doi:10.1175/1520-0493(2000)128<3320:TRBCTG>2.0.CO;2.

Snyder, J. P., 1987: *Map Projections: A Working Manual*. U.S. Government Printing Office, Washington, 104-110 pp.

Stolzenburg, M., W. D. Rust, and T. C. Marshall, 1998: Electrical structure in thunderstorm convective regions: 1. Mesoscale Convective Systems. *J. Geophys. Res.*, **103**, 14059–14078, doi:10.1029/97JD03547.

Takagi, N., T. Takeuti, and T. Nakai, 1986: On the occurrence of positive ground flashes. *J. Geophys. Res.*, **91**, 9905–9909, doi:10.1029/JD091iD09p09905.

Takahashi, T., 1978: Riming Electrification as a Charge Generation Mechanism in Thunderstorms. *J. Atmos. Sci.*, **35**, 1536–1548, doi:10.1175/1520-0469(1978)035<1536:REAACG>2.0.CO;2.

Takeuti, T., M. Nakano, M. Brook, D. J. Raymond, and P. Krehbiel, 1978: The anomalous winter thunderstorms of the Hokuriku Coast. *J. Geophys. Res.*, **83**, 2385–2394, doi:10.1029/JC083iC05p02385.

Tessendorf, S. A., S. A. Rutledge, and K. C. Wiens, 2007: Radar and Lightning Observations of Normal and Inverted Polarity Multicellular Storms from STEPS. *Mon. Weather Rev.*, **135**, 3682–3706, doi:10.1175/2007MWR1954.1.

Vonnegut, B., and C. B. Moore, 1958: *Giant Electrical Storms*. Little.

Wallace, J. M., and P. V. Hobbs, 2006: *Atmospheric Science: An Introductory Survey*. 2nd ed. Elsevier Inc.

Weckwerth, T. M., and Coauthors, 2004: An overview of the international H 2O project (IHOP_2002) and some preliminary highlights. *Bull. Am. Meteorol. Soc.*, **85**, 253–277, doi:10.1175/BAMS-85-2-253.

Weiss, S. A., W. D. Rust, D. R. MacGorman, E. C. Bruning, and P. R. Krehbiel, 2008: Evolving complex electrical structures of the STEPS 25 June 2000 multicell storm. *Mon. Weather Rev.*, **136**, 741–756, doi:10.1175/2007MWR2023.1.

Wiens, K. C., S. A. Rutledge, and S. A. Tessendorf, 2005: The 29 June 2000 supercell observed during STEPS. Part II: Lightning and charge structure. *J. Atmos. Sci.*, **62**, 4151–4177, doi:10.1175/JAS3615.1.

Wilks, D. S., 2011: *Statistical Methods in the Atmospheric Sciences*. 3rd ed. Academic Press.

Williams, E., V. Mushtak, D. Rosenfeld, S. Goodman, and D. Boccippio, 2005: Thermodynamic conditions favorable to superlative thunderstorm updraft, mixed phase microphysics and lightning flash rate. *Atmos. Res.*, **76**, 288–306, doi:10.1016/j.atmosres.2004.11.009.

Williams, E. R., 1989: The tripole structure of thunderstorms. *J. Geophys. Res. Atmos.*, **94**, 13151–13167, doi:10.1029/JD094iD11p13151.

Williams, E. R., R. Zhang, and J. Rydock, 1991: Mixed-Phase Microphysics and Cloud Electrification. *J. Atmos. Sci.*, **48**, 2195–2203, doi:10.1175/1520-0469(1991)048<2195:MPMACE>2.0.CO;2.

Wilson, C. T. R., 1921: Investigations on Lightning Discharges and on the Electric Field of Thunderstorms. *Philos. Trans. R. Soc. A Math. Phys. Eng. Sci.*, **221**.